



FABRICATION AND EVALUATION OF
SHELLAC/POLYVINYLPIRROLIDONE NANOFIBERS LOADED WITH
MONOLAURIN AS WOUND DRESSING MATS USING FACTORIAL DESIGNS



By
MISS Nawinda CHINATANGKUL

A Thesis Submitted in Partial Fulfillment of the Requirements
for Doctor of Philosophy (PHARMACEUTICAL TECHNOLOGY)
Department of PHARMACEUTICAL TECHNOLOGY
Graduate School, Silpakorn University
Academic Year 2018
Copyright of Graduate School, Silpakorn University



การเตรียมและประเมินเส้นใยนาโนเซลลูล์และพอลิไวนิลไพโรลิโดนที่บรรจุสารโม
โนลอรินสำหรับใช้เป็นวัสดุปิดแผลโดยการออกแบบเชิงตัวประกอบ



โดย
นางสาววินดา ชินะตั้งกูร

วิทยานิพนธ์นี้เป็นส่วนหนึ่งของการศึกษาตามหลักสูตรปรัชญาดุษฎีบัณฑิต
สาขาวิชาเทคโนโลยีสารสนเทศ แบบ 1.1 ปรัชญาดุษฎีบัณฑิต
ภาควิชาเทคโนโลยีสารสนเทศ
บัณฑิตวิทยาลัย มหาวิทยาลัยศิลปากร
ปีการศึกษา 2561
ลิขสิทธิ์ของบัณฑิตวิทยาลัย มหาวิทยาลัยศิลปากร

FABRICATION AND EVALUATION OF
SHELLAC/POLYVINYLPIRROLIDONE NANOFIBERS LOADED
WITH MONOLAURIN AS WOUND DRESSING MATS USING
FACTORIAL DESIGNS



A Thesis Submitted in Partial Fulfillment of the Requirements
for Doctor of Philosophy (PHARMACEUTICAL TECHNOLOGY)
Department of PHARMACEUTICAL TECHNOLOGY
Graduate School, Silpakorn University
Academic Year 2018
Copyright of Graduate School, Silpakorn University

Title	Fabrication and evaluation of shellac/polyvinylpyrrolidone nanofibers loaded with monolaurin as wound dressing mats using factorial designs
By	Nawinda CHINATANGKUL
Field of Study	(PHARMACEUTICAL TECHNOLOGY)
Advisor	Sontaya Limmatvapirat

Graduate School Silpakorn University in Partial Fulfillment of the Requirements for the Doctor of Philosophy

..... Dean of graduate school
(Associate Professor Jurairat Nunthanid, Ph.D.)

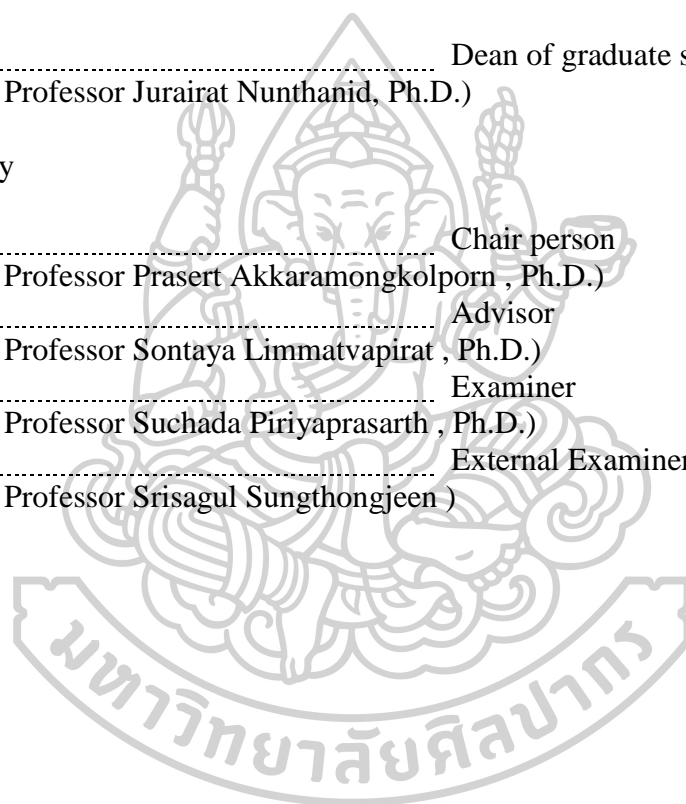
Approved by

..... Chair person
(Associate Professor Prasert Akkaramongkolporn , Ph.D.)

..... Advisor
(Associate Professor Sontaya Limmatvapirat , Ph.D.)

..... Examiner
(Associate Professor Suchada Piriyaprasarth , Ph.D.)

..... External Examiner
(Associate Professor Srisagul Sungthongjeen)



57353803 : Major (PHARMACEUTICAL TECHNOLOGY)

Keyword : shellac, polyvinylpyrrolidone, monolaurin, electrospun nanofibers, factorial design, wound dressing

MISS NAWINDA CHINATANGKUL : FABRICATION AND EVALUATION OF SHELLAC/POLYVINYLPIRROLIDONE NANOFIBERS LOADED WITH MONOLAURIN AS WOUND DRESSING MATS USING FACTORIAL DESIGNS THESIS ADVISOR : ASSOCIATE PROFESSOR SONTAYA LIMMATVAPIRAT, Ph.D.

Due to their ultrafine network structures, electrospun nanofibers have been potentially used for wound dressing application as they could provide a rapid wound epithelialization, an enhanced oxygen and nutrients delivery to cells, an improved drug loading capacity and release rate. In order to develop a desired wound dressing material, shellac (SHL), a natural biopolymer with excellent film forming and protective properties, was blended with polyvinyl pyrrolidone (PVP), a water-soluble synthetic polymer with good mechanical characteristic, for using as a polymeric carrier. Monolaurin (ML), which is a natural antimicrobial lipid, was incorporated into the SHL/PVP blended nanofibers to prevent the incidence of delayed wound healing resulting from microbial infection. In this study, a full factorial design with three replicated centre points was employed in order to determine the main and interaction effects of various factors including SHL ratio in SHL-PVP blended solution, ML content and applied voltage on the multiple responses such as morphology, surface wettability, absorbency and mechanical properties. According to the results, an increase in the PVP content could lead to a significant increase in the mechanical behavior resulting in the appearance of beadless fibres. In addition, the presence of PVP might contribute to an improvement in the drug loading capacity and dissolution rate. However, the wettability and absorbency of the fibres might be retarded by the hygroscopic nature and rapid erosion of PVP. The fabricated nanofibers loaded with ML exhibited an excellent activity against *Staphylococcus aureus* and *Candida albicans*, and also provided an enhanced ability in the cell adhesion. Therefore, SHL/PVP blended nanofibers loaded with ML might be effectively used for application in wound healing.

ACKNOWLEDGEMENTS

First of all, I would like to give a special thank to my thesis advisor, Associate Professor Dr. Sontaya Limmatvapirat, for his crucial guidance, financial support, patience and motivation during my graduate study period. Without his helpful advice and constant assistance, I could not be able to finish my PhD degree successfully.

Besides, I wish to express my gratitude to Associate Professor Dr. Suchada Piriyaprasarth for her worthy guidance and suggestion on the concept of experimental design. In addition, I am also grateful to Associate Professor Dr. Jurairat Nunthanid, Associate Professor Dr. Manee Luangtana-anan and Professor Dr. Pornsak Sriamornsak at the Department of Pharmaceutical Technology and Pharmaceutical Biopolymer Group (PBiG), Faculty of Pharmacy, Silpakorn University, for their insightful opinion and discussion in my research.

I cannot forget to thank all laboratory members at Pharmaceutical Technology Building for their kind assistance and warm friendship. They are important to my meaningful success.

I would like to acknowledge the Higher Education Commission, Faculty of Pharmacy, Silpakorn University for financial support. My thesis work was also supported by Silpakorn University Research and Development Institute and the Thailand Research Fund.

Lastly, I would like to thank my beloved mom, family and friends for their emotional support and encouragement. To my dad, especially, I would like to give a huge thank for his all support. I could not get through any struggle without him. "I love you, DAD."

Nawinda CHINATANGKUL

TABLE OF CONTENTS

	Page
ABSTRACT.....	D
ACKNOWLEDGEMENTS.....	E
TABLE OF CONTENTS.....	F
LIST OF TABLES.....	J
LIST OF FIGURES.....	L
CHAPTER 1 Introduction.....	1
CHAPTER 2 Literature review.....	5
2.1 Types of wound dressings.....	7
2.2 Methods for nanofiber preparation.....	10
2.3 Polymers used for the synthesis of electrospun nanofibers.....	15
2.4 The active compounds incorporated into electrospun nanofibers.....	22
2.5 A design of experiments approach for fabrication process of electrospun nanofibers.....	37
CHAPTER 3 Methodology.....	45
3.1 Materials and methods.....	47
3.1.1 Materials.....	47
3.1.2 Preparation of SHL solutions.....	47
3.1.3 Electrospinning.....	48
3.1.4 Characterization.....	48
3.1.5 Experimental design.....	48
3.1.6 Fabrication and physicochemical characterization of ML loaded SHL films 50	
3.1.6.1 Powder X-ray diffraction (PXRD).....	50
3.1.6.2 Differential scanning calorimetry (DSC).....	50
3.1.6.3 Fourier transformed infrared spectroscopy (FTIR).....	50

3.1.7	Fabrication and physicochemical characterization of ML loaded SHL fibers	51
3.1.7.1	Preparation and evaluation of SHL-ML solutions.....	51
3.1.7.2	Preparation and evaluation of SHL-ML fibers	51
3.1.7.3	Physicochemical characterization of SHL-ML fibers	51
3.1.8	Experimental design	52
3.1.9	Time-kill kinetics.....	52
3.1.10	Experimental design	53
3.1.11	Preparation of blended solutions of SHL and PVP loaded with ML	54
3.1.12	Evaluation of properties of the blended solution.....	54
3.1.13	Preparation of electrospun SHL-PVP nanofibers loaded with ML	54
3.1.14	Morphology of electrospun nanofibers.....	54
3.1.15	Physicochemical and physical characterization of electrospun nanofibers	55
3.1.15.1	Mechanical properties	55
3.1.15.2	Wettability.....	55
3.1.15.3	Absorbency	56
3.1.16	Time-kill kinetics.....	56
3.1.17	Cell attachment assay	57
3.1.18	<i>In vitro</i> MTT assay	57
CHAPTER 4 Design of Experiment Approach for Fabrication Process of Electrospun Shellac Nanofibers Using Factorial Designs		
4.1	Introduction	59
4.2	Results and discussion.....	59
4.2.1	Properties of SHL solution	59
4.2.2	Results of the experimental design.....	60

4.2.2.1 Effects of the independent parameters on the morphology of SHL nanofibers	60
4.2.2.2 The validation of the models	63
4.3 Summary.....	64
CHAPTER 5 Design and characterisation of monolaurin loaded electrospun shellac nanofibers with antimicrobial activity	65
5.1 Introduction	66
5.2 Results and discussion.....	67
5.2.1 Evaluation of physical state and compatibility of the components in ML loaded SHL matrix	67
5.2.1.1 Powder X-ray diffractometry (PXRD)	67
5.2.1.2 Differential scanning calorimetry (DSC)	69
5.2.1.3 Fourier transform infrared spectroscopy (FTIR)	70
5.2.2 Evaluation of SHL-ML solution properties.....	72
5.2.3 Experimental design.....	74
5.2.3.1 Effects of the independent parameters on the morphology of SHL-ML nanofibers	74
5.2.3.2 Optimization of SHL-ML nanofibers.....	79
5.2.3.3 The validation of the models	80
5.2.4 Time-kill kinetic study.....	81
5.3 Conclusions	83
CHAPTER 6 Design and characterisation of electrospun shellac/polyvinylpyrrolidone blended nanofibers loaded with monolaurin for application in wound healing	85
6.1 Introduction	86
6.2 Results and discussion.....	86
6.2.1 Evaluation of physical characteristics and compatibility of SHL-PVP nanofibers loaded with ML	86
6.2.1.1 Powder X-ray diffractometry (PXRD)	87
6.2.1.2 Differential scanning calorimetry (DSC)	88

6.2.1.3 Fourier transform infrared spectroscopy (FTIR)	90
6.2.2 Evaluation of SHL-PVP-ML solution properties	93
6.2.3 Experimental design	94
6.2.3.1 Effects of the independent parameters on the morphology of SHL-PVP nanofibers loaded with ML	94
6.2.3.2 Effects of the independent parameters on the mechanical properties of SHL-PVP nanofibers loaded with ML	98
6.2.3.3 Effects of the independent parameters on the wettability of SHL-PVP nanofibers loaded with ML	101
6.2.3.4 Effects of the independent parameters on the absorbency of SHL-PVP nanofibers loaded with ML	103
6.2.4 The antimicrobial activity of SHL-PVP nanofibers loaded with ML	106
6.2.5 Cell attachment assay	108
6.3 Cytotoxicity screening by the MTT bioassay	110
6.4 Conclusions	112
CHAPTER 7 Summary and general conclusions	113
APPENDIX	116
REFERENCES	120
VITA	128

LIST OF TABLES

	Page
Table 1 The MIC and MBC values against <i>S. aureus</i> (the units of antimicrobial agents are mg/mL for lauric acid and monolaurin and % (v/v) for virgin coconut oil and lactic acid) (42).	27
Table 2 Inactivation of <i>H. pylori</i> by lipids (46).....	29
Table 3 MIC (mg/mL) of monolaurin, citric, succinic, fumaric, malic and lactic acid against <i>E. coli</i> , <i>Salmonella</i> spp. and <i>Cl. Perfringens</i> grown on glucose (incubation in triplicate for 1 day) (45).....	30
Table 4 Viral inactivation by incubation with fatty acids at 37 °C for 30 min (50). 34	
Table 5 Viral inactivation by incubation with monoglycerides at 37 °C for 30 min (50). 35	
Table 6 Effect of applied voltage and tip to collector distance on nanofiber diameter based on a 3 ² factorial experimental design with two replicates.....	39
Table 7 ANOVA analysis of parameters including applied voltage, distance and their interaction on the fibre diameter.....	39
Table 8 Independent parameters, including distance, voltage, flow rate, pH, PVP and TTIP contents, and their levels for the central composite design.	41
Table 9 Independent parameters, including bioactive glass content, applied voltage, tip-to-collector distance and flow rate, and their levels for the Box-Behnken design. 43	
Table 10 Summary of the ANOVA results for the average fibre diameter.....	43
Table 11 Experimental range and levels of selected independent parameters including SHL content, applied voltage and flow rate.	49
Table 12 Experimental range and levels of selected independent parameters including SHL and ML contents, applied voltage and flow rate.	52
Table 13 Experimental range and levels of selected independent parameters including SHL ratio in blended solution, ML content, applied voltage and flow rate.....	54
Table 14 The effect of different SHL concentrations on viscosity, conductivity and surface tension.	60

Table 15	Full factorial design and experimental responses, including nanofiber diameter and bead amount, for each design point of SHL content, applied voltage and flow rate.	61
Table 16	Analytical results for diameter and bead amount of SHL fibres.....	63
Table 17	Comparison between the actual and predicted values of diameter and bead amount of test data set.....	63
Table 18	Effect of SHL and ML concentrations on viscosity, conductivity and surface tension.	73
Table 19	Full factorial design and experimental responses, including fibre diameter and bead amount, for each design point of SHL and ML contents, applied voltage and flow rate.	75
Table 20	Analytical results for diameter and bead amount of SHL-ML fibres.....	78
Table 21	Comparison between the actual and predicted values of diameter and bead amount of test data set.....	81
Table 22	Effect of SHL ratio in blended solution and ML content on the solution properties.	93
Table 23	Analytical results for different responses, including morphology and mechanical properties.	97
Table 24	Analytical results for different responses, including surface wettability and absorbency.....	103



LIST OF FIGURES

	Page
Figure 1 Schematic of nanofiber fabrication by drawing.	11
Figure 2 Schematic of nanofiber fabrication by template synthesis.	12
Figure 3 Schematic of nanofiber fabrication by phase separation.	13
Figure 4 Schematic illustration of the basic setup for electrospinning.	14
Figure 5 Progress in polymer processing.	17
Figure 6 Potential effect on polymer blend properties as component concentration changes.	18
Figure 7 DSC thermograms of various compositions such as (a) Gati pure, (b) PCL pure, (c) PNIPAM pure, (d) EA pure, (e) PNIPAM(10%) nanofibers, (f) PNIPAM(6%) / EA(4%) nanofibers, (g) PNIPAM(5%) / EA(2%) / PCL(6%) nanofibers, (h) PNIPAM(3%) / EA(2%) / PCL(8%) / Gati(10%) nanofibers and (i) PCL(8%) nanofibers.	19
Figure 8 Antimicrobial activity (zone of inhibition) against <i>Staphylococcus aureus</i> of various formulations.	20
Figure 9 The structure of lauric acid.	23
Figure 10 Fatty acid composition of virgin coconut oil (40).	23
Figure 11 Glycerolysis of triglycerides to form monolaurin.	24
Figure 12 SEM of <i>S. aureus</i> CH1 in Mueller Hinton broth containing antimicrobials: (A) control, (B) 10% virgin coconut oil, (C) 0.4% lactic acid, (D) 10% virgin coconut oil + 0.4% lactic acid, (E) 3.2 mg/mL of lauric acid, (F) 0.2 mg/mL of lauric acid + 0.1% of lactic acid, (G) 0.1 mg/mL of monolaurin and (H) 0.05 mg/mL of monolaurin + 0.1% of lactic acid. Cell membranes were disturbed and leaked (solid arrow) and subsided (hatched arrow) (42).	25
Figure 13 TEM of <i>S. aureus</i> CH1 in Mueller Hinton broth containing antimicrobials: (A) control, (B) 10% virgin coconut oil, (C) 0.4% lactic acid, (D) 10% virgin coconut oil + 0.4% lactic acid, (E) 3.2 mg/mL of lauric acid, (F) 0.2 mg/mL of lauric acid + 0.1% of lactic acid, (G) 0.1 mg/mL of monolaurin and (H) 0.05 mg/mL of monolaurin + 0.1% of lactic acid. Cell membranes were disturbed and leaked (solid arrow) and subsided (hatched arrow) (42).	26
Figure 14 The outer surface of <i>E. coli</i>	30

Figure 15 Inhibition index expressed by ML against <i>E. coli</i> . O157:H7 in PC broth. Data represent the average (n=2) \pm SD (49).	31
Figure 16 Inhibition index expressed by ML against <i>Salmonella</i> spp. in PC broth. Data represent the average (n=2) \pm SD (49).	32
Figure 17 The effect of linoleic acid against VSV: (a) control (b) linoleic acid 0.5 mg/mL (c) linoleic acid 1 mg/mL (50).	33
Figure 18 in vitro effect of ML on the growth of <i>C. albicans</i> (A) and <i>G. vaginalis</i> (B) which were cultured for 24 h in the presence of various concentrations of ML at 37 °C (51). 36	36
Figure 19 Diagram of central composite design for two factors.	41
Figure 20 Diagram of Box-Behnken design for three factors.	43
Figure 21 SEM images of SHL nanofibers at the concentrations of (A) 35% w/w, (B) 37.5% w/w and (C) 40% w/w.....	60
Figure 22 Pareto charts of the response values (A) nanofiber diameter and (B) bead amount. 61	61
Figure 23 Powder X-ray diffraction patterns of SHL, ML, their physical mixture, nanofibers and films in the weight ratio of 40: 3.	68
Figure 24 Powder X-ray diffraction patterns of (A) SHL-ML physical mixtures with different amounts of ML and (B) their corresponding films.	69
Figure 25 DSC thermograms of SHL, ML, their physical mixture, nanofibers and films in the weight ratio of 40: 3.....	70
Figure 26 FTIR spectra of SHL, ML, their physical mixture, nanofibers and films in the ratio of 40: 3. 72	72
Figure 27 Pareto charts of the response values (A) nanofiber diameter and (B) bead amount. 76	76
Figure 28 Schematic diagram representing the influence of ML on fibre diameter. 76	76
Figure 29 SEM images and diameter distribution of SHL-ML nanofibers at the weight ratio of (A) 35: 1, (B) 35: 3, (C) 37.5: 2, (D) 40: 1 and (E) 40: 3.....	77
Figure 30 Two-dimensional contour plots presenting the effects of SHL and ML contents on (A) fibre diameter and (B) bead amount.	79
Figure 31 Overlay plot for optimization of SHL nanofibers loaded with ML.	80
Figure 32 Kill kinetics of nanofibers for (A) <i>S. aureus</i> , (B) <i>E. coli</i> and (C) <i>C. albicans</i> over a period of 9 h.	83

Figure 33 Powder X-ray diffraction patterns of ML, PVP, SHL and nanofibers at various ratios of SHL and PVP, and different amounts of loaded ML.	88
Figure 34 DSC thermograms of ML, PVP, SHL and nanofibers at various ratios of SHL and PVP, and different amounts of loaded ML.	90
Figure 35 FTIR spectra of ML, PVP, SHL and nanofibers at various ratios of SHL and PVP, and different amounts of loaded ML.	92
Figure 36 Pareto charts of nanofiber diameter.	94
Figure 37 SEM images and diameter distributions of (A) SHL:PVP (25:75) + 5ML at 9 kV, (B) SHL:PVP (25:75) + 5ML at 27 kV, (C) SHL:PVP (25:75) + 35ML at 9 kV, (D) SHL:PVP (25:75) + 35ML at 27 kV, (E) SHL:PVP (50:50) + 20ML at 18 kV, (F) SHL:PVP (75:25) + 5ML at 9 kV, (G) SHL:PVP (75:25) + 5ML at 27 kV, (H) SHL:PVP (75:25) + 35ML at 9 kV and (I) SHL:PVP (75:25) + 35ML at 27 kV.	95
Figure 38 Interaction graph between the ratio of SHL in blended solution and ML amount.	96
Figure 39 Pareto charts of (A) tensile strength, (B) elongation, (C) contact angle, (D) polarity and (E) absorbency.	99
Figure 40 SEM images of SHL-PVP-ML nanofibers at the weight rate of (A) 75:25:5, (B) 50:50:5 and (C) 25:75:5.	101
Figure 41 The degree of absorption of nanofibers (at 27 kV) over a period of 15 min.	105
Figure 42 Kill kinetics of nanofibers (at 27 kV) for <i>S. aureus</i> over a period of 6 h.	107
Figure 43 Kill kinetics of nanofibers at (A) 9 kV and (B) 27 kV for <i>C. albicans</i> over a period of 6 h.	108
Figure 44 The morphology of cell after seeding on nanofibers at different time points.	109
Figure 45 Percentage of cell viability at (A) different concentrations and (B) 0.001 mg/mL.	111

CHAPTER 1

Introduction

Wound is an injury which damages the skin, a protective barrier against the external environment. When a wound is exposed to the air, the scab, a crust of dried pus, blood or serum, would be formed to cover the wound (1). However, delayed wound healing might be occurred because the scab formation could trap white blood cells, thus preventing their functions in wound healing, and the epidermal cells cannot move through the scab formed. The surface temperature of the wound exposed to the air would decline causing peripheral vasoconstriction affecting the supply of oxygen, nutrition and other factors to the wound (2,3). Moreover, the dry scab, which is the stratum corneum layer acting as the body's barrier to water vapor loss, is normally detached from the wound leading to significant transepidermal water loss (1).

Wound dressing is applied to a wound to promote natural wound healing and protect the wound. Although traditional wound dressings are effective barriers which could absorb exudate and prevent bacterial contamination, they keep wound dry causing the formation of scab contributing to delayed wound healing process (1). Therefore, prevention of the formation of scab with preserving moisture and aiding the different stages of healing should be considered.

Electrospun nanofibers wound dressings work on the concept of moist wound healing which retains fluid contacting with wound. The benefits of moist wound healing include inhibiting dry scab formation, decreasing the pH of environment affecting bacterial growth, shortening of the inflammatory phase of wound healing and providing an environment rich in enzymes, white blood cells and growth factors favourable for wound healing (3). Due to their ultrafine network structures, electrospun nanofibers can be used for the replacement of natural extracellular matrix (ECM) resulting in greatly rapid epithelialization, allowing the reduction of scar formation (4,5). The porous nature of nanofiber dressings also enhances oxygen and nutrients transferring to cells leading to an increased healing rate (6). In addition, they can improve drug loading capacity, and release rate because of their high surface to volume ratio properties (7).

Shellac (SHL) is a natural polymer secreted by the lac insect found on specific trees in China, India and Thailand. It is nontoxic and physiologically harmless (8). Based on its excellent film forming and protective properties, SHL is commonly used as an enteric coating material to protect from acid in gastrointestinal tract and as an additive in fruit coating to prevent water loss and microbial entry (9,10). Additionally, SHL could be easily electrospun in to nanofibers (11). Therefore, SHL demonstrates good promising properties as a carrier polymer for wound dressing application.

However, nanofibers containing only SHL indicate some disadvantages, including hydrophobicity, lacking cell affinity and poor mechanical properties. In order to solve the problems, the fabrication of electrospun nanofibers from blend solutions of SHL with another polymer that possesses more hydrophilicity, higher mechanical strength and better cell adhesion might be investigated. Polyvinylpyrrolidone (PVP), a water soluble synthetic polymer, has been frequently utilized for biomedical applications such as hydrogels for skin substitutes and wound healing due to its biocompatibility, biodegradable, low toxicity and good mechanical properties (12,13). However, the highly hygroscopic property of PVP might attribute to storage and quick-dissolving problems. Therefore, SHL blending with PVP might offer an excellent nanofiber mats for wound dressing with the improvement of the physiological properties.

Infection might cause a delay in wound healing. To prevent the multiplication of pathogen, an antimicrobial agent should be incorporated. Apparently, antibiotic resistance has become an increasing worldwide problem for infection treatment. In addition to treatment with synthetic drugs, safe and effective antimicrobials which are not easily subjected to resistance are greatly required. Among these simple antimicrobial compounds, natural lipids seem to be an achievable choice (14). Monolaurin (ML), a monoester form of lauric acid which is a medium chain fatty acid found naturally in human breast milk, coconut oil and palm kernel oil, exhibits broad-spectrum activity against Gram-positive bacteria from superficial skin infections and also has an antifungal effect by inhibiting spore germination and preventing the radial growth (15–17). It is non-toxic used as a food emulsifier and used for spoilage and microorganism control in food processing industries (18). However, there is little

study exploring the possibility of ML as an alternative antimicrobial agent in the pharmaceutical dosage forms, including wound dressing.

The morphology and physicochemical properties of electrospun nanofibers could be affected by various parameters which are broadly divided into formulation parameters, process parameters and ambient parameters (19). Experimental design techniques might be applied aiming to determine the main and interaction effects of possible parameters, and also reduce development time and the number of experimental trials. In this study, a full factorial design was conducted to optimize the effect of variable parameters. In addition, the optimum conditions which provide antimicrobial dressings with proper properties are obtained (20).

In order to develop a perfect wound dressing material, the combination of the property of individual material might be considered. Antimicrobial agents, especially from natural sources, should be additionally incorporated to prevent the post wound infection and reduce the risk of antibiotic resistance. In this work, a nanofiber mat of SHL-PVP containing ML is conducted through electrospinning. The optimum parameters in response to fabricating the antimicrobial nanofibers with desired properties were investigated by the full factorial design method.

The study is divided into 3 main parts according to the development of results.

Part I: Fabrication and morphology analysis of electrospun SHL nanofibers using factorial designs

SHL might be potentially used as a carrier polymer for wound dressing application. The objectives of this part is to investigate the main and interaction effects of some parameters such as SHL content, applied voltage and flow rate on the morphology of the SHL nanofibers, and to find the optimum process conditions by using a full factorial design with three replicated centre points.

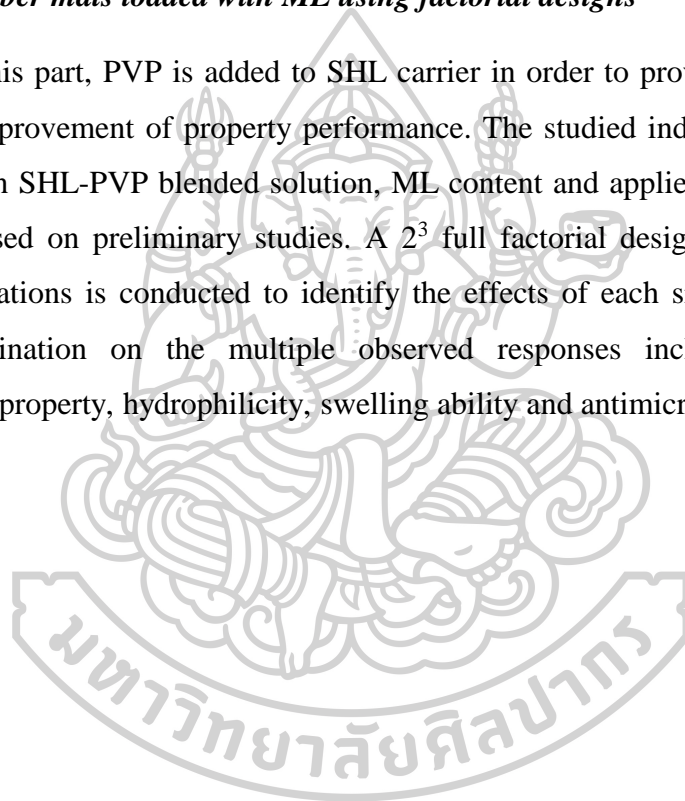
Part II: Fabrication and characterisation of ML loaded electrospun SHL nanofibers using factorial designs

The aims of this section are to investigate which factors (SHL and ML concentrations, applied voltage and flow rate) and interaction effects between these

factors would have the most impact on the morphology of SHL nanofibers loaded with ML. The fabrication conditions are optimized by using a full factorial design with three replicated centre points. Various instrumental analyses including powder x-ray diffraction, differential scanning calorimetry and FTIR spectroscopy are also employed in order to investigate the physicochemical characteristics of ML in SHL nanofibers.

Part III: Fabrication, analysis and characterisation of electrospun SHL / PVP nanofiber mats loaded with ML using factorial designs

In this part, PVP is added to SHL carrier in order to provide wound dressing with the improvement of property performance. The studied independent factors are SHL ratio in SHL-PVP blended solution, ML content and applied voltage, which are selected based on preliminary studies. A 2^3 full factorial design with three centre-point replications is conducted to identify the effects of each significant factor and their combination on the multiple observed responses including morphology, mechanical property, hydrophilicity, swelling ability and antimicrobial activities.

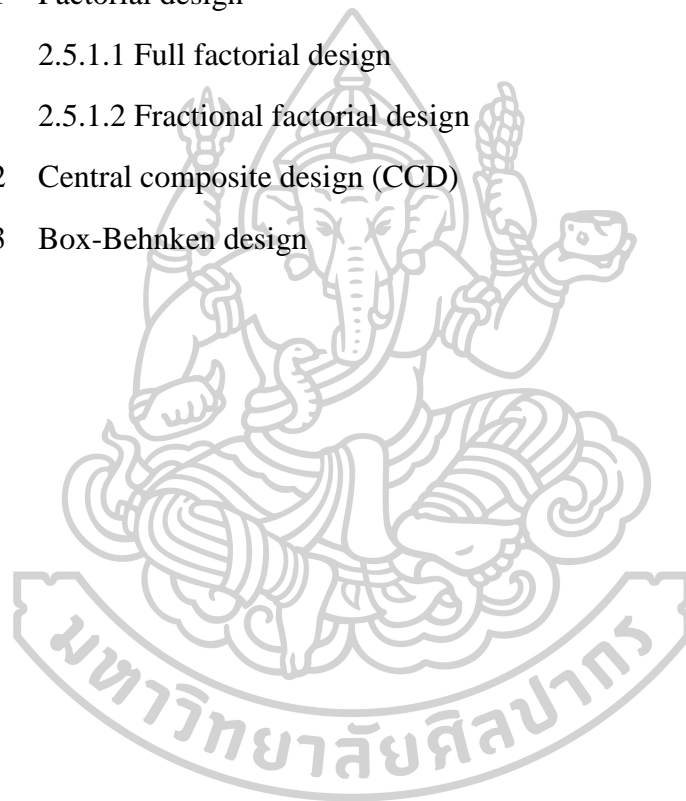


CHAPTER 2

Literature review

- 2.1 Types of wound dressings
 - 2.1.1 Passive dressings
 - 2.1.2 Interactive dressings
 - 2.1.2.1 Semi-permeable films
 - 2.1.2.2 Semi-permeable foams
 - 2.1.2.3 Hydrogels
 - 2.1.3 Bioactive materials or active wound dressing materials (AWD)
 - 2.1.3.1 Hydrocolloids
 - 2.1.3.2 Alginates
 - 2.1.3.3 Collagens
 - 2.1.3.4 Hydrofibers
 - 2.1.3.5 Nanofibers
- 2.2 Methods for nanofiber preparation
 - 2.2.1 Drawing
 - 2.2.2 Template synthesis
 - 2.2.3 Phase separation
 - 2.2.4 Self-assembly
 - 2.2.5 Electrospinning
- 2.3 Polymers used for the synthesis of electrospun nanofibers
 - 2.3.1 Synthetic polymers
 - 2.3.2 Natural polymers
 - 2.3.3 Polymer blends
 - 2.3.3.1 Types of polymer blends
 - 2.3.3.2 Applications of electrospun polymer blend nanofibers in wound healing and tissue engineering
 - 2.3.4 Shellac (SHL)
 - 2.3.5 Polyvinyl pyrrolidone (PVP)

- 2.4 The active compounds incorporated into electrospun nanofibers
 - 2.4.1 Lauric acid
 - 2.4.2 Monolaurin (ML)
 - 2.4.2.1 The mechanism of action
 - 2.4.2.2 The properties of ML and its applications
- 2.5 A design of experiments approach for fabrication process of electrospun nanofibers
 - 2.5.1 Factorial design
 - 2.5.1.1 Full factorial design
 - 2.5.1.2 Fractional factorial design
 - 2.5.2 Central composite design (CCD)
 - 2.5.3 Box-Behnken design



2.1 Types of wound dressings

Wound dressing is a suitable material designed to be in direct contact with the wound to promote effective healing and prevent further harm. In the last few years, various wound dressings have been designed in order to produce the ideal wound dressing materials which should be nontoxic, prevent dehydration and maintain a moist environment at the wound interface, physically protect the wound against dust and microorganisms, remove excess exudates, allow gaseous exchange, provide thermal insulation, be removed easily without trauma to the wound and promote wound healing (21). Recently, there is a variety of wound dressings available, which has been broadly classified from different aspects as follows (22);

2.1.1 Passive Dressings

For many years the conventional wound dressings, gauze and tulle (paraffin gauze), have been simply served as a protective cover on a wound leading to rehabilitation underneath. Gauze dressings are used for debridement of highly contaminated exudative wounds because of their fine and wide meshed weaved cotton composite. However, the passive dressings fulfill very few of the properties of an ideal dressing. They are not suitable for a wound as rapid healing is required. Gauze can also disrupt the wound bed causing trauma when removed, while tulle produces paraffin cover the wound leading to maceration as the water vapor and exudation can be trapped within wound (3,22,23).

2.1.2 Interactive dressings

Interactive dressings are comprised of polymeric films and foams which are mostly transparent, prevent bacterial entry to the wound, but allow gas and vapor permeation.

2.1.2.1 Semi-permeable films

These dressings are composed of polyurethane membrane coated with acrylic adhesive making them waterproof and flexible. They are transparent barriers which are permeable to oxygen and vapor but impermeable to liquid and bacteria. These films are objected to allow excess fluid to be lost by vapor transmission, but preventing dehydration of the wound. However, as films are non-absorbent, they are

not suitable for heavily exudative wounds. Film dressings are normally used for superficial and clean wounds, especially post-operative wounds because they could protect from shear and friction (3,24).

2.1.2.2 Semi-permeable foams

These dressings consist of a hydrophobic backing layer of semi-permeable film and a soft hydrophilic inner layer of polyurethane foam. They could absorb a large amount of exudates preventing the risk of maceration, while providing an environment for moist wound healing. In addition, they are easily applied and removed without influencing the healing tissue. They are also thermally insulating. Therefore, foam dressings meet many of the ideal dressing criteria (3,24).

2.1.2.3 Hydrogels

Hydrogels are a network of hydrophilic polymers containing high water content. These polymers are insoluble in water, but swell extensively in water. They are available in the form of sheets or gels designed to rehydrate necrotic tissue creating a moist wound healing environment to facilitate autolytic debridement, and able to absorb exudate into the polymer matrix. These dressings could be used for burn and painful wounds because of their cooling properties, and also used to deliver active compounds such as topical medications and growth factors because of their cross-linked structure. The moist interface between dressing and the wound surface prevents dressing adherence resulting in non-traumatic dressing removal (3,24).

2.1.3 Bioactive materials or active wound dressing materials (AWD)

Bioactive dressings, produced from a variety of biopolymers, are aimed to deliver active substances in wound healing either by delivery of bioactive compounds such as antimicrobials, vitamins, minerals and growth factors, or the dressings made from material having endogenous activity which might control the biochemical environment of a wound in order to assist its healing process. They could increase and manage cell migration leading up to highly desired healing events. Furthermore, frequency of dressing changes is minimized (22,23).

2.1.3.1 Hydrocolloids

These dressings consist of hydrocolloid base which is a combination of gelatin, pectin and gel-forming agents such as sodium carboxymethylcellulose secured onto a polyurethane film or foam backing acting as a barrier to external bacteria, but allowing the passage of water vapor and gases. When they are placed on wounds, they would combine with the exudate to form a moist gel at the wound interface. Hydrocolloids could encourage autolysis to aid in the removal of slough from a wound, and remain in place for up to 7 days reducing the frequency of dressing changes. They exhibit fibrinolytic, chemotactic and angiogenic effects leading to rapid wound healing. Hydrocolloid dressings also come in paste and powders used in a deeper ulcer or cavity (3,23,24).

2.1.3.2 Alginates

Alginate dressings contain calcium or sodium alginate obtained from seaweed. When applied to an exuding wound, calcium ions in the dressing would exchange with sodium ions in serum or wound fluid to form a hydrophilic gel creating a moist interface and making for easier dressing removal. They are useful for moderate to heavily exuding wounds. These dressings have the ability to activate macrophages within a wound bed and generate a pro-inflammatory signal resulting in the stimulating of granulation tissue formation. Moreover, the calcium content within the dressing also acts as a hemostat which is beneficial to bleeding wounds (1,3,24).

2.1.3.3 Collagens

These dressings are available in pads, gels or particles which could activate the deposition of newly formed collagen in wound bed, and absorb wound fluids providing a moist environment leading to rapid wound healing (22).

2.1.3.4 Hydrofibers

Hydrofibers are non-woven sheet or ribbon packing dressings made from sodium carboxymethyl cellulose fibres. They would form a firm gel in contact with exudate to maintain a moist wound healing environment. Moreover, maceration of surrounding skin is decreased because of the vertical wicking of exudate. These dressings are highly absorbent leading to easily peeling off (22,23).

2.1.3.5 Nanofibers

Nanofiber, an important class of nanostructured materials, is an ultrafine fiber with the diameter in the range of 1-100 nm. Currently, polymeric nanofibers have become increasing attention and also play significant roles in biomedical and healthcare due to their biocompatible and biodegradable properties (25).

2.2 Methods for nanofiber preparation

Recently, several techniques available for the production of polymeric nanofibers are drawing, template synthesis, phase separation, self-assembly and electrospinning.

2.2.1 Drawing

The fabrication of nanofibers could be performed by the process of drawing. As shown in Figure 1, a micropipette with a few micrometer diameter is dripped into the liquid near the contact line, and then withdrawn from the droplet rapidly at a speed of approximately $1 \times 10^{-4} \text{ ms}^{-1}$, resulting in a pulled nanofiber deposited at the end of the micropipette. However, the viscoelastic property of materials is required, and the process is also discontinuous. The drawing of nanofibers might be repeated several times (19).



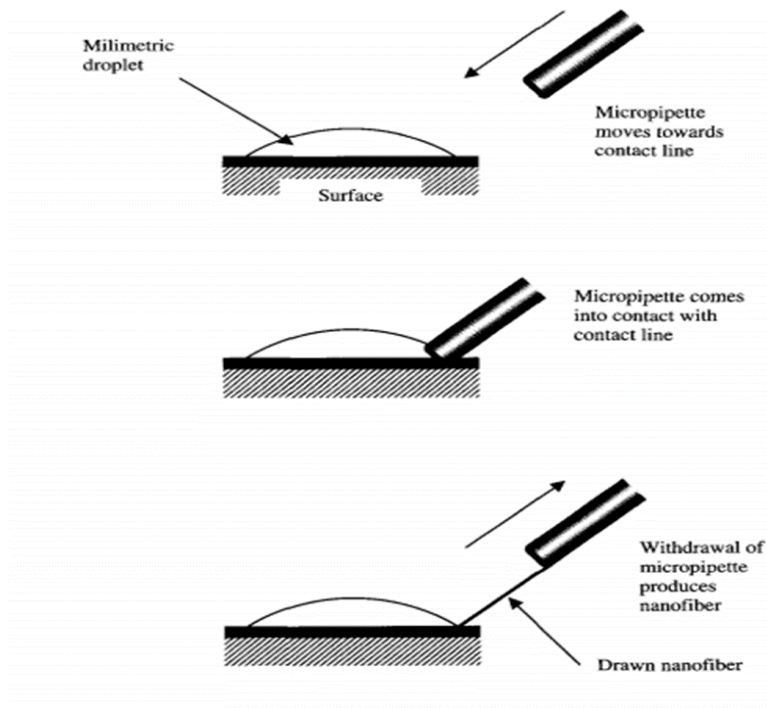


Figure 1 Schematic of nanofiber fabrication by drawing.

2.2.2 Template synthesis

Different nanoporous membranes are used as templates to produce nanofibers of a fibril or a tube shape with desired diameter. Various materials such as electronically conducting polymers, semiconductors, metals and carbons could be applied, but one-by-one continuous nanofibers cannot be obtained from this method (26). In Figure 2, metal oxide membrane with nano pores was used as a template. Under the application of water pressure on one side, the extrusion of polymer through porous membrane will contact with a solidifying solution resulting in nanofibers (19).

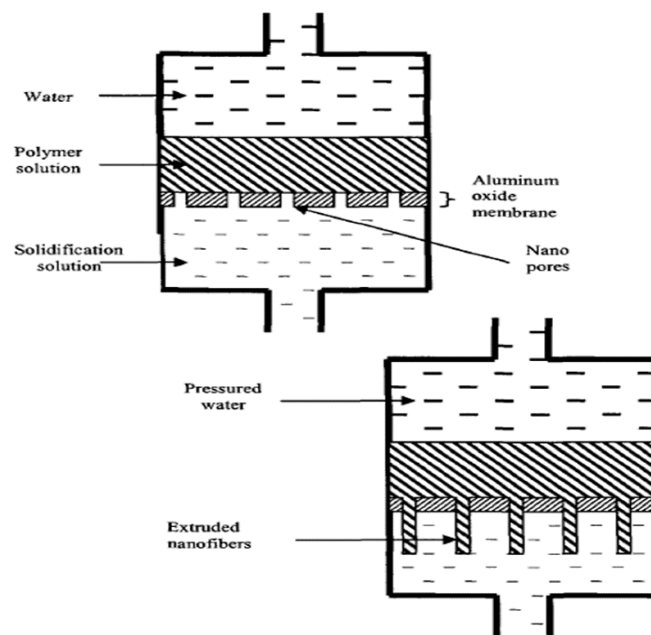


Figure 2 Schematic of nanofiber fabrication by template synthesis.

2.2.3 Phase separation

The main mechanism of this technique is the induced phase separation by introducing nonsolvent to the polymer solution or using thermal energy (cooling of solution). In the process, a polymer is added to a solvent for making a polymeric solution before undergoing gelation. After gelation, the solvent is removed from the gel by extraction with water. The gel is transferred to a freezer and then freeze-dried under vacuum leading to the formation of nanofibers with a size similar to the natural collagen of the extracellular matrix (ECM) which could enhance cell adhesion, migration and proliferation (see Figure 3). Nevertheless, it is a laboratory-scale process which is restricted to produce nanofiber scaffold (19,25).

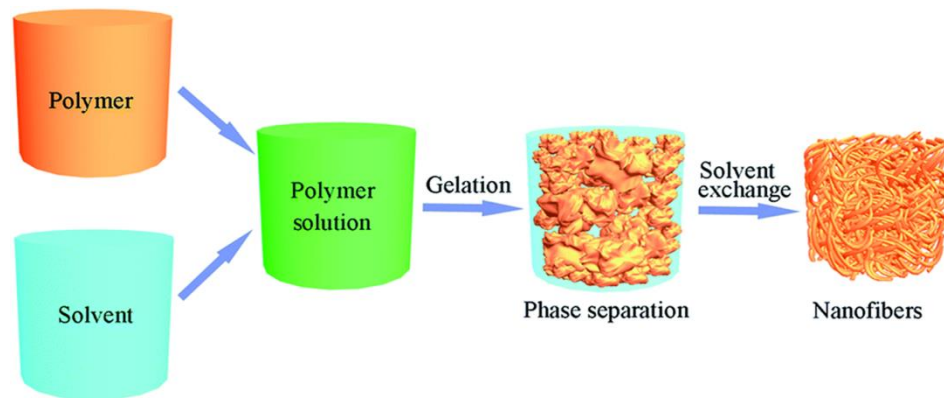


Figure 3 Schematic of nanofiber fabrication by phase separation.

2.2.4 Self-assembly

Nanofibers are built up by using small molecules as basic building blocks. The intermolecular forces lead to the arrangement of small molecules in a concentric manner, and the extension in the plane's normal would result in the longitudinal axis of a nanofiber. In order to mimic the human ECM, biomaterials are introduced. However, self-assembly is not potential for mass production likely to phase separation (19).

2.2.5 Electrospinning

Electrospinning is the most widely studied technique. It is highly flexible and seems to be the only method which can be further developed for industrial processing. During the process, the polymeric solution is held in a syringe. High direct current voltage is then supplied leading to an electric field between the collector and the filled syringe. When the surface charges overcome the surface tension of the polymer solution, the nanofibers are formed at the surface of the collector (see Figure 4) (19,25).

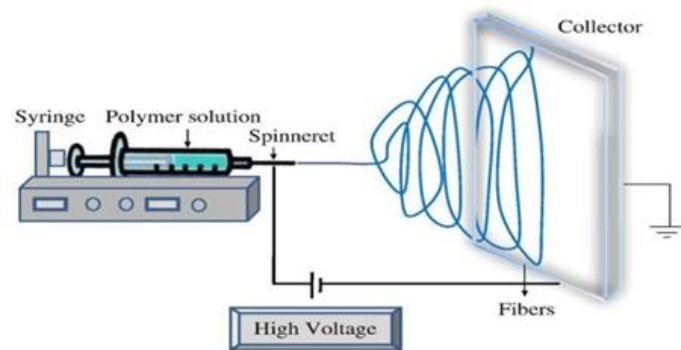


Figure 4 Schematic illustration of the basic setup for electrospinning.

Currently, electrospun nanofibers are increasingly introduced to wound healing management. With electrospinning, submicron fibers are developed from biodegradable polymers. Due to their microporous structure and high surface area, nanofibers would have the characteristics as follows (22);

Hemostasis: The ultrafine holes and high effective surface area properties of nanofibers could promote hemostasis phase, the clotting process, without using any hemostatic agents.

Absorbability: Because of the high surface area to volume ratio, the water absorption of nanofiber dressings is 17.9-213% which is more than that of typical film dressings (2.3%). Therefore, nanofibers especially made from hydrophilic polymers might be effectively used for highly exudative wounds.

Semi-permeability: Nanofibers act as semi-permeable barriers allowing gas permeation, but protecting the wound from bacterial infection and dehydration. The porous structure of nanofiber dressings reduces moisture transmission through the dressing from the wound surface in order to maintain moist wound conditions. The fine pore size can also prevent the permeation of bacteria to the wound.

Conformability: These dressings are flexible and resilient due to the fineness of fibers. They have been proposed for the ability to conform to irregular shape of the wound leading to excellent coverage and protection of the wound from infection.

Scar-free: Electrospun nanofibers could be used for tissue repair. According to the structure with similarity to the natural ECM in tissue and large surface area

available, nanofibers would encourage normal skin to develop immediately prior to scar formation resulting in wound healing with little scar. In addition, they have good cell conductivity, and can improve other factors to facilitate wound healing and skin regeneration. From previous studies, nanofibers would be beneficial for partial and full-thickness wounds by enhancing fibroblast cell proliferation, whereas hydrogels and foam dressings are used for partial thickness wounds (4,5,27).

Functional ability: Therapeutic compounds including antiseptics, antifungal, vasodilators (e.g. minoxidil), growth factors (e.g. FGF, EGF and TGF), and cells (e.g. keratinocytes) are easily integrated into nanofiber dressings to produce multifunctional bioactive nanofiber dressings. Unlike other commercial dressings, various functional materials could be electrospun into one blended layer instead of using multilayer configuration to achieve desired objectives, and the frequency in dressing changes, which may affect the regeneration of neotissue, might be reduced.

2.3 Polymers used for the synthesis of electrospun nanofibers

A wide range of natural and synthetic biomaterials has been used to electrospin nanofibers.

2.3.1 Synthetic polymers

Synthetic polymers are biocompatible, biodegradable and also not expensive. Due to the diversity of their physicochemical properties, synthetic polymers have been extensively used for nanofiber productions (25). Synthetic polymers such as polylactic acid (PLA), polyurethane (PU), polystyrene (PS), polycaprolactone (PCL), polyvinyl chloride (PVC), poly (methyl methacrylate) (PMMA), poly (lactic-co-glycolic acid) (PLGA), poly (ethylene-co-vinylacetate) (PEVA), poly (ethylene terephthalate) (PET), poly (ethylene oxide) (PEO), polyacrylonitrile (PAN) and cellulose acetate (CA) have been well studied (6,22,28–31). However, in order to develop nanofibers which could mimic a biological environment, natural polymers seem to be more attractive (25).

2.3.2 Natural polymers

Regarding to their structures, which are very similar to the macromolecular substances in the human body such as ECM, nanofibers prepared from natural

polymers might interact favourably with the biological environment leading to stimulating natural cell and tissue responses (25). Natural polymers including gelatin, chitosan, dextran, hyaluronic acid, silk fibroin and collagen have been commonly used for the fabrication of nanofibers (6,22,28–31). Nevertheless, the risk of batch variability, antigenicity, and disease transmission could occur especially from animal-originated polymeric nanofibers (25).

2.3.3 Polymer blends

The polymer blend technique have been widely applied in order to create new materials with the modification or improvement of the physicochemical properties, and also provide materials with the desired mechanical and biological properties at the lowest price. Additionally, blending might lead to improved processability and performance. A number of structurally different polymers or copolymers is blended and interacted with secondary forces without covalent bonding such as hydrogen bonding, charge-transfer complexes and dipole-dipole forces. The morphology, permeability, degradation and mechanical properties of polymer blends might different from homopolymers (32).

2.3.3.1 Types of polymer blends

Polymer blends could be broadly divided into three types which are miscible, immiscible and compatible polymer blends.

Miscible polymer blends (homogeneous polymer blends): it exhibits a single-phase structure associated with the negative value of the free energy of mixing ($\Delta G_m \approx \Delta H_m \leq 0$). The properties of mixtures might be the average values between the values of its contents depending upon the proportion of each polymer present (see Figure 5). In this case, only one glass transition temperature (T_g), which is between the T_g of both blend components, is observed (32).

Immiscible polymer blends (heterogeneous polymer blends): the mixtures display phase separation related to the positive free energy of mixing ($\Delta G_m \approx \Delta H_m > 0$). If two polymers are blended, two values of T_g might be found. However, the adhesion between both blend phases is low leading to poor structural integrity and

poor mechanical properties. These blends without being compatibilized seem to be useless (32).

Compatible polymer blends: immiscible polymer blends are modified by various techniques in order to reduce the interfacial tension, provide adhesive force between two phases and stabilize the desired morphology against thermal or shear effects during processing. The process of modification might be by incorporation of polymer or copolymer, by physical methods such as high stress field, thermal treatment and irradiation, or by reactive extrusion or injection molding. When the interface and morphology of an immiscible blend are modified, a polymer alloy is obtained. The properties of compatibilized blends are a synergistic combination of favourable properties from each polymer (see Figure 6) (32).

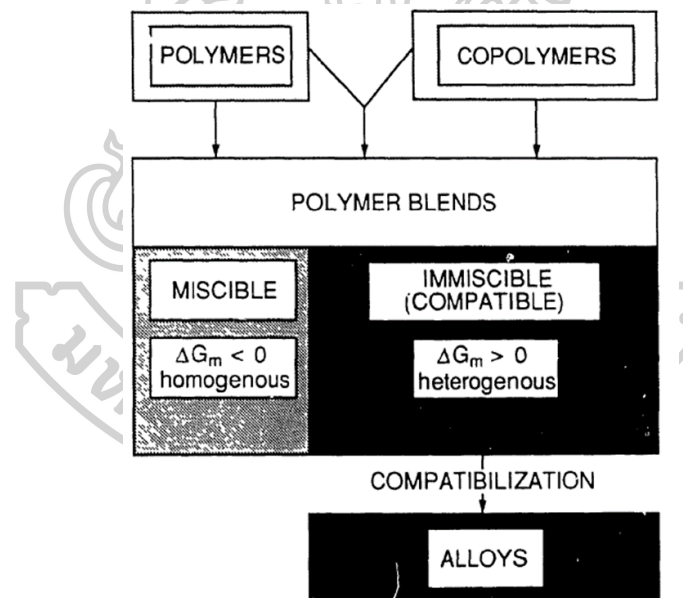


Figure 5 Progress in polymer processing.

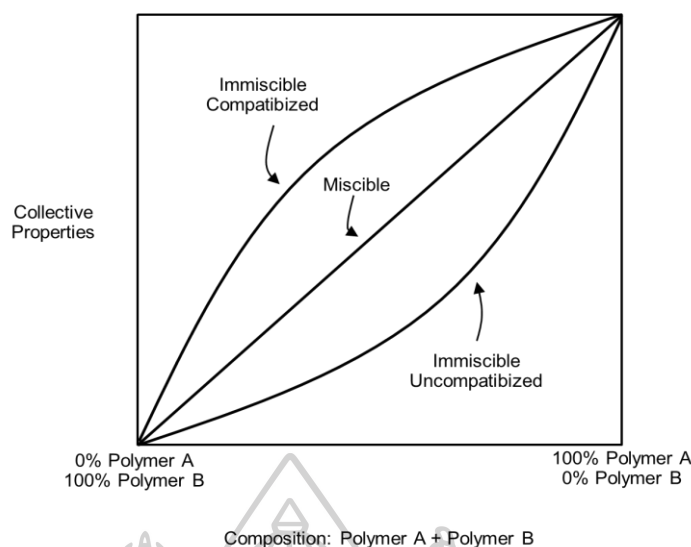


Figure 6 Potential effect on polymer blend properties as component concentration changes.

2.3.3.2 Applications of electrospun polymer blend nanofibers in wound healing and tissue engineering

Recently, polymer blends has been increasingly interesting and widely used in various fields including wound healing and tissue engineering applications aimed to produce high performance materials.

Regarding the study of Pawar et al. (33), the new bioactive thermoresponsive polymer blend nanofibers were fabricated for wound healing materials. Poly(ϵ -caprolactone) (PCL) offers hydrophobic, biodegradable and biocompatible properties. In order to enhance the hydrophilicity, rate of degradation and cell adherence characteristics thus leading to rapid tissue regeneration, blends of PCL nanofibers might be investigated. Poly(N-isopropylacrylamide) (PNIPAM), a thermoresponsive polymer, has a lower critical solution temperature (LCST) between 32 and 33 °C. Above LCST, PNIPAM is hydrophobic, whereas below LCST, PNIPAM is hydrophilic. The thermosensitivity property might be considered for cell attachment and also enabled easy removal of the dressing. Additionally, the structure of egg albumen (EA) resembles the fibrous collagen which is the major protein in the ECM. Therefore, the EA composite nanofibers could promote the regeneration of damaged tissues. In this study, gatifloxacin hydrochloride (Gati), which exhibited

good antibacterial activities at very low concentrations, was chosen as a model drug aiming to be engaged as wound dressing material.

The obtained polymer blend nanofibers of PNIPAM, PCL and EA incorporated with and without Gati were evaluated by FTIR, XRD and DSC.

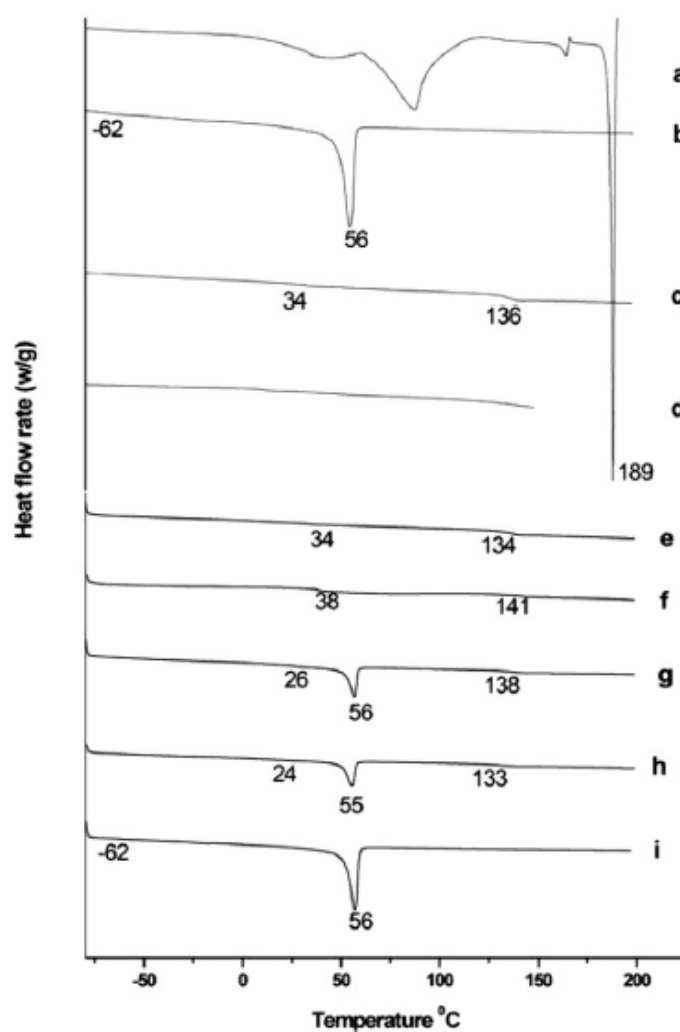


Figure 7 DSC thermograms of various compositions such as (a) Gati pure, (b) PCL pure, (c) PNIPAM pure, (d) EA pure, (e) PNIPAM(10%) nanofibers, (f) PNIPAM(6%) / EA(4%) nanofibers, (g) PNIPAM(5%) / EA(2%) / PCL(6%) nanofibers, (h) PNIPAM(3%) / EA(2%) / PCL(8%) / Gati(10%) nanofibers and (i) PCL(8%) nanofibers.

Based on DSC thermograms (Figure 7), assuming that the recorded LCST of PNIPAM/EA/PCL composite electrospun nanofibers was at 26 °C which was less than that of pure PNIPAM (34 °C). The reduction of LCST might be attributed to the interaction between PNIPAM and PCL and the reduced interaction between polymer chains of PNIPAM. Nevertheless, T_g of PNIPAM (138 °C) was more slightly increased than T_g of pure PNIPAM (136 °C) due to the rigid structure of nanofibers after crosslinking. The melting temperature of PCL, which is a semi-crystalline polymer, was not different from the pure PCL (56 °C), but the intensity of a peak seemed to be reduced because of disorganization of polymer chains during electrospinning. The nanofibers of PNIPAM/EA/PCL blend loaded with Gati showed a decrease in LCST (24 °C), T_m (55 °C, PCL), T_g (133 °C, PNIPAM) exhibiting good interaction between polymers and drug. Most of the Gati crystals were changed to amorphous form and dispersed in the nanofibers of polymer blend.

The polymer blend nanofibers of PNIPAM/PCL/EA incorporated with Gati were evaluated for their antimicrobial activities against *Staphylococcus aureus* (*S. aureus*) which is mostly found in wounds. The disc diffusion method was performed. The nanofibers without drug were used as a control. Regarding to the results (Figure 8), the significant inhibitory zones were observed for the electrospun nanofibers loaded with Gati after overnight incubation, while the nanofiber mats without Gati showed no antibacterial activity. In addition, as increasing the amount of drug loading in nanofibers, the zone of inhibition tended to be linearly increased.

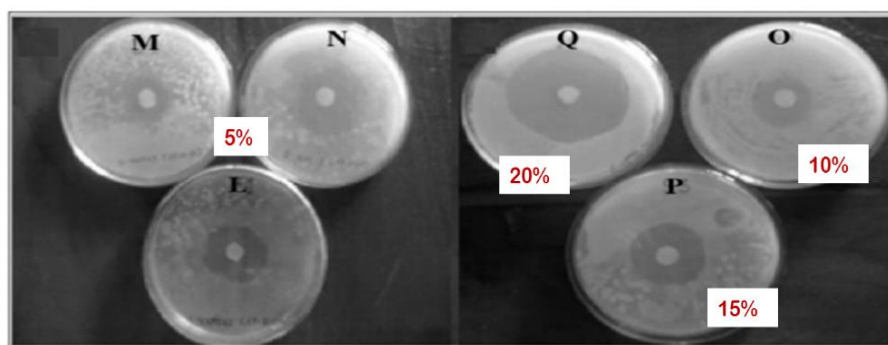


Figure 8 Antimicrobial activity (zone of inhibition) against *Staphylococcus aureus* of various formulations.

2.3.4 Shellac (SHL)

SHL is a natural polymer derived from the hardened secretion of the lac insect which grows on specific trees in China, India and Thailand. It is a nontoxic material listed as GRAS (Generally Recognized as Safe) by the FDA (8). It consists of polyesters and single esters, which contain hydroxyl and carboxyl groups. The ionization constant (pK_a) is 6.7. SHL is not soluble in water, but is dissolved in alcohol and alkaline solutions. Due to the ability to form an excellent protective film, it is widely used for coating applications in food and pharmaceutical industries to provide various functional properties (34,35). Only a few studies have been made on the application of SHL in wound healing management.

According to previous studies, the silk fibroin (SF) fabric coated with SHL wax was developed to be used as a non-adhesive wound dressing. It showed less adhesive than the commercial wound dressing “Sofra-tulle[®]” due to its hydrophobic property leading to loosely adherence to the hydrophilic wound surface, thus minimizing pain and risk of injury during removal (36).

Alzahrani et al. (2013) determined the effect of SHL solution compared with 10% povidone-iodine (PVP-I) solution applied to dry gangrene in order to prevent microbial infection and progression to wet gangrene. The result showed that the amputation rate in the conventional treatment group was 60% which was higher than 46.2% of the amputation rate in the SHL group. Thus, SHL could be used as a natural barrier to protect the underlying sterile gangrenous tissue in selected diabetic patients (9).

There were few studies on the application of SHL in wound healing management, especially through electrospinning process. However, according to its properties, SHL seems to be an alternative natural polymeric material which could be used as a carrier polymer for wound dressing application.

2.3.5 Polyvinyl pyrrolidone (PVP)

PVP is a water soluble polymer which has good compatibility, good transparency and non-toxic used as a blood plasma expander. Regarding the study of Hilmy, Darwis and Hardiningsih (1993), PVP hydrogel composites were prepared as

wound dressings. The obtained hydrogels were elastic, flexible, transparent and bacteria impermeable. Moreover, they could absorb high amount of water and be removed easily (37). Therefore, PVP could be added to SHL in order to fabricate wound dressing materials with the desired properties.

2.4 The active compounds incorporated into electrospun nanofibers

In addition to structural control of electrospun nanofibers, loading suitable active compounds must be considered in order to formulate an active wound dressing. Bioactive compounds can be growth factors which have a direct impact on the proliferation stage and stimulation of fibroblasts. Vasodilators such as minoxidil could be used to promote wound epithelialization and neovascularization. A vast range of antibiotics including ciprofloxacin, levofloxacin, tetracycline hydrochloride, streptomycin sulfate, itraconazole, benzalkonium chloride, fusidic acid and silver nanoparticles, is the most preferred to be incorporated to attain antibiotic properties (6,7,22).

Fatty acids and their corresponding esters might have little or no toxicity and also exert antimicrobial activity. Isaacs, Litov and Thormar (1995) found that fatty acids and monoglycerides with medium chain lengths varying from 8 to 14 carbons yielded more biologically active than long chain monoglycerides in killing viruses and bacteria (38).

2.4.1 Lauric acid

Among medium chain fatty acids (C8 to C14), lauric acid (C12) (See Figure 9) has more antimicrobial activity than other fatty acids such as myristic acid (C14), capric acid (C10) or caprylic acid (C8). It could be found in human breast milk, skin surface and other natural foods such as coconut oil and palm kernel oil. Lauric acid, which is rich in mother's milk as a component of triglycerides, would be hydrolysed to monoglycerides by the newborn playing a significant role in innate immune response protecting infants from microbial infections (16). It is also a minor component of skin lipids which take part in the self-sterilizing activity of the skin surface preventing invading pathogens (39).

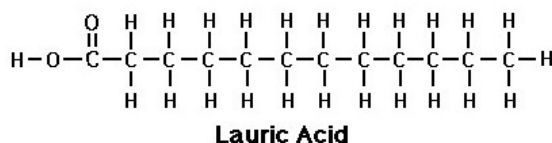


Figure 9 The structure of lauric acid.

Coconut trees are mostly grown in Southeast Asia involving Philippine, Indonesia, Malaysia and Thailand. Coconut oil is mainly derived from the dried kernel which contains about 65%-75% oil (40). It consists of 87% saturated fatty acids, 6% monounsaturated fatty acids and 2% polyunsaturated fatty acids. Of the saturated fatty acids, coconut oil is rich in medium chain fatty acids especially lauric acid (approximately 50%) (See Figure 10), which has the greatest antimicrobial activity of all medium chain aliphatic fatty acids. Trilaurin is the predominant triacylglycerol of the coconut oil (16,40). However, diglycerides and triglycerides do not exhibit antimicrobial property (16).

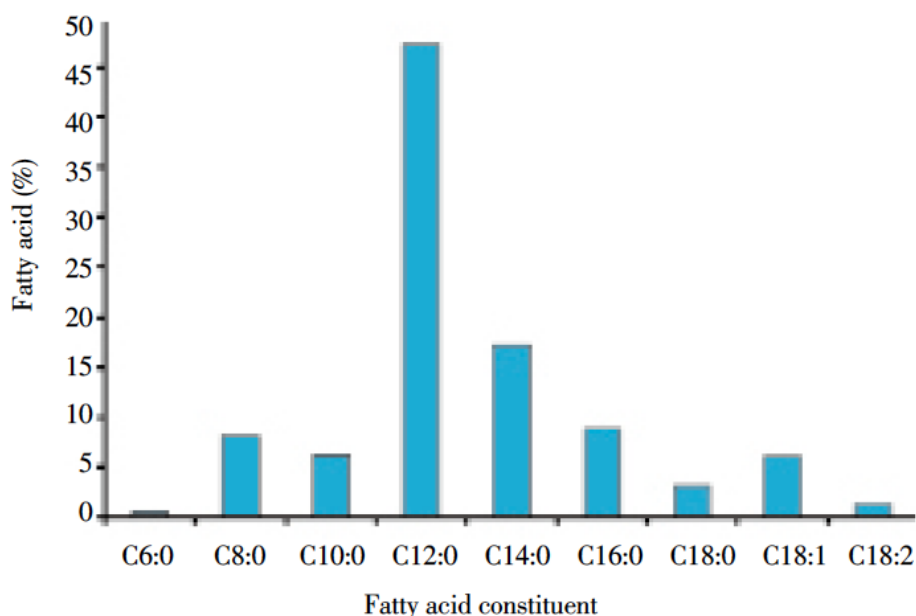


Figure 10 Fatty acid composition of virgin coconut oil (40).

As mentioned above, coconut oil is high in medium chain triglycerides. Trilaurin is the main component which is inactive against microorganisms. To potentiate this effect, triacylglycerol might be altered to monolaurin, the potential monoglyceride with medium chain. Recently, there are various methods used for synthesis of monoglycerides from triglycerides such as hydrolysis, esterification, glycerolysis and the ring-opening reaction. Glycerolysis is one of the processes which is carried out to convert triglycerides to monoglycerides at industrial level (See Figure 11). The reaction of triglycerides with glycerol is performed at high temperatures (250 °C) in order to increase the solubility of glycerol in the oil part. Inorganic alkaline such as NaOH, KOH, and Ca(OH)₂ is used as a catalyst to accelerate the process. After the reaction, the resultant product, which is a mixture of monoglycerides (30-40%), diglycerides, triglycerides, free fatty acids and its metallic soap, would be obtained (41).

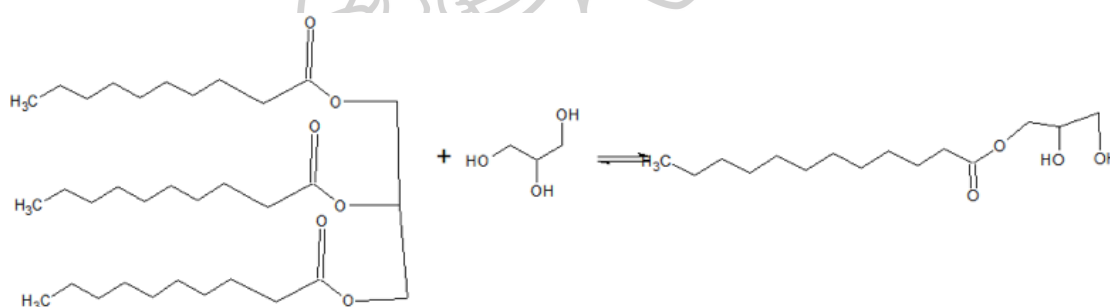


Figure 11 Glycerolysis of triglycerides to form monolaurin.

2.4.2 Monolaurin (ML)

ML, also known as glycerol monolaurate, is a monoester form of lauric acid. It has many times greater antibacterial and antiviral activity than lauric acid. Tangwatcharin and Khopaibool (2012) revealed that minimum bactericidal concentrations (MBC) of lauric acid and ML were 3.2 mg/mL and 0.1 mg/mL, respectively (42). The lower MBC values of ML indicate stronger antimicrobial activity than that of lauric acid. ML has Generally Recognized As Safe (GRAS) status considered to be nontoxic (16). ML is approved in the US as a food emulsifier and has

been used to control growth of pathogenic organisms and spoilage in food processing industries (18).

2.4.2.1 The mechanism of action

ML has wide-spectrum activity against bacteria, fungi and viruses. The antimicrobial effects are produced by several mechanisms. ML, a lipophilic compound, might be accumulated into the membrane bilayer, and consequently disintegrates the microbial membrane by fluidizing the lipids and phospholipids in the envelope of the organism, changing in the hydrogen bonding and the dipole-dipole interaction between acyl chains exerting bactericidal and virucidal effects (42).

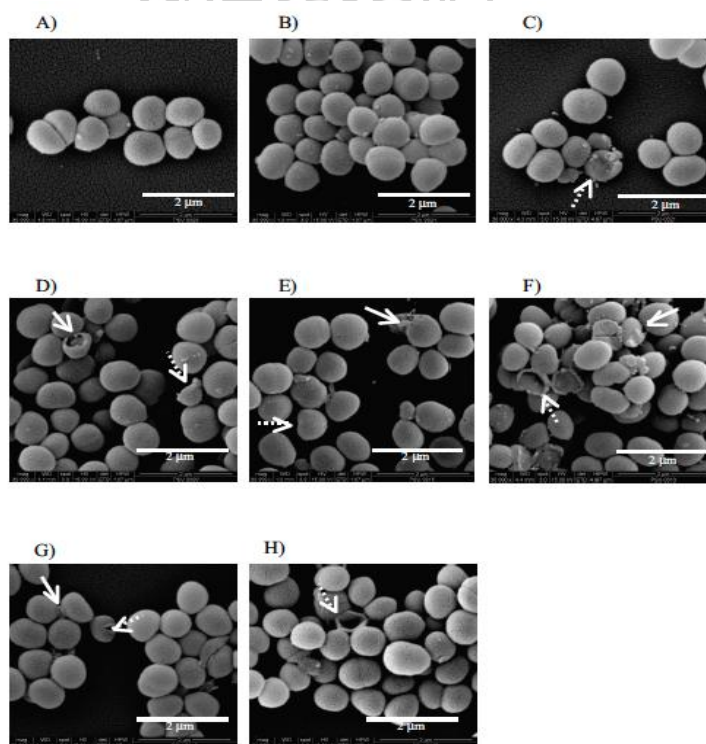


Figure 12 SEM of S. aureus CH1 in Mueller Hinton broth containing antimicrobials: (A) control, (B) 10% virgin coconut oil, (C) 0.4% lactic acid, (D) 10% virgin coconut oil + 0.4% lactic acid, (E) 3.2 mg/mL of lauric acid, (F) 0.2 mg/mL of lauric acid + 0.1% of lactic acid, (G) 0.1 mg/mL of monolaurin and (H) 0.05 mg/mL of monolaurin + 0.1% of lactic acid. Cell membranes were disturbed and leaked (solid arrow) and subsided (hatched arrow) (42).

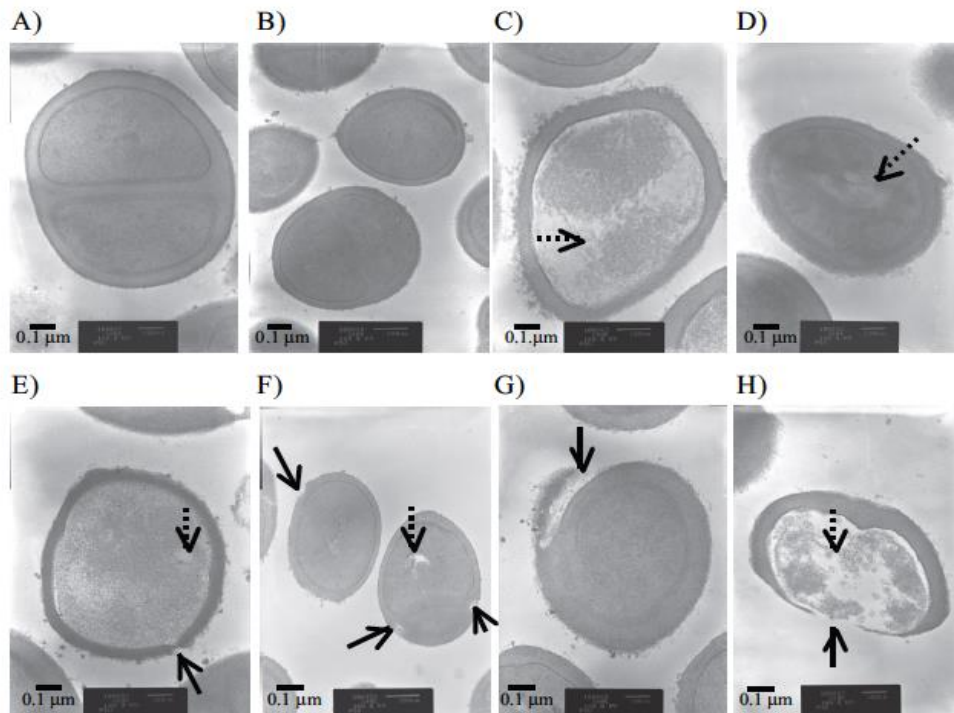


Figure 13 TEM of *S. aureus* CHI in Mueller Hinton broth containing antimicrobials: (A) control, (B) 10% virgin coconut oil, (C) 0.4% lactic acid, (D) 10% virgin coconut oil + 0.4% lactic acid, (E) 3.2 mg/mL of lauric acid, (F) 0.2 mg/mL of lauric acid + 0.1% of lactic acid, (G) 0.1 mg/mL of monolaurin and (H) 0.05 mg/mL of monolaurin + 0.1% of lactic acid. Cell membranes were disturbed and leaked (solid arrow) and subsided (hatched arrow) (42).

As shown in Figure 12 and 13, some membrane leakage of *S. aureus* cells treated with lauric acid and ML was observed, whereas bacterial cells treated with lactic acid displayed some loss and change of cytoplasm in cells. However, the membrane and cytoplasm of cells exposed to virgin coconut oil were not different from control (42).

Some research indicated that ML might interrupt the signal transduction in cell replication and also reduce the production of various exoenzymes and virulence factors such as protein A, toxic shock syndrome toxin 1, alpha-hemolysin and β -lactamase (16,42). Kabara (1993) reported that ML inhibited enzymes involved in oxygen uptake affecting respiratory activity. Furthermore, it exhibited an antifungal effect by inhibiting spore germination and preventing the

radial growth (16,43). Currently, the development of resistance of the pathogen to its antimicrobial effects seems to be very little (16).

2.4.2.2 The properties of ML and its applications

Bactericidal effects: ML is effective against Gram-positive and Gram-negative bacteria (15). Previous studies revealed that the topical use of ML at doses up to 100 mg/mL could inhibit the growth of *S. aureus*, a significant cause of skin and mucosal infections (44). In addition to *S. aureus*, *Mycobacterium terrae* (*M. terrae*), *Listeria monocytogenes* (*L. monocytogenes*), *Streptococcus agalactiae* (*S. agalactiae*), and Groups A, F, and G streptococci might be killed by ML (16).

Staphylococcal food poisoning is a common cause of foodborne illness. Meat and meat products are the most frequent vehicles of intoxication. In recent years, lactic acid is widely used to control the growth of pathogens on the surface of meat and meat products by spraying or dipping food with lactic acid solutions. The mode of action of lactic acid seems to be pH dependent. At low pH, most of the organic acid would be in the undissociated form that could penetrate the lipid membrane of cell, and dissociate in the interior. The excess protons might be exported in order to maintain a neutral pH of the cytoplasm, which consumes cellular ATP resulting in depletion of energy. However, lactic acid is difficult to be stabilized on the surface of meat because of evaporation, neutralization and diffusion into the matrix. Therefore, other lipids such as ML and lauric acid might be considered (42,45).

Table 1 The MIC and MBC values against S. aureus (the units of antimicrobial agents are mg/mL for lauric acid and monolaurin and % (v/v) for virgin coconut oil and lactic acid) (42).

Antimicrobials	<i>S. aureus</i> ATCC 25923		<i>S. aureus</i> CH1	
	MIC	MBC	MIC	MBC
Virgin coconut oil	NI	NI	NI	NI
Lauric acid	1.6	3.2	1.6	3.2
Monolaurin	0.1	0.1	0.1	0.1
Lactic acid	0.1	0.4	0.1	0.4

Table 1 showed the minimal inhibitory concentration (MIC) and minimal bactericidal concentration (MBC) values of lipid and lactic acid against *S. aureus*. While MIC was recorded as the lowest concentration which could limit the turbidity of the broth to be not more than 0.05 at absorbance of 600 nm, MBC was recorded as the lowest concentration which could kill at least 99.9% of the initial amount of bacteria. The results revealed that lauric acid, ML and lactic acid expressed beneficial effect against *S. aureus*. When comparing with lauric acid, ML which is the monoacrylglycerol was more active than lauric acid which is the free fatty acid form. Nevertheless, virgin coconut oil did not exhibit inhibitory activity because it contained low amount of ML (42).

Besides Gram-positive bacteria, some Gram-negative organisms such as *Haemophilus influenzae* (*H. influenzae*) and *Helicobacter pylori* (*H. pylori*) could be also eliminated by ML (16,46).

Due to inflammatory mechanism, *H. pylori* could cause chronic gastritis and duodenal ulceration, and might be a risk factor in gastric cancer. The problem of resistant strains of *H. pylori* seems to be significant that can cause relapse after complete remission. Therefore, new methods are required to prevent or to treat gastrointestinal ulcers caused by *H. pylori*. Regarding to the study of Bergsson et al. (2002), 12 of fatty acids and monoglycerides were evaluated for the antibacterial effect against *H. pylori*, and the bactericidal activity could be indicated as the number of viable cells per millilitre. As shown in Table 2, all of the lipids except oleic acid, monoolein and monocaprylin had activity against *H. pylori* at the concentration of 10 mM after 10 min incubation at 37 °C. When tested at the lowest concentration, ML was the most active among these lipids (46).

Table 2 Inactivation of *H. pylori* by lipids (46).

Lipids	Number of viable bacteria (log 10/ml) ^a after treatment with the following concentrations of lipids (mM) ^b						
	10.00	5.00	2.50	1.25	0.63	0.31	0.15
Caprylic acid (8:0) ^c	2.40 ± 0.69 ^d	6.40 ± 2.77	ND ^e	ND	ND	ND	ND
Capric acid (10:0)	≤ 2.00 ^f ± NA ^g	≤ 2.00 ± NA	2.33 ± 0.35 ^d	7.43 ± 0.87	ND	ND	ND
Lauric acid (12:0)	≤ 2.00 ± NA	≤ 2.00 ± NA	≤ 2.00 ± NA	≤ 2.00 ± 0NA	4.00 ± 3.46	7.83 ± 0.47	ND
Myristic acid (14:0)	≤ 2.00 ± NA	≤ 2.00 ± NA	3.20 ± 1.11	8.27 ± 0.40	ND	ND	ND
Palmitoleic acid (16:1)	≤ 2.00 ± NA	≤ 2.00 ± NA	≤ 2.00 ± NA	≤ 2.00 ± NA	2.07 ± 0.12 ^d	5.53 ± 3.07	ND
Oleic acid (18:1)	6.17 ± 2.02	ND	ND	ND	ND	ND	ND
Monocaprylin (8:0)	8.00 ± 0.26	ND	ND	ND	ND	ND	ND
Monocaprin (10:0)	≤ 2.00 ± NA	≤ 2.00 ± NA	≤ 2.00 ± NA	≤ 2.00 ± NA	≤ 2.00 ± NA	4.60 ± 2.82	8.23 ± 0.32
Monolaurin (12:0)	≤ 2.00 ± NA	≤ 2.00 ± NA	≤ 2.00 ± NA	≤ 2.00 ± NA	2.17 ± 0.29 ^d	2.73 ± 1.27 ^h	2.23 ± 0.40 ^d
Monomyristin (14:0)	3.97 ± 0.46 ^d	ND	ND	ND	ND	ND	ND
Monopalmitolein (16:1)	2.68 ± 1.15 ^d	2.63 ± 1.10 ^d	ND	ND	ND	ND	ND
Monoollein (18:1)	6.30 ± 1.61	ND	ND	ND	ND	ND	ND
Control	8.20 ± 0.26						

^a Mean (± S.D.) of three *H. pylori* strains which are defined in the text.

^b Final concentration of fatty acids.

^c Number of carbon atoms: number of double bonds.

^d Significantly different from control ($P < 0.01$).

^e ND, not done.

^f ≤, Indicates that no colonies were detectable in 100 µl of the 10⁻¹ dilution, which was the lowest dilution tested.

^g NA, not available.

^h Significantly different from control ($P < 0.05$).

Nevertheless, many studies reported that *Escherichia coli* (*E. coli*) and *Salmonella* spp. were found to be less affected by ML (45). The difference in the killing effects of lipids against Gram-negative bacteria might depend on differences in the outer membrane. Based on the structures of *E. coli* and *Salmonella* spp., the external membrane consists of proteins and lipopolysaccholine (LPS) which is composed of the O polysaccharide chains demonstrating hydrophilic surface property (See Figure 14). Therefore, lipids, which are hydrophobic molecules, could difficultly enter the bilayer, and hardly diffuse in the cytoplasm (46,47).

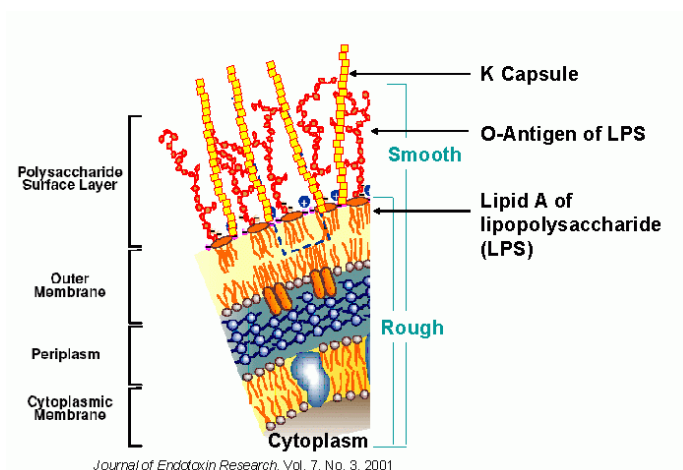


Figure 14 The outer surface of *E. coli*.

In the experiments of Skrivanova et al. (2006), ML and citric acid could inhibit the growth of *Clostridium perfringens* (*Cl. perfringens*), which is a Gram-positive bacteria, with MIC of 3 and 4 mg/mL, respectively, whereas other acids (succinic, fumaric, malic and lactic acid) did not show any inhibitory effects at 5 mg/mL. However, the inhibitory activities of ML and these organic acids against other Gram-negative bacteria such as *E. coli* and *Salmonella* spp. were not observed (See Table 3) (45). To magnify the effect against Gram-negative bacteria, some chelating agents such as EDTA might be added in order to disrupt the outer membrane (48).

Table 3 MIC (mg/mL) of monolaurin, citric, succinic, fumaric, malic and lactic acid against *E. coli*, *Salmonella* spp. and *Cl. Perfringens* grown on glucose (incubation in triplicate for 1 day) (45).

Compounds tested	<i>E. coli</i> (2 strains)	<i>Salmonella</i> sp. (3 species)	<i>Cl. Perfringens</i> (2 strains)
Monolaurin	r	r	3
Citric acid	r	r	4
Succinic, fumaric, malic, lactic acid	r	r	r

r = resistant (MIC > 5 mg/mL)

The experiment of Altieri et al. (2009) was in contrast to the above statement. The effectiveness of ML was determined as Inhibition Index (I.I.), where

Abs_c is the absorbance of the control and Abs_a is the absorbance of the active sample at the time t .

$$I.I. = (Abs_c - Abs_a) \times 100 / Abs_c$$

The inhibition index (%) of ML against *E. coli* and *Salmonella* spp. in PC broth was shown in Figure 15 and 16, respectively. As can be seen in Figure 15, the bioactivity of ML could be strongly expressed within 10 h and decreased for a prolonged incubation time. The reduction of its bioactivity may be due to possible mechanism of adaptation of bacteria or reversible mode of action. The effectiveness of ML tended to be dose-dependent. The I.I. increased from 27% to 90.77%, when increasing the concentration of ML from 20 ppm to 50 ppm. The 50 ppm of ML exhibited a nearly complete inhibition with I.I. of approximately 90-95% for the entire running time (49).

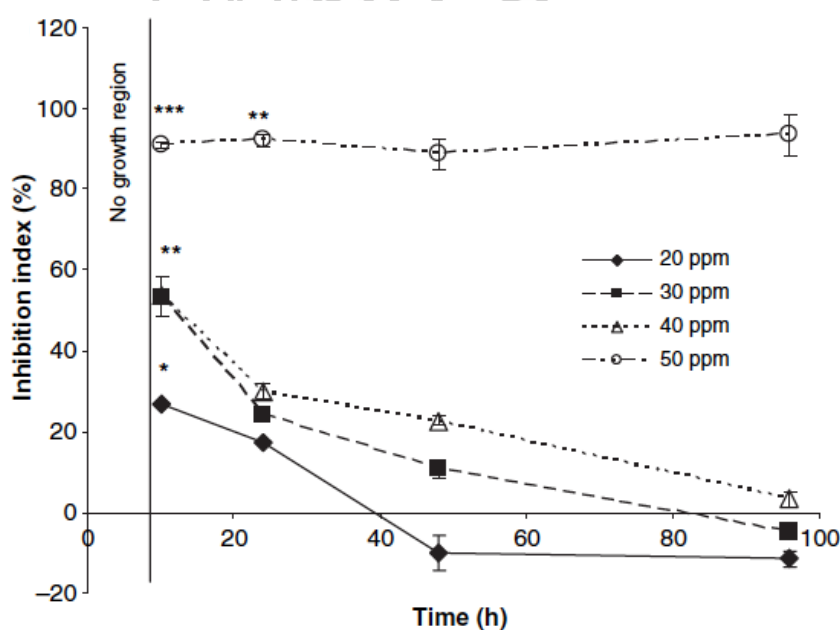


Figure 15 Inhibition index expressed by ML against *E. coli*. O157:H7 in PC broth. Data represent the average ($n=2$) \pm SD (49).

Figure 16 demonstrated the I.I. of ML against *Salmonella* spp. The lowest amount of ML, which was 20 ppm, could perform a slight activation effect after 24 h of incubation. Nevertheless, the higher concentrations (30-50 ppm) might

inhibit *Salmonella* spp. with I.I. of approximately 30-40%. According to the results, it can be concluded that ML displayed a strong inhibition against *E. coli* O157:H7, but exhibited a moderate activity against *Salmonella* spp (49).

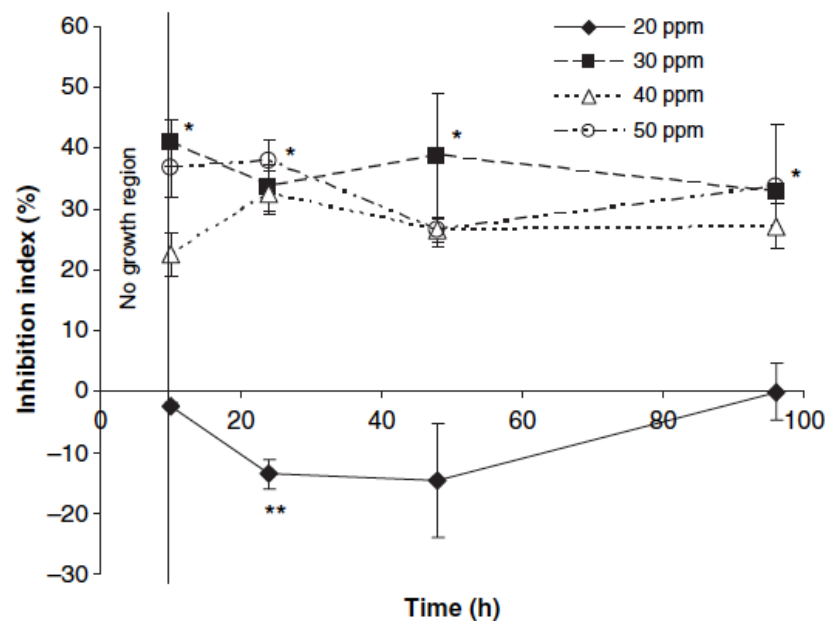


Figure 16 Inhibition index expressed by ML against *Salmonella* spp. in PC broth. Data represent the average ($n=2$) \pm SD (49).

Virucidal effects: As mentioned above, ML could be incorporated into the viral envelope causing leakage of the bilayer membrane leading to cell lysis and death. Thormar et al. (1986) evaluated the effect of fatty acids and their monoglycerides against both enveloped viruses, including vesicular stomatitis virus (VSV), herpes simplex virus and visna virus (VV), and a nonenveloped virus, poliovirus (50).

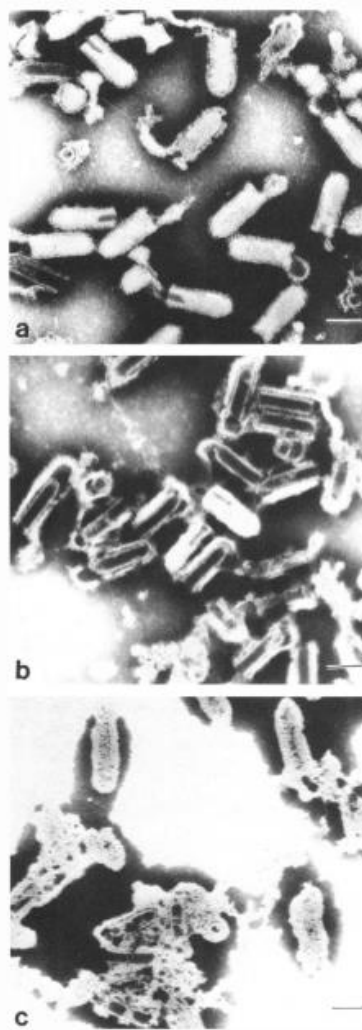


Figure 17 The effect of linoleic acid against VSV: (a) control (b) linoleic acid 0.5 mg/mL (c) linoleic acid 1 mg/mL (50).

The effects of linoleic acid against VSV were shown in Figure 17. VSV was incubated at 37 °C for 30 min in the maintenance medium (MM) with or without linoleic acid. As seen in Figure 17a, MM without linoleic acid showed normal intact particles covered with spikes. The leakage of viral envelopes could be observed after incubation with 0.5 mg of linoleic acid (see Figure 17b). When adding the higher amount of linoleic acid (1 mg), the disintegration of virus particles was illustrated (see Figure 17c). These results seemed to follow the above statement.

The comparison of the antiviral effect of fatty acids and their monoglycerides was displayed in Table 4 and Table 5, respectively. According to Table 4, butyric, caproic, caprylic, palmitic and stearic acids exhibited no or little

antiviral activity, while medium-chain saturated and long-chain unsaturated fatty acids could decrease the amount of VSV, HSV and VV considerably. Poliovirus, a nonenveloped virus, was also incubated with various fatty acids with the concentration of 8 mg/mL at 37 °C for 30 min. In contrast, a significant reduction of virus was not obtained (50).

Table 4 Viral inactivation by incubation with fatty acids at 37 °C for 30 min (50).

Fatty acid	Concn ^a in mg/mL (mM)	Reduction of virus titer (log ₁₀)		
		VSV	HSV-1	VV ^b
Butyric (4:0) ^c	10 (113)	0	ND ^d	ND
Caproic (6:0)	10 (86)	0	ND	ND
Caprylic (8:0)	10 (69)	1.8	ND	≥3.2
Capric (10:0)	4 (22)	≥4.0 ^e	≥4.0	≥3.2
Lauric (12:0)	2 (10)	≥4.0	≥4.0	≥3.2
Myristic (14:0)	4 (16)	≥4.0	≥4.0	1.7
Palmitic (16:0)	20 (78)	1.0	1.0	0.7
Palmitoleic (16:1)	2 (15)	≥4.0	≥4.0	≥3.2
Stearic (18:0)	20 (70)	0	ND	ND
Oleic (18:1 <i>cis</i>)	2 (7)	≥4.0	≥4.0	≥3.2
Elaidic (18:1 <i>trans</i>)	2 (7)	≥4.0	ND	ND
Linoleic (18:2)	1 (3.5)	≥4.0	≥4.0	≥3.2
Linolenic (18:3)	1 (3.6)	≥4.0	≥4.0	≥3.2
Arachidonic (20:4)	0.5 (1.6)	≥4.0	ND	ND

^a Concentration of fatty acid in virus mixtures incubated at 37 °C for 30 min.

All fatty acids were tested in a series of twofold concentrations. Shown is either the lowest concentration which reduced the VSV titer by ≥4.0 log₁₀ units or the highest concentration tested (butyric, caproic, caprylic, palmitic and stearic).

^b VV, Visna virus.

^c Carbon atoms: double bonds.

^d ND, Not done.

Table 5 Viral inactivation by incubation with monoglycerides at 37 °C for 30 min (50).

Monoglyceride	Concn ^a in mg/mL (mM)	Reduction of virus titer (log ₁₀)	
		VSV	HSV-1
Monocaprylin (8:0) ^b	2.0 (9)	≥4.0	ND ^c
Monocaprin (10:0)	0.5 (2)	≥4.0	≥3.7
Monolaurin (12:0)	0.25 (0.9)	≥4.0	≥3.7
Monomyristin (14:0)	2.0 (13)	3.0	ND
Monoolein (18:1)	1.0 (2.8 ^d)	2.3	ND
Monolinolein (18:2)	0.25 (0.7)	≥4.0	ND

^a Lowest concentration causing ≥3.0 log₁₀ reduction in virus titer.

^b Carbon atoms: double bonds.

^c ND, Not done.

The antiviral effect of monoglycerides was shown in Table 5. All of the monoglycerides tested except monoolein and monomyristin were found to be 5 to 10 times more active than the corresponding fatty acids. Monolaurin and monocaprin had the most effect against both VSV and HSV compared to other monoglycerides (50).

The clinical trial using ML as monotherapy on 15 HIV-infected patients was performed. These 15 patients, who never having received anti-HIV treatment, were randomly assigned to 3 treatment groups which were 7.2 g (low dose) and 22 g (high dose) of ML and 45 mL of coconut oil daily for 6 months. Viral load, CD4 and CD8 counts, complete blood count, ALT, AST, urea N, creatinine, cholesterol, triglycerides, HDL, and body weight were examined at the beginning of the study and after 3 and 6 months of treatment. The results showed that 7 of all the patients (~ 50%) exhibited decreased viral load on the 3rd month, and 8 patients (2 given high dose of ML, 4 given low dose of ML and 3 given coconut oil) had reduced viral count on the 6th month. Moreover, no serious side effects were observed. This trial confirmed that the antiviral action could be seen from both ML and coconut oil (50).

Antifungal effects: A number of fungi, yeast, and protozoa are also inactivated or killed by ML. The fungi include several species of ringworm. The yeast

reported to be affected is *Candida albicans*. The protozoan parasite *Giardia lamblia* is killed by monoglycerides from hydrolyzed human milk (16,51).

Candida albicans (*C. albicans*) and *Gardnerella vaginalis* (*G. vaginalis*) are normally related to vaginal infections in women. Bacterial vaginosis is a chronic infection caused by vaginal flora changes. During infection, the number of *lactobacilli*, which could maintain acidic pH, is decreased leading to the elevation of vaginal pH allowing other bacterial groups such as *G. vaginalis* to grow. Vulvovaginal candidiasis is also a common infection dominated by *C. albicans*. Lately, the recurrence rates of vaginal infection become increased indicating the limitation of antimicrobial therapy. Thus, the better therapeutics might be considered.

According to the study of Strandberg et al. (2010), ML was determined its antimicrobial effects on *Lactobacillus*, *Candida* and *G. vaginalis*. The *in vitro* activities of ML on the growth of *C. albicans* and *G. vaginalis* were demonstrated in Figure 18. As shown in the figure below, when increasing the concentration of ML, the reduction in *C. albicans* and *G. vaginalis* counts was observed. The concentration of ML used as candidicidal was 500 µg/mL, while the amount used as bactericidal for *G. vaginalis* was 10 µg/mL. *G. vaginalis* is a Gram-negative bacteria consisting of a lipooligosaccharide (LOS) in the outer membrane. LOS lacks of O side chains leading to be sensitive to the inhibition effect by ML. Strandberg et al. (2010) also revealed that *lactobacilli*, normal vaginal flora, was not affected by ML (51).

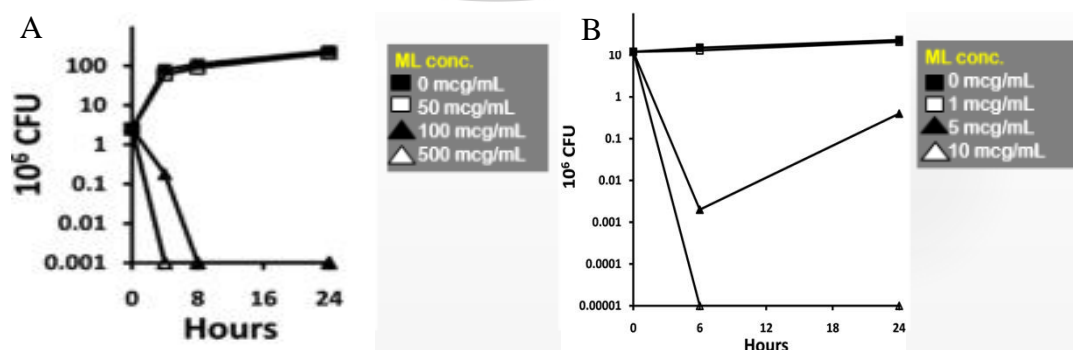


Figure 18 *in vitro* effect of ML on the growth of *C. albicans* (A) and *G. vaginalis* (B) which were cultured for 24 h in the presence of various concentrations of ML at 37 °C (51).

2.5 A design of experiments approach for fabrication process of electrospun nanofibers

The electrospinning process could be influenced by various parameters including solution parameters (viscosity, surface tension and conductivity), processing parameters (applied voltage, feed rate and distance between tip and collector) and ambient parameters (humidity and temperature) (19). The number of parameters affecting the morphology of nanofibers is relatively high; thus, evaluating all of them in the single framework is impossible. The effect of parameters on a process could be studied by the conventional method which is called one factor at a time (OFAT). In this procedure, one parameter is varied, whereas the other parameters are held constant. However, the interaction effects between parameters are not carried out. Therefore, the optimum conditions could not be obtained. These disadvantages might be discarded by introducing the use of the experimental design for studying the impact of parameters (20).

Experimental design is the design of tests with the aims to determine which factors have the most effect on the response and determine which the range of the setting for factors can result in the target response with less variability. The application of experimental design might lead to an increase in process yields, a closer conformance to the target response and a decrease in variability, time consuming and total costs (20).

The first step of the design of experiments is to characterise a process. In this step, the screening experiments might be performed in order to examine which parameters have the influential impact on the response, and can also estimate the magnitude of the parameter effects and the direction of the relationship between the test parameters and the response. The obtained data from this step would be used to identify the most important parameters and investigate the modification direction of these parameters. The next step is optimization. The objective of this step is to find the optimum process conditions which yield the best desirable response (20).

2.5.1 Factorial design

2.5.1.1 Full factorial design

All combinations of the levels of the parameters are evaluated. Therefore, it is necessary when the interactions are considered resulting in accurate interpretation. However, an independent estimate of error might not be provided unless several observations at some runs would be performed. The design with the replicate measurements at the centre point is commonly used to obtain an experimental error estimation and to examine the curvature of the middle area of the design space. The required number of experiments could be calculated by the following equation

$$\text{The number of experimental runs} = l^k$$

where l is the number of levels of each factor, k is the number of factors (20,52).

According to the study of Yanilmaz et al. (2013), the effect of process parameters on the morphology of polyurethane nanofibers were investigated by using factorial design. In this study, two process parameters, which were the applied voltage and the distance from the tip to the collector, were considered. The observed response was the nanofiber diameter. A 3^2 full factorial design with two replicates was conducted, thus providing a total of 18 experimental runs as shown in Table 6.

Table 6 Effect of applied voltage and tip to collector distance on nanofiber diameter based on a 3² factorial experimental design with two replicates.

Exp.	Applied voltage	Distance	Diameter	St. Dev.
1	3	3	585.8	162,360
2	1	1	825.9	95,960
3	1	1	831.0	95,572
4	3	1	647.6	128,000
5	1	3	608.4	120,674
6	1	2	1023.3	151,542
7	2	3	541.2	116,866
8	3	2	780.4	128,146
9	3	2	823.9	113,966
10	1	2	1063.0	109,925
11	3	1	614.8	187,709
12	3	3	604.4	226,460
13	2	2	845.6	172,393
14	2	2	896.0	169,091
15	2	1	917.2	109,247
16	2	3	538.4	119,280
17	2	1	874.6	116,759
18	1	3	590.9	170,405

Regarding the ANOVA results (Table 7), the degree of freedom of each parameter and the sum of squares are represented by DF and Seq SS, respectively. The results presented that the *P* values of the applied voltage, the distance from the tip to the collector and their interaction were less than 0.05, indicating that they might have an influential impact on the fibre diameter. In addition, the distance with Seq SS of 328.684 seemed to have greater effect on fibre diameter than the applied voltage which had Seq SS of 66.784. The fitting of data was excellent with the R^2 of 98.99% (53).

Table 7 ANOVA analysis of parameters including applied voltage, distance and their interaction on the fibre diameter.

Source	DF	Seq SS	Adj SS	Adj MS	F	<i>P</i>
Applied voltage	2	66784	66784	33392	62.71	0.000
Distance	2	328684	328684	164342	308.62	0.000
Applied voltage x Distance	4	75005	75005	18751	35.21	0.000
Error	9	4793	4793	533		
Total	17	475265				
S = 23.0762		R-Sq = 98.99%		R-Sq(adj) = 98.10%		

2.5.1.2 Fractional factorial design

When the effect of four to five or more of variables was investigated, it is unnecessary to perform all of the combinations of the specified factor settings. Generally, fractional factorial design might be adopted when the high order interactions could be negligible, whereas the main effects and lower order interactions are still investigated. A fractional factorial design might be used instead of full factorial design. The required number of experiments could be calculated by the following equation

$$\text{The number of experimental runs} = I^{k-p}$$

where I is the number of levels of each factor, k is the number of factors and p describes the size of the fraction of the full factorial used (20,52).

2.5.2 Central composite design (CCD)

Central composite design (CCD) is composed of a factorial or fractional factorial design with centre points and the addition of the star or axial points for the curvature estimation based on a second-order fitting model (quadratic model) as demonstrated in Figure 19. The number of star points is twice of the number of parameters in the design. Therefore, a central composite design with k parameters would have the additional $2k$ star points

$$\text{The number of experimental runs} = 2^k \text{ (full) or } 2^{k-p} \text{ (fractional) } + 2k + n_c$$

where $2k$ is the number of axial points and n_c is the number of centre points (20,52).

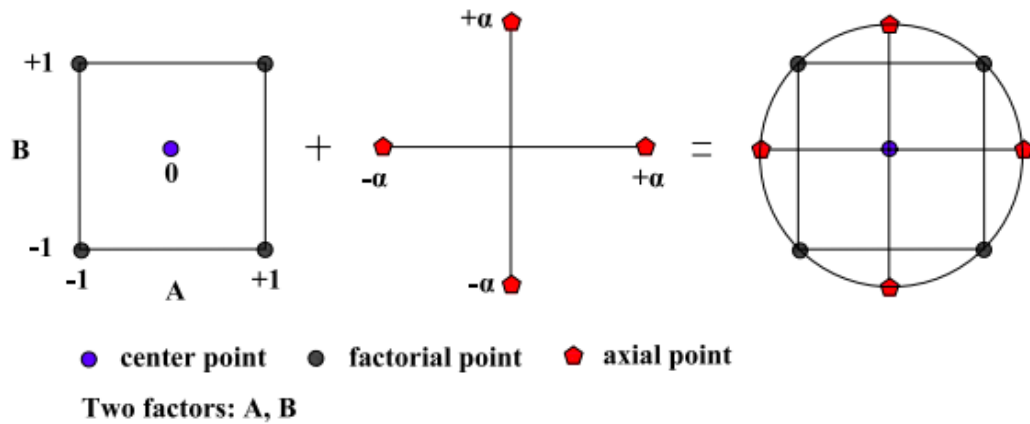


Figure 19 Diagram of central composite design for two factors.

Based on the study of Sarlak et al. (2012), the aims of this study are to evaluate the effect of six factors on the morphology of the TiO₂ nanofibers and to find the optimum conditions for fabricating TiO₂ nanofibers with desired morphology. In this research, the test variables were polyvinylpyrrolidone (PVP) content, titanium isopropoxide (TTIP) content, applied voltage, tip-to-collector distance, flow rate and pH of precursor solution, whereas the response was the diameter of the obtained nanofibers. These factors were varied according to the central composite design consisting of 32 runs of a fractional factorial design (1/2 fractional) with 9 runs of the replicated central points and 12 runs of the star points. The parameters and their levels are listed in Table 8.

Table 8 Independent parameters, including distance, voltage, flow rate, pH, PVP and TTIP contents, and their levels for the central composite design.

Independent parameters	Symbol	Coded levels				
		$-\alpha$	-1	0	+1	$+\alpha$
Distance (cm)	X ₁	16.55	20	22.5	25	28.44
Voltage (kV)	X ₂	6.55	10	12.5	15	18.44
Flow rate (mL/h)	X ₃	0.15	0.5	0.75	1	1.34
PVP content (% w/w)	X ₄	1.55	5	7.5	10	13.44
TTIP (% w/w)	X ₅	-1.89	5	10	15	21.89
pH	X ₆	2.31	3	3.5	4	4.68

The following equation presenting a relationship between the parameters and the nanofiber diameter was attained in coded unit.

$$Y = 476.5 + 549.685X_4 + 381.338X_5 - 295.568X_6 + 645.124X_4^2$$

Due to the ANOVA results, the *P* value of the model was less than 0.05 indicating that this regression model was significant. The R^2 value of 0.831 showed good reliability of the model. As mentioned earlier, the obtained model could provide the magnitude of the parameter effects and the direction of the relationship between the test parameters and the response. According to the equation, the PVP content (X_4) was the most significant with the scaled estimate of +549.685, while pH (X_6) had an indirect relationship with the nanofiber diameter (scaled estimate = -295.568). Moreover, the response surface plots were employed in order to find the optimum conditions. As a result, the TiO₂ nanofibers with minimum diameter around 105.5 ± 20 nm were fabricated at the distance of 25 cm, the voltage of 18.4 kV, the flow rate of 0.7 mL/h, the PVP content of 6.5% w/w, the TTIP content of 5% w/w and the solution pH of 3.2 (54).

2.5.3 Box-Behnken design

The Box-Behnken design is composed of 2^k factorials with incomplete block designs. It contains the treatment combinations which are placed at the middle of edges of the process space and at the centre as illustrated in Figure 20. This design requires three levels of each parameter and is rotatable (or nearly rotatable).

In this design, the fewer number of treatment combinations were required compared to the central composite design in the case of three or four parameters. In addition, all of the treatment combinations located at the corner points are discarded to avoid the experimental runs which seem to be expensive or impossible to test due to the physical process limitations (20).

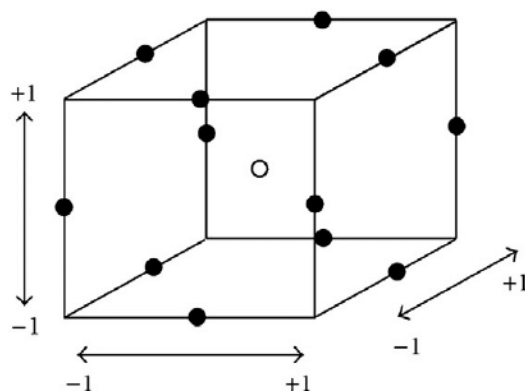


Figure 20 Diagram of Box-Behnken design for three factors.

Gönen et al. (2016) investigated the most appropriate factor settings for producing the gelatin/poly(ϵ -caprolactone) nanofibers loaded with bioactive glass particles with targeted fibre diameter by using Box-Behnken design. Bioactive glass content, applied voltage, tip-to-collector distance, and flow rate were selected to be the test variables in this work. The observed response were the average fiber diameter and its standard deviation. A total of 27 experimental runs including two replicates at the centre point was performed. The parameters and their levels are illustrated in Table 9.

Table 9 Independent parameters, including bioactive glass content, applied voltage, tip-to-collector distance and flow rate, and their levels for the Box-Behnken design.

Independent parameters	Symbol	Coded levels		
		-1	0	1
Bioactive glass content (% w/v)	X_1	2.5	5	7.5
Applied voltage (kV)	X_2	20	22.5	25
Tip-to-collector distance (cm)	X_3	7.5	10	12.5
Flow rate (mL/h)	X_4	1	2	3

Table 10 Summary of the ANOVA results for the average fibre diameter.

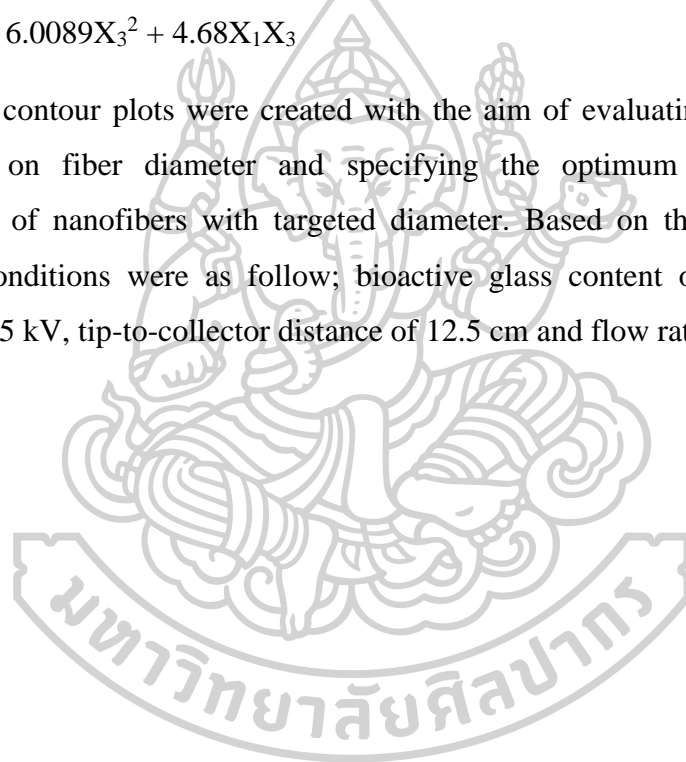
	Average fibre diameter		Standard deviation	
	F-value	P-value	F-value	P-value
Regression	14.40	0.000	17.76	0.000
Linear	0.89	0.487	1.95	0.155
Square	46.79	0.000	38.76	0.000
Interaction	3.66	0.071	2.18	0.156
Lack-of-fit	1.97	0.389	2.61	0.092

Regarding the ANOVA analysis as presented in Table 10, the P value of the model was less than 0.05, while the P value of the lack-of-fit was more than 0.05, indicating that this model was suitable. The equations for the fiber diameter and the standard deviation were developed. These models were good reliable represented by the R^2 values of 84.14% and 86.74%, respectively.

$$\text{Fibre diameter} = 346.903 - 423.617X_1 + 13.4X_2 + 193.867X_3 - 129.75X_4 + 37.2217X_1^2 - 9.9983X_3^2 + 25.8X_1X_4$$

$$\text{Standard deviation} = -2846.89 - 273.544X_1 + 280.467X_2 + 91.8444X_3 + 23.0511X_1^2 - 6.0289X_2^2 - 6.0089X_3^2 + 4.68X_1X_3$$

The contour plots were created with the aim of evaluating the impact of the parameters on fiber diameter and specifying the optimum conditions for the formulation of nanofibers with targeted diameter. Based on the contour plots, the optimum conditions were as follow; bioactive glass content of 7.5%w/v, applied voltage of 25 kV, tip-to-collector distance of 12.5 cm and flow rate of 1 mL/h (55).



CHAPTER 3

Methodology

3.1 Materials and methods

3.1.1 Materials

Part 1 Design of experiment approach for fabrication process of electrospun SHL nanofibers using factorial designs

3.1.2 Preparation of SHL solutions

3.1.3 Electrospinning

3.1.4 Characterization

3.1.5 Experimental design

Part 2 Design and characterization of ML loaded electrospun SHL nanofibers with antimicrobial activity

3.1.6 Fabrication and physicochemical characterization of ML loaded SHL films

3.1.6.1 Powder X-ray diffraction

3.1.6.2 Differential scanning calorimetry

3.1.6.3 Fourier transform infrared spectroscopy (FTIR)

3.1.7 Fabrication and physiochemical characterization of ML loaded SHL fibers

3.1.7.1 Preparation and evaluation of SHL-ML solutions

3.1.7.2 Preparation and evaluation of SHL-ML fibers through electrospinning process

3.1.7.3 Physicochemical characterization of SHL-ML fibers

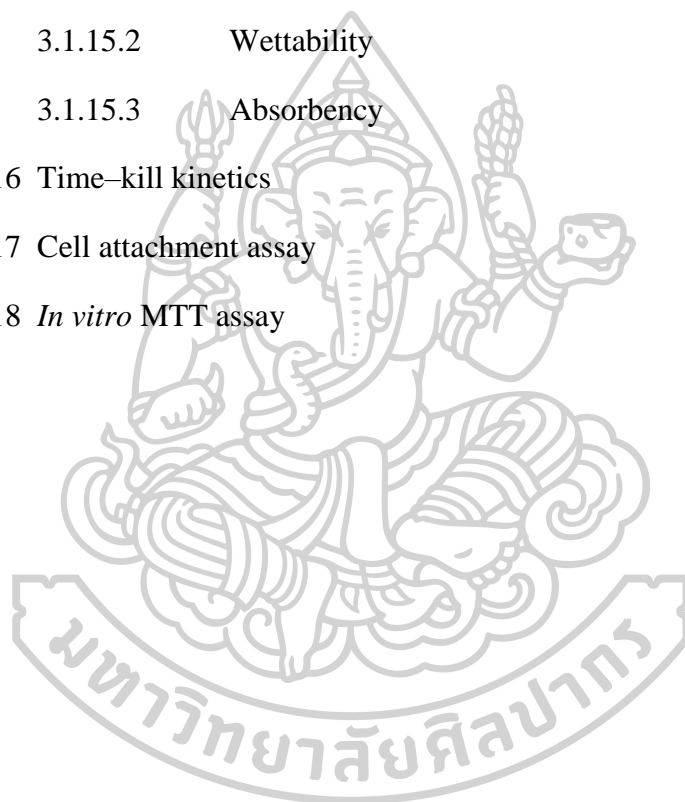
3.1.8 Experimental design

3.1.9 Time-kill kinetics

Part 3 Design and characterisation of electrospun SHL/PVP blended nanofibers loaded with monolaurin for application in wound healing

3.1.10 Experimental design

- 3.1.11 Preparation of blended solutions of SHL and PVP loaded with ML
- 3.1.12 Evaluation of properties of the blended solution
- 3.1.13 Preparation of electrospun SHL-PVP nanofibers loaded with ML
- 3.1.14 Morphology of electrospun nanofibers
- 3.1.15 Physicochemical and physical characterization of electrospun nanofibers
 - 3.1.15.1 Mechanical properties
 - 3.1.15.2 Wettability
 - 3.1.15.3 Absorbency
- 3.1.16 Time-kill kinetics
- 3.1.17 Cell attachment assay
- 3.1.18 *In vitro* MTT assay



3.1 Materials and methods

3.1.1 Materials

SHL (Lot No. 55), PVP K90 (Lot No. 0001845847) and ML (Lot No. 150520) were obtained from Mahachai Shellac Part., Ltd. (Samut Sakhon, Thailand), P.C. Drug Center Co. Ltd. (Bangkok, Thailand) and Shanghai Terppon Chemical Co., Ltd. (China), respectively. The microorganismal strains used for the antimicrobial study were *S. aureus* DMST 8013, *E. coli* DMST 4212 and *C. albicans* DMST 5815, which were purchased from the Department of Medical Sciences, Thailand. Tryptic soy agar and broth (TSA, Lot No. VM221159 and TSB, Lot No. VM229958) were used as culture media for bacterial growth and obtained from Merck KGaA (Germany). Sabouraud dextrose agar and broth (SDA, Lot No. 3200237 and SDB, Lot No. VM331339) were used as culture media for fungal growth and obtained from Benton, Dickinson and Company (USA) and Merck KGaA (Germany), respectively. Sterile powders of ketoconazole (Lot No. KT/14/08/18514) and streptomycin (Lot No. 9/2015) were used as positive controls and obtained from Greater Pharma Co., Ltd. (Bangkok, Thailand) and General Drugs House Co., Ltd. (Bangkok, Thailand), respectively. Human fibroblast cells (Mrc-5) derived from lung tissue were employed for cell adhesion assay and cytotoxic analysis. Chitosan (90% DAC, MW ~ 22,000) purchased from Seafresh Chitosan Company Limited, Thailand was used for toxicity screening. Ethanol (95% v/v) used for the preparation of the electrospun solution was of reagent grade.

Part 1 Design of experiment approach for fabrication process of electrospun SHL nanofibers using factorial designs

3.1.2 Preparation of SHL solutions

Each finely ground SHL was separately dissolved in 95% v/v ethanol and stirred at room temperature for overnight before adjusting to the desired concentration. The obtained homogenous solution was then centrifuged at 8000 rpm for 30 min to eliminate insoluble contamination and subjected to further electrospinning process.

3.1.3 Electrospinning

The prepared SHL solution was filled in a syringe connected to a high-voltage supply. When the voltages were applied, an electric field was conducted between the needle tip of the syringe and the collector. Fibers were accumulated on the surface of a target plate wrapped with aluminum foil. The process of electrospinning was carried out under the controlled conditions (23 °C–26 °C and 40%–60% RH).

3.1.4 Characterization

The properties of SHL solution such as viscosity, conductivity and surface tension were evaluated by using rheometer (Malvern Kinexus, England), electrical conductivity meter (Hanna HI 4522, USA) and drop shape instrument (FTA 1000, USA), respectively. The morphology of electrospun SHL fibers was observed by scanning electron microscope (SEM) (LEO 1450 VP, UK). Based on SEM images, fiber diameters and bead amounts were analysed by J MicroVision 1.2.7 software.

3.1.5 Experimental design

The morphology of the resultant nanofibers could be altered by several factors. Based on preliminary experiments, SHL content (X_1), applied voltage (X_2) and flow rate (X_3) were chosen to be the most significant parameters, whereas some parameters could be maintained constant. In this research, a tip-to-collector distance was held at 20 cm. The electrospinning process was performed at ambient condition. The appropriate range of each parameter was investigated. SHL concentration should be from 35% to 40% w/w. With increasing the amount of SHL above 40% w/w, the fibers could not be formed. At the SHL concentration of below 35% w/w, droplets might be obtained instead of fibers. The desired range of voltage was between 9 and 27 kV. The applied voltages below 9 kV were not enough to draw the solution from the tip, while high voltages might produce electrical arcs. Moreover, a flow rate varying from 0.4 to 1.2 mL/h was considered as the effective range for the fabrication process. The parameters and their levels used in the experimental design are given in Table 11. In this study, a 2^3 full factorial design with three replicates at the center point were exploited, and the responses studied were the diameter of SHL nanofibers, the distribution of diameter and the amount of beads presented in bead-to-fiber ratio.

The results of the factorial design were analysed using Design Expert 8.0.7.1 (Stat-Ease Inc., USA).

To investigate the most influential factors on the studied responses and their interactions, the Pareto charts were performed and described in the sequence of bar graphs consisting of two different t limits (the Bonferroni-corrected t and the standard t). On the bar graphs, values of critical factors would be displayed above both t limits, whereas those of possible factors might be presented above the t value limit. Factor effects indicated as not important would appear below the t value limit (56). The positive and negative impacts of factors are represented by vertical bars with orange and blue colours, respectively. Based on the analysis results, the predicted model was reliable as the P value of model displaying the statistical significant of the model was less than 0.05. The lack of fit illustrating the model related with errors was not significant. The coefficient of determination (R^2) indicating the goodness of fitted model was high. The developed mathematic models were also validated for the ability of models in describing the response changes in the design space by conducting the additional experiments. The difference between the experimental measurements and the predicted values presented by the root mean square error (RMSE) was calculated as following formula (57):

$$RMSE = \sqrt{\frac{\sum_{i=0}^N (P-O)^2}{N}}$$

where P and O are the model predicted value and the observed value, respectively. N is the number of tested data. In addition, the optimum conditions for the preparation of nanofibers with desired morphology were determined by defining the required criteria for each response.

Table 11 Experimental range and levels of selected independent parameters including SHL content, applied voltage and flow rate.

Parameters	Symbol	Variable levels		
		Low (-1)	Central point (0)	High (+1)
SHL content [% w/w]	X ₁	35	37.5	40
Applied voltage [kV]	X ₂	9	18	27
Flow rate [mL/h]	X ₃	0.4	0.8	1.2

Part 2 Design and characterization of ML loaded electrospun SHL nanofibers with antimicrobial activity

3.1.6 Fabrication and physicochemical characterization of ML loaded SHL films

The SHL-based polymeric films containing different concentrations of ML were initially prepared aiming to investigate the highest content of loaded ML by dissolving definite amount of SHL (40% w/w) and varied amounts of ML in the range of 3%–15% w/w in 95% v/v ethanol under overnight stirring at room temperature followed by solvent evaporation. The highest level of ML loading in the obtained films was accordingly analyzed using powder X-ray diffraction (PXRD). Consequently, SHL nanofibers loaded with the maximum amount of incorporated ML were fabricated and further evaluated for the physicochemical characteristics using powder X-ray diffraction (PXRD), differential scanning calorimetry (DSC) and Fourier transformed infrared spectroscopy (FTIR).

3.1.6.1 Powder X-ray diffraction (PXRD)

The crystalline or amorphous characteristic of the samples was evaluated using powder X-ray diffractometer (MiniFlex II, Rigaku, Japan). The scan was performed at 30 kV and 15 mA in the 2θ range of 5° to 40° with the speed of $4^\circ/\text{min}$ using Cu $K\alpha$ radiation ($\lambda = 0.154 \text{ nm}$).

3.1.6.2 Differential scanning calorimetry (DSC)

The thermal characteristic of materials was investigated using differential scanning calorimeter (Sapphire, Perkin Elmer, Germany) under nitrogen gas flow with the rate of 20 mL/min. Samples were sealed in standard liquid aluminum pans and heated from 25 to 200 $^\circ\text{C}$ with the rate of 10 $^\circ\text{C}/\text{min}$.

3.1.6.3 Fourier transformed infrared spectroscopy (FTIR)

The molecular behavior and interaction of ML in SHL matrix was examined using FTIR spectrophotometer (Nicolet Avatar 360, USA). During the process, each sample was ground and triturated with dry potassium bromide (KBr), and consequently compacted by hydraulic press machine to form pellet. The obtained pellet was placed in the sample holder. The scan was processed from 4000 to 400

cm^{-1} at 4 cm^{-1} resolution. The FTIR spectrum of each sample was obtained and analyzed using the OMNIC FTIR software.

3.1.7 Fabrication and physicochemical characterization of ML loaded SHL fibers

3.1.7.1 Preparation and evaluation of SHL-ML solutions

The solutions at selected SHL-ML ratios were prepared by dissolving finely ground SHL and ML in 95% v/v ethanol and then magnetically stirring for overnight at room temperature before adjusting to the desired content. In order to eliminate insoluble contamination, the homogenous solution was centrifuged at 8000 rpm for 30 min. The obtained solution was further subjected to study solution property, and fiber morphology after fabrication via electrospinning process.

The properties of SHL-ML solutions including viscosity, surface tension and conductivity were examined by rheometer (Malvern Kinexus, UK), drop shape instrument (FTA 1000, USA) and electrical conductivity meter (Extech EC500, USA), respectively.

3.1.7.2 Preparation and evaluation of SHL-ML fibers

SHL-ML nanofibers were prepared as mentioned in section 3.1.3. The morphology of the obtained fibers was investigated using scanning electron microscope (SEM) (LEO 1450 VP, UK). Based on SEM images, J MicroVision 1.2.7 software was utilized to measure the diameter of the fibers and the amount of beads. The influence of independent factors; formulation and process parameters including viscosity, surface tension, conductivity, applied voltage and feed rate, on the morphological characteristics of fibers were determined in order to find the significant factors for further design of experiment.

3.1.7.3 Physicochemical characterization of SHL-ML fibers

The prepared electrospun SHL-ML fibers were examined for the physicochemical characteristics compared with their physical mixtures derived from the blend of each finely ground excipient and pure compounds using powder X-ray

diffraction (PXRD), differential scanning calorimetry (DSC) and Fourier transformed infrared spectroscopy (FTIR) as described in section 3.1.6.

3.1.8 Experimental design

A 2⁴ full factorial design with three replicates at the center point was performed in order to find the optimized significant independent factors for the multiple responses of fiber properties. The diameter of fibers and the amount of beads (bead-to-fiber ratio) were the observed responses. The critical variables and their levels considered in the design of experiment are shown in Table 12. The optimum concentration of ML was in a range of 1% to 3% w/w. At a content of ML above 3% w/w, the loaded nanofibers were found to be liquefied. The Design Expert 8.0.7.1 software (Stat-Ease Inc., USA) was used for the analysis of the resultant data. In addition, the optimum conditions for the fabrication of nanofibers with desired morphology were also determined.

Table 12 Experimental range and levels of selected independent parameters including SHL and ML contents, applied voltage and flow rate.

Parameters	Symbol	Variable levels		
		Low (-1)	Central point (0)	High (+1)
SHL content [% w/w]	X ₁	35.0	37.5	40.0
ML content [% w/w]	X ₂	1.0	2.0	3.0
Applied voltage [kV]	X ₃	9.0	18.0	27.0
Flow rate [mL/hr]	X ₄	0.4	0.8	1.2

3.1.9 Time-kill kinetics

Time-kill assays were performed in order to study the pharmacodynamics of antimicrobial agents, showing a profile of antimicrobial activity over time. Prior to the kinetic test, *S. aureus* and *E. coli* were cultured in TSB media. Whereas *C. albicans* were cultured in SDB media. After overnight incubation at 37 °C, the density of inoculation was further diluted to 10⁴ CFU/mL. For the kinetic test, 30 min UV-sterilized SHL nanofibers loaded with ML and ML in a solution form were added in the media broth to give the same final concentration of ML (2 mg/mL). SHL fibers without ML were used as the negative control, while streptomycin and ketoconazole in the concentrations of 1 mg/mL were used as positive controls for antibacterial and

antifungal test, respectively. All tubes were shaken and incubated at 37 °C. At different time points (0, 15, and 30 min, 1, 3, 6 and 9 h), 100 µL of each sample was taken and spread on a media agar. All plates were then incubated for 24 h at 37 °C. The number of colonies was counted and calculated for the percentage of living microbial cells as following equation.

$$\text{The percentage of living microbial cells} = (C_t \times 100) / C_0$$

where C_0 and C_t are the number of colonies at initial time (before adding the sample) and each time point, respectively.

Part 3 Design and characterisation of electrospun SHL/PVP blended nanofibers loaded with monolaurin for application in wound healing

3.1.10 Experimental design

PVP was added to the SHL carrier to generate a wound dressing with improved performance properties. Monolaurin was incorporated to provide antimicrobial activity. The studied independent factors were the SHL ratio in the SHL/PVP blended solution (X_1), ML content (X_2) and applied voltage (X_3), which were selected on the basis of preliminary studies. A 2^3 full factorial design with three centre-point replications was conducted to identify the effects of each significant factor and their combination on multiple observed responses, including morphology, mechanical properties, hydrophilicity and absorbability. The evaluated samples were obtained from solutions that were varied according to selected parameters as illustrated in Table 13. In this part, the encapsulated content of ML seemed to increase with the addition of PVP, thus the selected concentration range of ML was between 5% and 35% w/w. The resultant data were analysed using the Design Expert 8.0.7.1 software. The optimum production conditions for electrospun SHL/PVP nanofibers comprising ML with the desired properties were also investigated.

Table 13 Experimental range and levels of selected independent parameters including SHL ratio in blended solution, ML content, applied voltage and flow rate.

Parameters	Symbol	Variable levels		
		Low (-1)	Central point (0)	High (+1)
SHL ratio in blended solution	X ₁	25	50	75
ML content [% w/w]	X ₂	5	20	35
Applied voltage [kV]	X ₃	9	18	27

3.1.11 Preparation of blended solutions of SHL and PVP loaded with ML

SHL (35% w/w) and PVP (8% w/w) solutions were separately prepared by dissolving fine powders of SHL and PVP in 95% v/v ethanol. The dissolved solutions were then stirred overnight at room temperature and adjusted to the required concentrations. Prior to concentration adjustment, insoluble contaminants that may have been present in the SHL solution were removed by centrifugation at 8000 rpm for 30 min. The blends of SHL and PVP solutions with ML at different ratios were subsequently prepared and subjected to further evaluation and fabrication.

3.1.12 Evaluation of properties of the blended solution

Properties of the drug/polymer blended solution such as viscosity, surface tension and conductivity were determined using a rheometer (Malvern Kinexus, UK), drop shape instrument (FTA 1000, USA) and electrical conductivity meter (Extech EC500, USA), respectively.

3.1.13 Preparation of electrospun SHL-PVP nanofibers loaded with ML

The electrospun SHL-PVP fibers were prepared as mentioned earlier (section 3.1.3).

3.1.14 Morphology of electrospun nanofibers

The morphology of the obtained fibres was investigated using scanning electron microscope (SEM) (LEO 1450 VP, UK). Based on SEM images, J MicroVision 1.2.7 software was utilized to measure the diameter of the fibres and the amount of beads.

3.1.15 Physicochemical and physical characterization of electrospun nanofibers

The obtained electrospun nanofibers were investigated for their physicochemical properties using powder X-ray diffractometry (PXRD), differential scanning calorimetry (DSC) and Fourier transform infrared spectroscopy (FTIR) as illustrated in section 3.1.6. Physical characteristics, including mechanical properties, wettability and absorbability were also studied.

3.1.15.1 Mechanical properties

Mechanical properties, including tensile strength and elongation, were measured using a texture analyser (TA.XT plus, Stable Micro Systems, UK). The fibre mats were cut to a length of 25 mm and a width of 5 mm (58). The thickness of nanofibers was evaluated using a thickness tester. The tensile strength and elongation were calculated as following equations:

$$\text{Tensile strength (MPa)} = \frac{\text{Force (N)}}{\text{Cross sectional area (mm}^2\text{)}}$$

$$\text{Elongation (\%)} = \frac{\Delta L \times 100}{L}$$

where ΔL is the change in length of the original gage length measured after a rupture and L is the original gage length.

3.1.15.2 Wettability

The hydrophilicity of wound dressing mats influences the behaviours of cell adhesion and growth, thus affecting the rate of wound healing. Moreover, wound dressing membranes should be applied effectively and firmly adhered to the moist wound bed during the wound-healing process. In order to determine the hydrophilicity of the obtained fibres, the wettability, as indicated by contact angle, surface free energy and polarity, was measured using a drop shape instrument. During the process, two liquids, water and diiodomethane, used as polar and nonpolar solvents, were dropped onto each fibre mat, and the contact angle, surface free energy and polarity were then calculated according to the Wu's harmonic mean equation as follows:

$$\gamma_L(1+\text{Cos}\theta) = 4 [(\gamma_S^d \gamma_L^d) / (\gamma_S^d + \gamma_L^d) + (\gamma_S^p \gamma_L^p) / (\gamma_S^p + \gamma_L^p)]$$

where γ_L and γ_S were the liquid surface tension and solid surface free energy, respectively. The dispersive and polar components of the surface free energy were represented as γ^d and γ^p , accordingly (59).

3.1.15.3 Absorbency

Regarding the characteristics of ideal dressing materials, wound mats should absorb exudates and maintain a moist wound environment at the surface. The degree of swelling (DS) of the wound dressing was investigated and calculated according to the following formula (60):

$$DS = (W_w - W_d) \times 100 / W_d$$

where W_d was the weight of a dry dressing, and W_w was weight of a wet dressing following immersion in the medium for the given time periods (1, 5, 10 and 15 min). In this work, the medium was phosphate buffered saline (PBS) solution pH 7.4, which simulated the environment of a chronic wound. The samples were placed between two sieves. The excess fluid was removed with filter paper and by oven drying at 50 °C. The maximum values of absorbency at the same time point after immersion in medium were selected and evaluated using an experimental design approach.

3.1.16 Time-kill kinetics

S. aureus and *C. albicans*, majority causes of chronic wound infection, were used in this assay. *S. aureus* and *C. albicans* were incubated overnight at 37 °C in TSB and SDB, respectively, and then further diluted to 10⁴ CFU/mL. The nanofibers were UV sterilised for 30 min prior to the kinetic test. Based on time-kill kinetic methodology, the sterilised mats at different ratios of SHL/PVP loaded with ML and the solution of ML were introduced into liquid media in a final concentration of 2 mg/mL. Streptomycin and ketoconazole in the concentrations of 1 mg/mL were used as positive controls for the study of antibacterial and antifungal activities, whereas fibres without ML were used as a negative control. All tubes were cultured at 37 °C in a shaking incubator. At each time point (0, 15 and 30 min and 1, 3 and 6 h), 100 µL of each sample was drawn up, dispensed onto an agar plate and then incubated at 37 °C for 24 h. The percentage of living microbial cells calculated from the number of colonies at different time points was used to determine each activity over time.

3.1.17 Cell attachment assay

Human fibroblast cells suspended in Dulbecco's Modified Eagle's Medium comprising 10% foetal bovine serum and 0.01% L-glutamine were grown in T-75 cell culture flasks at 37 °C in a 5% CO₂ atmosphere. The nanofiber mats were cut into small pieces and subsequently UV sterilised for 20 min. The fibroblast cells were separated by trypsinisation, seeded onto the nanofibers at a density of 10⁵ cells/mat and incubated at 37 °C under 5% CO₂. During cell seeding, the characteristic of cell adhesion was observed continuously under a light microscope.

3.1.18 *In vitro* MTT assay

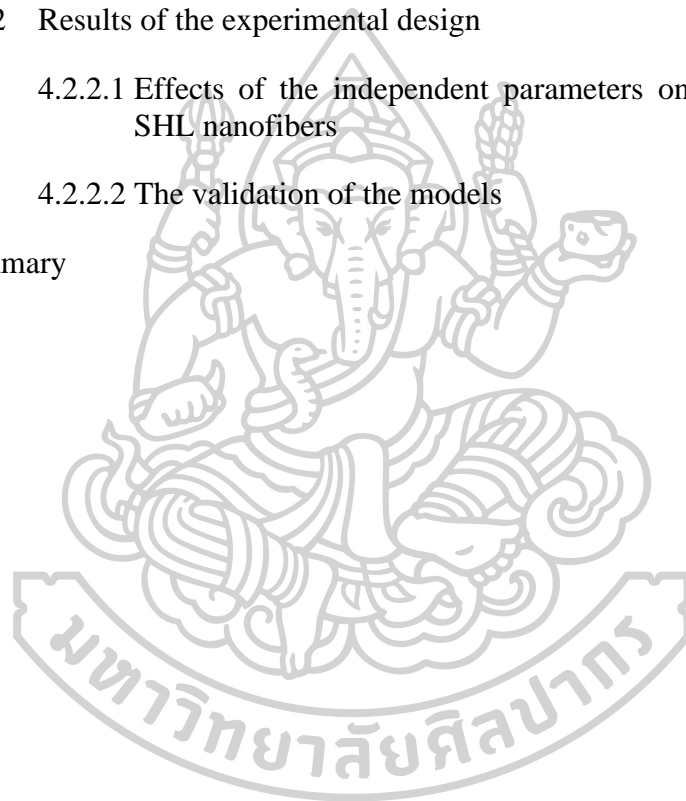
Prior to cytotoxicity test, SHL, PVP, ML and SHL/PVP blended nanofibers in the ratio of 50 to 50 containing 20% w/w ML, which should be preferable applied in wound healing application based on the experimental results, were prepared in the solutions by dissolving in 95% ethanol. Chitosan was stirred overnight in 2% acetic acid. Human fibroblast cells were grown in T-75 cell culture flask using a DMEM cell culture medium added with 0.01% L-glutamine and 10% FBS, and incubated at 37 °C in 5% CO₂. During the process of MTT assay, the fibroblast cells were separated by trypsinization and placed in a 96 well culture plate at the density of approximately 3 x 10⁴ cells/well. The cells were treated with various samples, including SHL, PVP, ML, chitosan, SHL/PVP blended nanofibers in the ratio of 50 to 50 loaded with 20% w/w ML, which were 4-fold serial diluted with DMEM cell culture medium to 0.064, 0.016, 0.004 and 0.001 mg/mL in each well. The 20 µg/mL of 5-FU was employed as a positive control, and the cells without samples were used as control cells. After 24 h incubation, all of the samples was removed. The MTT solution was added in the concentration of 0.5 mg/mL. The culture plates were covered with aluminum foil in order to protect from light, and then incubated for 3 h at 37 °C of 5% CO₂ atmosphere. The 50 µL of DMSO was added in each well to dissolve the cell formation of insoluble purple formazan. The cell viability was detected at the absorbance of 570 nm, and the percentage of cell viability was measured as following equation.

$$\text{Cell viability (\%)} = 100 \times \frac{\text{Mean absorbance of treated cell}}{\text{Mean absorbance of untreated cell}}$$

CHAPTER 4

Design of Experiment Approach for Fabrication Process of Electrospun Shellac Nanofibers Using Factorial Designs

- 4.1 Introduction
- 4.2 Results and discussion
 - 4.2.1 Properties of SHL solution
 - 4.2.2 Results of the experimental design
 - 4.2.2.1 Effects of the independent parameters on the morphology of SHL nanofibers
 - 4.2.2.2 The validation of the models
- 4.3 Summary



4.1 Introduction

Currently, electrospun nanofibers are increasingly introduced to wound healing management. Due to their ultrafine network structures, electrospun nanofibers could be used for the replacement of natural extracellular matrix (ECM) resulting in greatly rapid epithelialization, allowing the reduction of scar formation (4). The porous nature of nanofiber dressings also enhances oxygen and nutrients transferring to cells leading to an increased healing rate (6). Dressings are supposed to be placed in the physiological and biological environment of a wound; thus, the use of biopolymers for electrospun nanofibers is necessary.

SHL is a natural polymer secreted by the lac insect found on specific trees in China, India and Thailand. It is nontoxic and physiologically harmless (8). Based on its excellent film forming and protective properties, SHL is commonly used as an enteric coating material to protect from acid in gastrointestinal tract and as an additive in fruit coating to prevent water loss and microbial entry (9,10). Therefore, SHL might be potentially used as a carrier polymer for wound dressing application.

The electrospinning process could be influenced by various parameters including solution parameters, processing parameters and ambient parameters (19). In order to determine the single effect of each factor and interaction effects between factors, a factorial design was carried out with the aim to minimize time consuming and the number of experiments (20).

The objectives of this study were to investigate the main and interaction effects of some parameters such as SHL content, applied voltage and flow rate on the morphology of the SHL nanofibers, and to find the optimum process conditions by using a full factorial design with three replicated centre points.

4.2 Results and discussion

4.2.1 Properties of SHL solution

The electrical property, viscosity and surface tension might affect the stretching property of the solution influencing in the electrospinning process. From Table 14, an increase in the concentration of SHL resulted in the increased viscosity and the decreased conductivity of the solution, while the surface tension was not

significantly different. When the SHL content was increased, the beaded fibres were gradually altered to smooth fibres as shown in Figure 21 due to a high interaction between the solvent and polymer molecules, thus reducing the tendency of aggregation of the solvent molecules (19).

Table 14 The effect of different SHL concentrations on viscosity, conductivity and surface tension.

SHL content [% w/w]	Solution properties		
	Viscosity [mPa.s]	Conductivity [μ S]	Surface tension [mN/m]
35	225.80	25.70	24.6
37.5	442.50	23.49	24.3
40	628.03	21.46	25.4

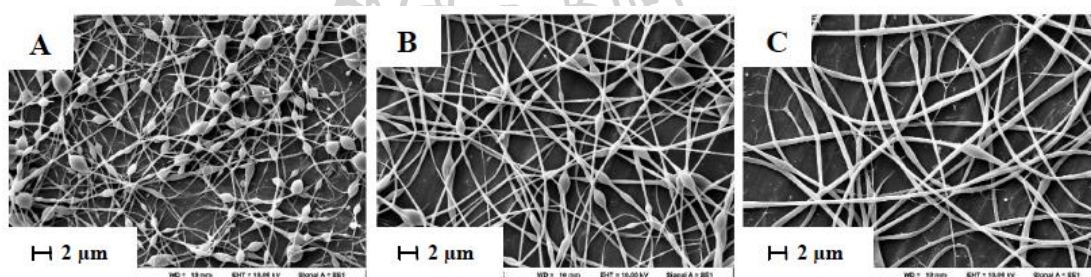


Figure 21 SEM images of SHL nanofibers at the concentrations of (A) 35% w/w, (B) 37.5% w/w and (C) 40% w/w.

4.2.2 Results of the experimental design

4.2.2.1 Effects of the independent parameters on the morphology of SHL nanofibers

The results were measured based on a 2^3 full factorial design with three replicated centre points consisting of 11 experiments (Table 15). The most significant effects and their interactions were evaluated by using Pareto charts as demonstrated in Figure 22.

Table 15 Full factorial design and experimental responses, including nanofiber diameter and bead amount, for each design point of SHL content, applied voltage and flow rate.

Run	SHL content (X ₁)	Applied voltage (X ₂)	Flow rate (X ₃)	Nanofiber diameter (Y ₁) [nm]	Bead amount (Y ₂)
1	-1	-1	-1	251.16	1.64
2	+1	-1	-1	533.74	0.11
3	-1	+1	-1	256.87	1.12
4	+1	+1	-1	646.93	0.06
5	-1	-1	+1	289.09	1.50
6	+1	-1	+1	604.52	0.18
7	-1	+1	+1	293.23	1.01
8	+1	+1	+1	698.41	0.08
9	0	0	0	389.44	0.85
10	0	0	0	429.34	0.80
11	0	0	0	404.10	0.89

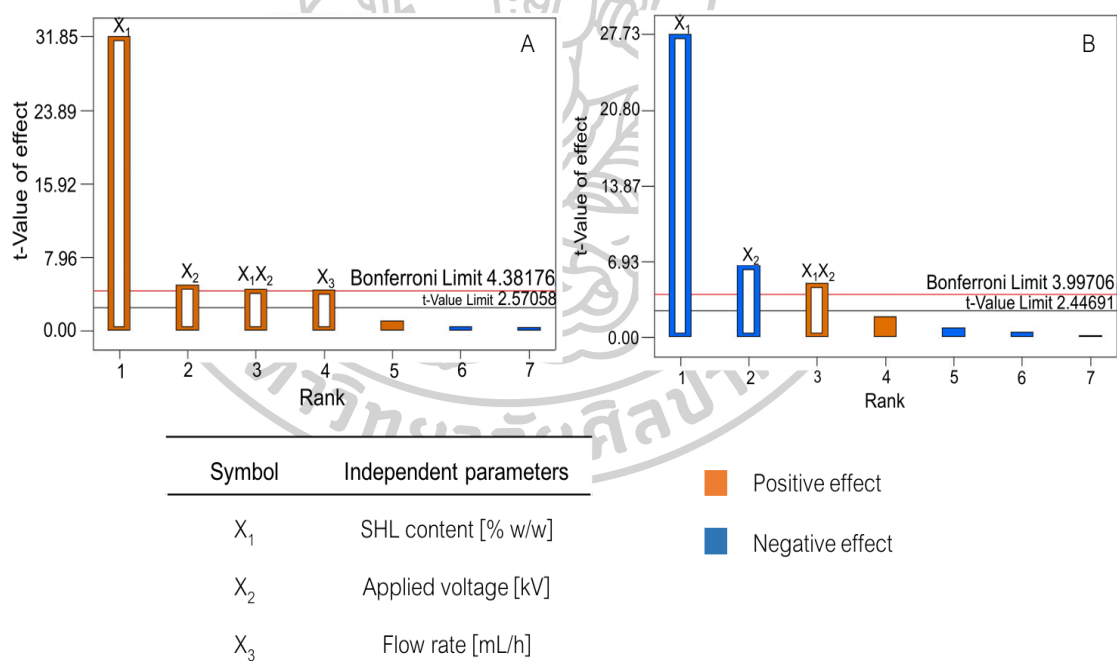


Figure 22 Pareto charts of the response values (A) nanofiber diameter and (B) bead amount.

The Pareto charts presented that SHL content had the most important effect on the SHL fibre diameter, while applied voltage, interaction between SHL content and voltage, and feed rate were minor factors, respectively. When the

concentration of SHL was increased, the stretching of the solution might be reduced due to an increase in the viscosity and a decrease in the conductivity resulting in the formation of large diameter nanofibers (19). Moreover, the high applied voltages might facilitate the polymer ejection leading to the increased diameter (61). Fibres with large diameter could be obtained from the high feed rate because of the increased volume of solution drawn from the tip, thus consuming long time to be dried. The fibres would be fused together (19).

SHL content and applied voltage had negative relationships with bead amount. As previously mentioned, the solution containing low amount of SHL might produce beaded fibres instead of smooth fibres due to a low interaction between the solvent and polymer molecules. The solvent molecules tended to easily compact together. In addition, when the high voltages were applied, the amount of charges would be increased causing the fast drawing of the solution; therefore, the beadless fibres could be formed (19).

The mathematical models were performed to predict the effect of independent parameters on fibre diameter and bead amount as shown in the following equations referring to coded factors (Eq. 1,2) with R^2 values of 0.9827 and 0.9803, respectively.

$$\text{Diameter} = 174.16(X_1) + 27.12(X_2) + 24.57(X_3) + 24.66(X_1X_2) + 436.07 \quad (1)$$

$$\text{Bead amount} = 0.75 - 0.6(X_1) - 0.14(X_2) + 0.11(X_1X_2) \quad (2)$$

Regarding Table 16, the P values of the models were less than 0.05 indicating that these models were significant. In the same way, the P values for the lack of fit of diameter and bead amount were 0.3271 and 0.1524, which were greater than 0.05, determining that the models were suitable. The sign of coefficients represented the positive and negative relationships between factors and responses.

Table 16 Analytical results for diameter and bead amount of SHL fibres.

Responses	Coefficients	*P value	Std. Dev.	%CV	Mean value	R ²	F-value
Y ₁ (nanofiber diameter)			27.49	6.30	436.08	0.9827	
X ₁	174.16	< 0.0001					
X ₂	27.12	0.0316					
X ₃	24.57	0.0448					
X ₁ X ₂	24.66	0.0443					
Intercept	436.07						
Model		< 0.0001					85.42
Lack of fit		0.3271					2.28
Y ₂ (bead amount)			0.095	12.79	0.75	0.9803	
X ₁	-0.60	< 0.0001					
X ₂	-0.14	0.0037					
X ₁ X ₂	0.11	0.0148					
Intercept	0.75						
Model		< 0.0001					116.03
Lack of fit		0.1524					5.85

*P values < 0.05 indicate that the model terms are significant.

An overlay plot was created in order to find the optimum conditions. Nanofibers with thinner diameter (~ 493 nm) and less number of beads (~ 0.47) might be obtained at the SHL content of 38.5% w/w, the voltage of 21 kV and the feed rate of 0.4 mL/h.

4.2.2.2 The validation of the models

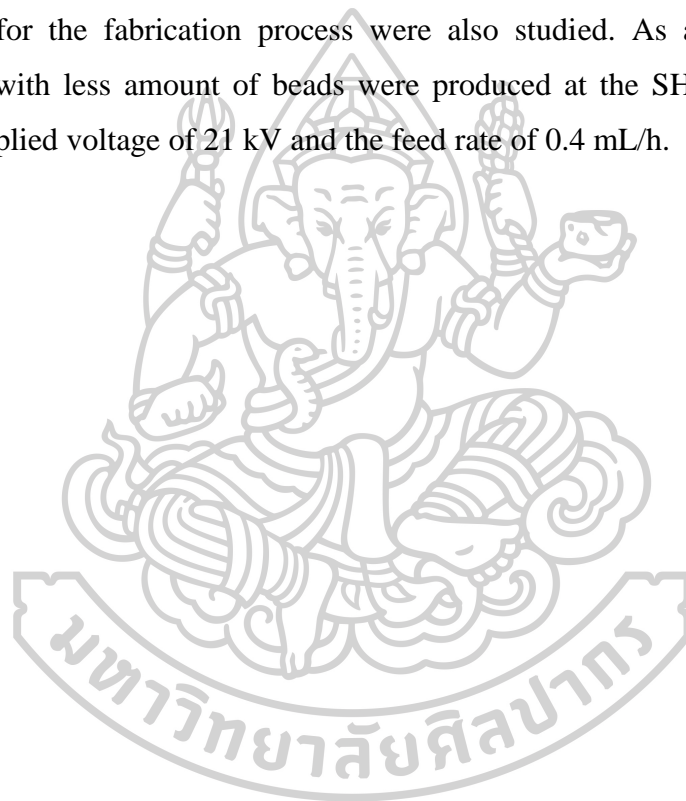
In order to evaluate the correlation between the expected values calculated from the developed mathematic models and the actual experimental results, the additional test data set was exploited. According to Table 17, there was a relative agreement between the actual and predicted values of fibre diameter and bead amount as displayed by the calculated RMSE values of 14.48 and 0.05, describing the effectiveness of the equations.

Table 17 Comparison between the actual and predicted values of diameter and bead amount of test data set.

	Diameter (nm)			Bead amount		
	Actual value	Predicted value	RMSE	Actual value	Predicted value	RMSE
38% w/w SHL (25.5 kV / 1 mL/h)	493.83	509.90	14.48	0.93	1.18	0.05
38.9% w/w SHL (25.5 kV / 1 mL/h)	562.93	579.99		0.77	1.01	
39.4% w/w SHL (21 kV / 0.5 mL/h)	577.09	565.29		0.47	0.52	

4.3 Summary

The SHL nanofibers could be developed as a carrier polymer for wound dressing application by using a full factorial design aiming to examine the main and interaction effects of parameters on the morphology of the SHL fibres. Based on the results, SHL content was the most important effect on fibre diameter. Whereas applied voltage, interaction between SHL content and voltage, and feed rate were minor factors, respectively. On the other hand, an increase in the concentration of SHL and voltage might lead to a decrease in the amount of beads. The optimum conditions for the fabrication process were also studied. As a result, the thinner nanofibers with less amount of beads were produced at the SHL content of 38.5% w/w, the applied voltage of 21 kV and the feed rate of 0.4 mL/h.



CHAPTER 5

Design and characterisation of monolaurin loaded electrospun shellac nanofibers with antimicrobial activity

- 5.1 Introduction
- 5.2 Results and discussion
 - 5.2.1 Evaluation of physical state and compatibility of the components in ML loaded SHL matrix
 - 4.3.1.1 Powder X-ray diffractometry (PXRD)
 - 4.3.1.2 Differential scanning calorimetry (DSC)
 - 4.3.1.3 Fourier transform infrared spectroscopy (FTIR)
 - 5.2.2 Evaluation of SHL-ML solution properties
 - 5.2.3 Experimental design
 - 5.2.3.1 Effects of the independent parameters on the morphology of SHL-ML nanofibers
 - 5.2.3.2 Optimization of SHL-ML nanofibers
 - 5.2.3.3 The validation of the models
 - 5.2.4 Time-kill kinetic study
- 5.3 Conclusions

5.1 Introduction

Infection might cause a delay in wound healing. To prevent the multiplication of pathogens, an antimicrobial agent should be incorporated. Apparently, antibiotic resistance has become an increasing worldwide problem for infection treatment. Therefore, safe and effective antimicrobials which are not easily subjected to resistance are greatly required. Among these simple antimicrobial compounds, natural lipids seem to be an achievable choice (14). Fatty acids and their corresponding esters might have little or no toxicity and also exert antimicrobial activity. Isaacs, Litov and Thormar (1995) found that fatty acids and monoglycerides with medium chain lengths yielded more biologically active than long chain monoglycerides in killing viruses and bacteria (38). Among medium chain fatty acids (C8 to C14), lauric acid (C12) has more antimicrobial activity than other fatty acids such as myristic acid (C14), capric acid (C10) or caprylic acid (C8) (16). It could be found in human breastmilk, skin surface and other natural foods such as coconut oil and palm kernel oil (16). ML, known as glycerol monolaurate, is a monoester form of lauric acid. It has many times greater antibacterial and antiviral activity than lauric acid. Tangwatcharin and Khopaibool (2012) revealed that minimum bactericidal concentrations (MBC) of lauric acid and ML were 3.2 mg/mL and 0.1 mg/mL, respectively (42). The lower MBC value of ML indicated the stronger antimicrobial activity than that of lauric acid. ML has Generally Recognized As Safe (GRAS) status considered to be nontoxic (16). It is approved in the US as a food emulsifier and has been used to control growth of pathogenic organisms and spoilage in food processing industries (18). ML exhibits a broad-spectrum bactericidal activity against Gram positive bacteria from superficial skin infections and also has an antifungal effect by inhibiting spore germination and preventing the radial growth (15,16,43,62). Previous studies revealed that the topical use of ML could inhibit the growth of *S. aureus*, a significant cause of skin and mucosal infections (62). Besides the killing effect, ML might stabilize mucosal and skin surfaces, thus avoiding inflammation and further infection (62). In addition to *S. aureus*, *S. pyrogenes*, *Cl. perfringens*, *M. terrae*, *L. monocytogenes*, *S. agalactiae*, and Groups C, F, and G streptococci could be killed by ML (16,62). Fungi, yeast, and protozoa were also reported to be inactivated by ML. *C. albicans*, an opportunistic human yeast pathogen found in the oral pharynx, gut, genito-urinary tract and skin,

was potentially affected by ML (63). Additionally, the development of microbial resistance to ML was also considered rare to occur (62). However, there are few studies exploring the possibility of ML as an alternative antimicrobial agent in the pharmaceutical dosage forms, including wound dressing.

The aims of this research were to investigate which factors (SHL and ML concentrations, applied voltage and flow rate) and interaction effects between these factors would have the most impact on the morphology of SHL nanofibers loaded with ML. The fabrication conditions were optimized by using a full factorial design with three replicated centre points. Various instrumental analyses including powder X-ray diffraction, differential scanning calorimetry and FTIR spectroscopy were also employed in order to investigate the physicochemical characteristics of ML in SHL matrix.

5.2 Results and discussion

5.2.1 Evaluation of physical state and compatibility of the components in ML loaded SHL matrix

The physicochemical characterisations of ML loaded SHL matrix including crystallinity property, thermal characterisation and molecular behaviour and interaction were determined by using PXRD, DSC and FTIR as described below.

5.2.1.1 Powder X-ray diffractometry (PXRD)

The PXRD patterns of SHL powder, ML powder, their physical mixture, nanofibers and films in the weight ratio of 40: 3 are illustrated in Figure 23. The crystalline peaks as indicated by the diffraction peaks at 2θ values of 9.6° , 19.6° , 20.5° and 23.0° were clearly observed in the PXRD pattern of ML powder while SHL powder was in amorphous state as presented in a halo PXRD pattern. After encapsulation of ML in SHL nanofibers or films, the characteristic crystalline peaks of ML were absent assuming that ML might be entrapped in the SHL matrix. It was also noted that fast drying rate during electrospinning was not the cause of disappearance of ML diffraction peak (amorphization) since slow evaporation during the film casting also demonstrated the similar PXRD pattern as that obtained from electrospinning. In this case, the ML molecules should be molecularly dispersed

among the polymer chains of SHL, resulting in the disappearance of crystalline structure.

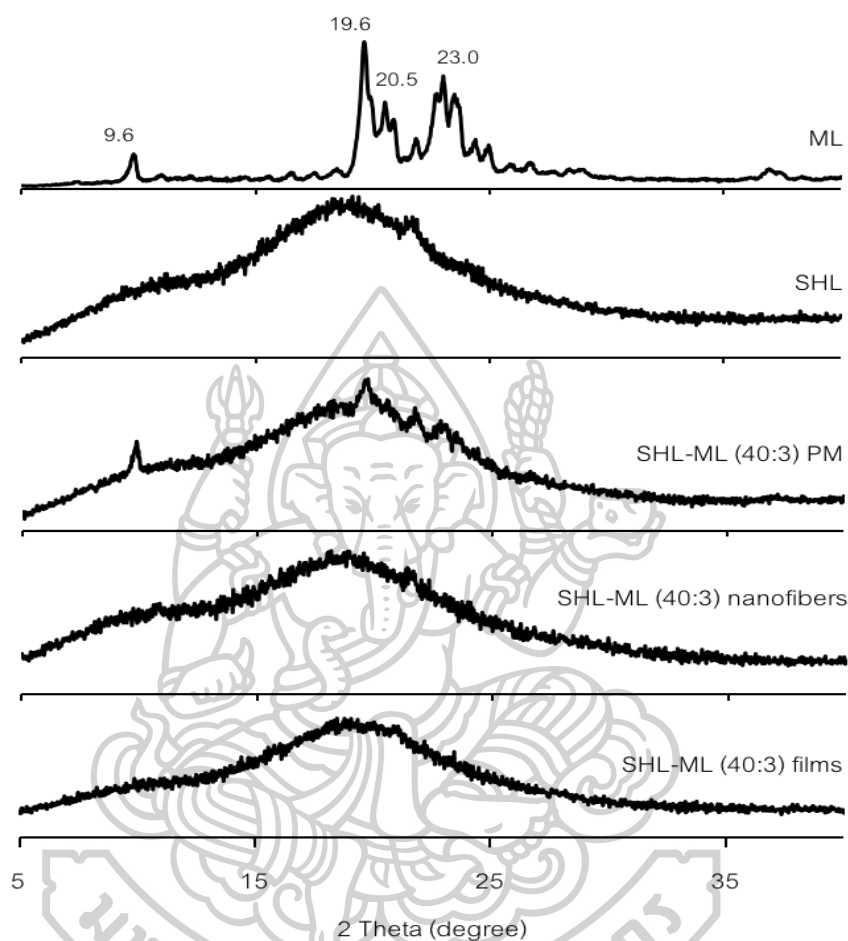


Figure 23 Powder X-ray diffraction patterns of SHL, ML, their physical mixture, nanofibers and films in the weight ratio of 40: 3.

The SHL films containing various amounts of ML were developed aiming to investigate the highest level of incorporated ML. Based on Figure 24A, the diffraction peaks due to crystalline ML were clearly observed in the PXRD patterns of all SHL-ML physical mixtures, especially at high fraction of ML. However, the peak intensity due to ML in PXRD patterns of SHL-ML films (Figure 24B) became obviously decreased as compared to that of the corresponding physical mixtures. According to the PXRD profiles of SHL-ML films at the ratios of 40: 5 and 40: 3, the diffraction peaks completely disappeared and changed to halo pattern, suggesting the

complete encapsulation or monomolecular dispersion of ML into SHL matrix films at these ratios. Thus, the suitable ratio of SHL to ML should be 40: 5 in which ML could be completely loaded in SHL nanofibers. Nevertheless after preliminary investigation by electrospinning process, nanofibers containing 40: 5 weight ratio of SHL to ML could not be performed because of tackiness. Therefore, the combination of SHL with ML at the ratio of 40: 3 was found to be the maximum loading amount of ML.

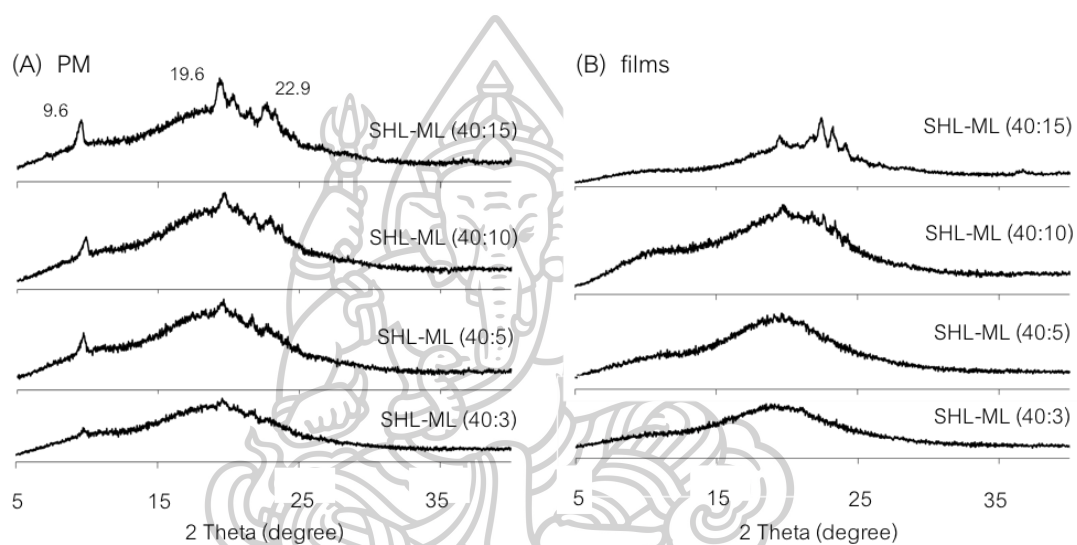


Figure 24 Powder X-ray diffraction patterns of (A) SHL-ML physical mixtures with different amounts of ML and (B) their corresponding films.

5.2.1.2 Differential scanning calorimetry (DSC)

DSC is one of the common tools for studying the interaction between the active drug and excipients and also assessing the possible incompatibilities which is significantly involved in the dosage form development (64). In this study, DSC was employed to study the interaction between SHL and ML. The DSC thermograms of SHL, ML and their corresponding samples are illustrated in Figure 25. Based on the DSC curve of ML, a large endothermic peak was obtained at about 66 °C indicating the melting temperature of ML. Meanwhile, pure SHL displayed the melting peak at about 69 °C which was almost the same position as ML. The physical mixture showed the broad endothermic peak, presumably due to the overlapped melting peaks of ML

and SHL, at 68 °C. However, the films and nanofibers demonstrated the different results as compared to those found in the physical mixture. The loss of endothermic peaks of ML and SHL was obviously observed in the DSC thermograms of the films and nanofibers which suggested the strong interaction between SHL and ML. The ML crystals might be changed from crystal state to molecular level and interacted with polymer structure of SHL during processing which was in accordance to the XRD results.

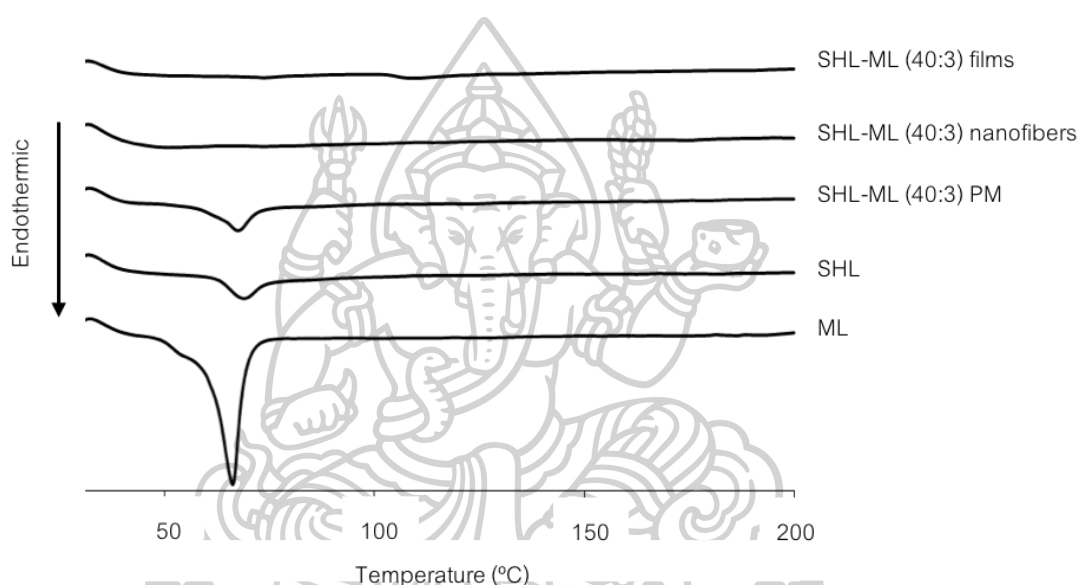
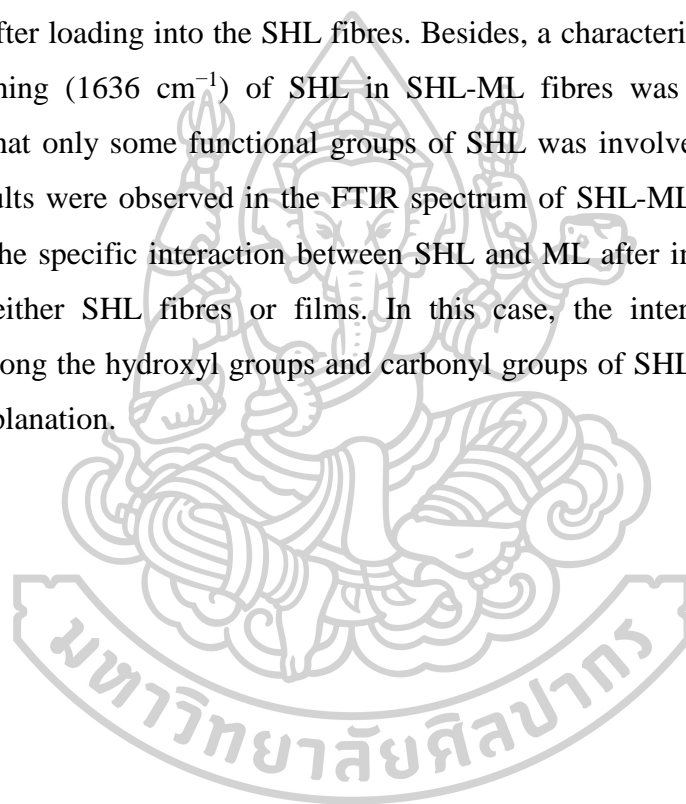


Figure 25 DSC thermograms of SHL, ML, their physical mixture, nanofibers and films in the weight ratio of 40: 3.

5.2.1.3 Fourier transform infrared spectroscopy (FTIR)

In order to provide more insight into the chemical interaction between components, FTIR was used for studying the molecular behaviour of ML in SHL matrix. As illustrated in Figure 26, ML showed a broad peak with the maxima around 3314 cm^{-1} which was assigned as O-H stretching of the hydroxyl groups at the glycerol backbone while the peaks at 1731 and 1182 cm^{-1} were attributed to carbonyl (C=O) stretching and C-O stretching of lauryl ester, respectively (65). SHL also demonstrated the peak due to O-H stretching of hydroxyl groups and C=O stretching but in the different positions of 3420 cm^{-1} and 1716 cm^{-1} , respectively. Additionally,

the peaks assigned to alkenyl (C=C) and C-O stretching band were observed at 1636 and 1255 cm^{-1} , respectively (66). For the physical mixture, the superimposed spectrum between SHL and ML was observed. However, the FTIR spectrum of ML loaded SHL fibres was clearly changed as compared to that of the physical mixture. After the incorporation of ML into SHL fibres, the shift of broad O-H bands of ML (3314 cm^{-1}) and SHL (3420 cm^{-1}) to the maxima around 3446 cm^{-1} was observed while the peaks assigned to C=O stretching of ML (1731 cm^{-1}) and SHL (1716 cm^{-1}) were shifted to 1717 cm^{-1} . Additionally, the peak intensity of ML was clearly decreased after loading into the SHL fibres. Besides, a characteristic peak assigned to C=C stretching (1636 cm^{-1}) of SHL in SHL-ML fibres was not changed which suggested that only some functional groups of SHL was involved in the interaction. Similar results were observed in the FTIR spectrum of SHL-ML films and therefore confirmed the specific interaction between SHL and ML after incorporation into the matrix of either SHL fibres or films. In this case, the intermolecular hydrogen bonding among the hydroxyl groups and carbonyl groups of SHL and ML might be a possible explanation.



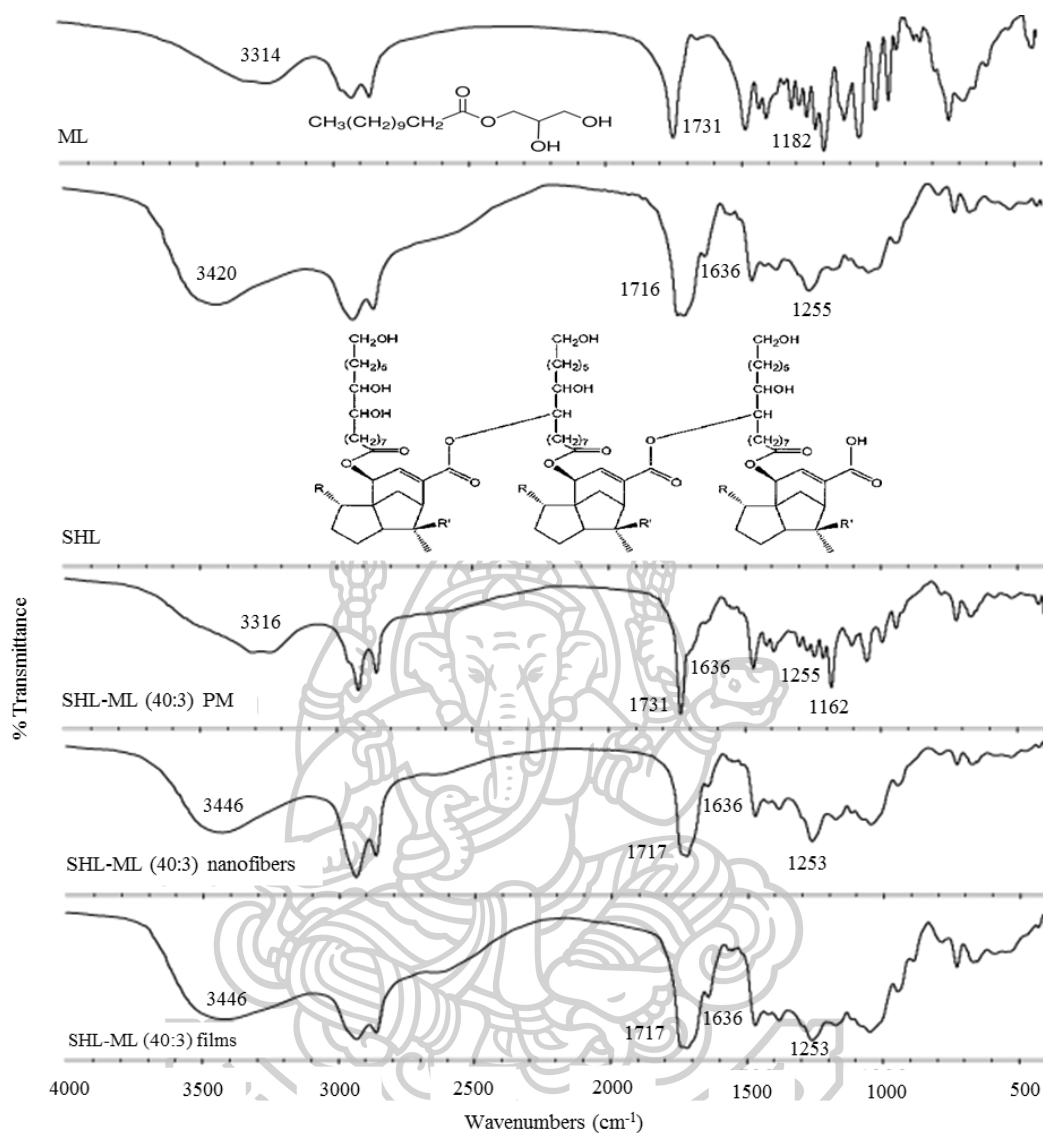


Figure 26 FTIR spectra of SHL, ML, their physical mixture, nanofibers and films in the ratio of 40: 3.

5.2.2 Evaluation of SHL-ML solution properties

The solution property might play a significant role in the electrospinning process affecting the morphology of the obtained nanofibers. During the electrospinning process, the solution was ejected from the needle tip depending on the stretching capacity of the solution which would be influenced by conductivity, viscosity and surface tension (19). Obviously, as illustrated in Table 18, the increased concentration of SHL led to a remarkable increase in viscosity, a slight decline in conductivity, but no significant change in surface tension. The viscosity was directly

related to SHL content. As the concentration of SHL was increased, the amount of polymer chain entanglement was also increased resulting in a significant elevation in viscosity (19). Generally, SHL is a non-ionic polymer with dielectric constant (ϵ) of 3.6 (67). When the SHL content was increased, the electrical conductivity of a solution seemed to decline as a result of the decreased charge carrier mobility. Meanwhile, the surface tension of a solution was not significantly different. This could be explained by the dispersed distribution of SHL molecules in the solution which was not projected to the surface.

In addition, the introduction of ML into the SHL solutions could also affect the solution properties. When the content of ML was increased, the solution tended to have a slight reduction in viscosity which was presumably owing to the change in chain conformation of SHL. As discussed earlier, ML could be entrapped between the chains of SHL during the process of electrospinning, thus reducing the entanglement of SHL chains and resulting in a slight decreased in viscosity. A slight decrease in conductivity might be induced by an increase in the amount of ML due to the non-ionic property of ML (68). However, the surface property of a solution was not changed after incorporating ML in the same manner as described above.

Table 18 Effect of SHL and ML concentrations on viscosity, conductivity and surface tension.

SHL content [% w/w]	ML content [% w/w]	Solution properties		
		Viscosity [mPa.s]	Conductivity [μ S]	Surface tension [mN/m]
35.0	1.0	454.2	26.41	22.4
35.0	2.0	335.4	26.33	21.8
35.0	3.0	251.5	26.29	21.6
37.5	1.0	676.7	23.75	22.0
37.5	2.0	561.9	23.27	22.1
37.5	3.0	411.8	23.05	21.3
40.0	1.0	750.8	22.23	22.4
40.0	2.0	705.3	20.97	21.8
40.0	3.0	643.4	20.64	21.6

5.2.3 Experimental design

5.2.3.1 Effects of the independent parameters on the morphology of SHL-ML nanofibers

A series of 19 experiments based on a 2^4 full factorial design with three replicated centre points was performed (Table 19). As demonstrated in Figure 27A and Figure 29, Pareto charts and the diameter distributions of nanofibers at different concentrations of SHL and ML revealed that the SHL content (X_1) had a tremendous effect on the diameter of fibres while the ML level (X_2) was the minor factor. For examples, electrospun fibres prepared from 40% w/w SHL (Figure 29D, 29E) indicated the larger diameter as compared to those prepared from 35% w/w SHL with the same concentration of ML (Figure 29A, 29E). Similarly, the electrospun fibres prepared from a higher concentration of ML (Figure 29A, 29B) demonstrated the larger fibre size as compared to those prepared from a lower concentration of ML (Figure 29D, 29E) although less extent was observed. As mentioned earlier (Table 18), the increased concentration of SHL resulted in the significant increase of viscosity and the slight decrease of conductivity leading to a reduction in the stretching capacity of the solution. As a result, nanofibers with large diameters might be obtained (19). Another factor affecting the fibre diameter was the concentration of ML. Based on theoretical expectation, an increase in the viscosity of electrospun solution contributes to an increase in the resultant fibre diameter due to a decrease in the stretching capacity during the electrospinning process (19). By contrast, the fabricated nanofibers appeared to be thicker with the presence of increased ML, although the reduced viscosity was clearly indicated. In this case, the influence of viscosity as well as the stretching capacity might be presumably dominated by another factor. As explained in the section 5.2.1, the possible interaction between SHL and ML was observed. We therefore assumed that the interaction of ML seemed to be the likely cause of the reduced stretching ability of solutions and thus increasing the fibre diameter. ML might interact with the SHL by intercalating among the polymeric chains and thus impeding the elongation or stretching capacity (as postulated in Figure 28). Additionally, the slight decrease of solution conductivity as increasing ML contents also reduced the charge density of electrospun solutions leading to the impaired elastic force within the jet (19) (Figure 27).

The occurrence of beads on the electrospun fibres is considered as defect. As indicated by Pareto chart in Figure 27B, only the content of SHL (X_1) had a remarkable impact on the appearance of beads. The number of beads had a tendency to decrease with increasing concentration of SHL while the smooth fibres were obtained from 40% w/w SHL and 3% w/w ML (Figure 29). Based on Table 15, an increase in the viscosity of SHL might lead to the high interaction between the polymers and solvent molecules. The aggregation probability of the solvent molecules was thus reduced. As a result, the beaded fibres were gradually changed to smooth fibres (19). In order to predict the impact of independent factors on the diameter of fibre (Y_1) and the amount of bead (Y_2) represented by bead-to-fibre ratio, mathematical models were performed as presented in the following equations. The Equation 3 and 4 referred to coded factors with R^2 values of 0.7480 and 0.7527, respectively indicating the good fit of the model.

$$\text{Diameter} = 173.81(X_1) + 60.69(X_2) + 542.89 \quad (3)$$

$$\text{Bead amount} = 0.48 - 0.39(X_1) \quad (4)$$

Table 19 Full factorial design and experimental responses, including fibre diameter and bead amount, for each design point of SHL and ML contents, applied voltage and flow rate.

Run	SHL content (X_1)	ML content (X_2)	Applied voltage (X_3)	Flow rate (X_4)	Fibre diameter (Y_1) [nm]	Bead amount (Y_2)
1	-1	-1	-1	-1	297	0.76
2	+1	-1	-1	-1	554	0.05
3	-1	+1	-1	-1	378	1.04
4	+1	+1	-1	-1	741	0.02
5	-1	-1	+1	-1	309	0.80
6	+1	-1	+1	-1	774	0.03
7	-1	+1	+1	-1	448	1.04
8	+1	+1	+1	-1	695	0.02
9	-1	-1	-1	+1	315	1.20
10	+1	-1	-1	+1	714	0.16
11	-1	+1	-1	+1	549	0.43
12	+1	+1	-1	+1	830	0.03
13	-1	-1	+1	+1	357	0.96
14	+1	-1	+1	+1	783	0.03
15	-1	+1	+1	+1	544	0.42
16	+1	+1	+1	+1	888	0.03
17	0	0	0	0	394	0.75
18	0	0	0	0	411	0.65
19	0	0	0	0	335	0.78

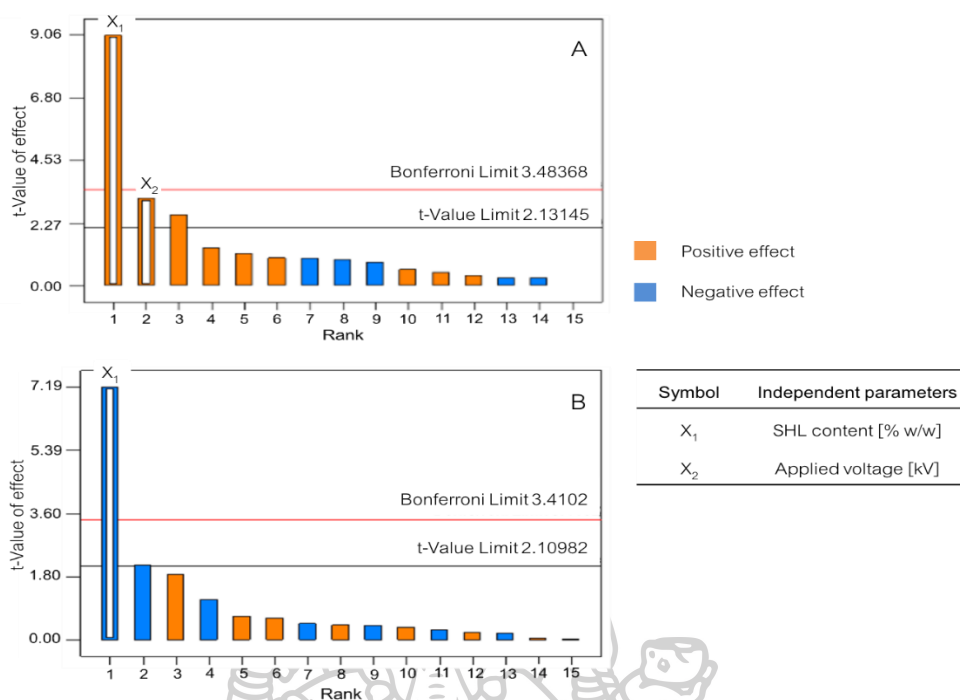


Figure 27 Pareto charts of the response values (A) nanofiber diameter and (B) bead amount.

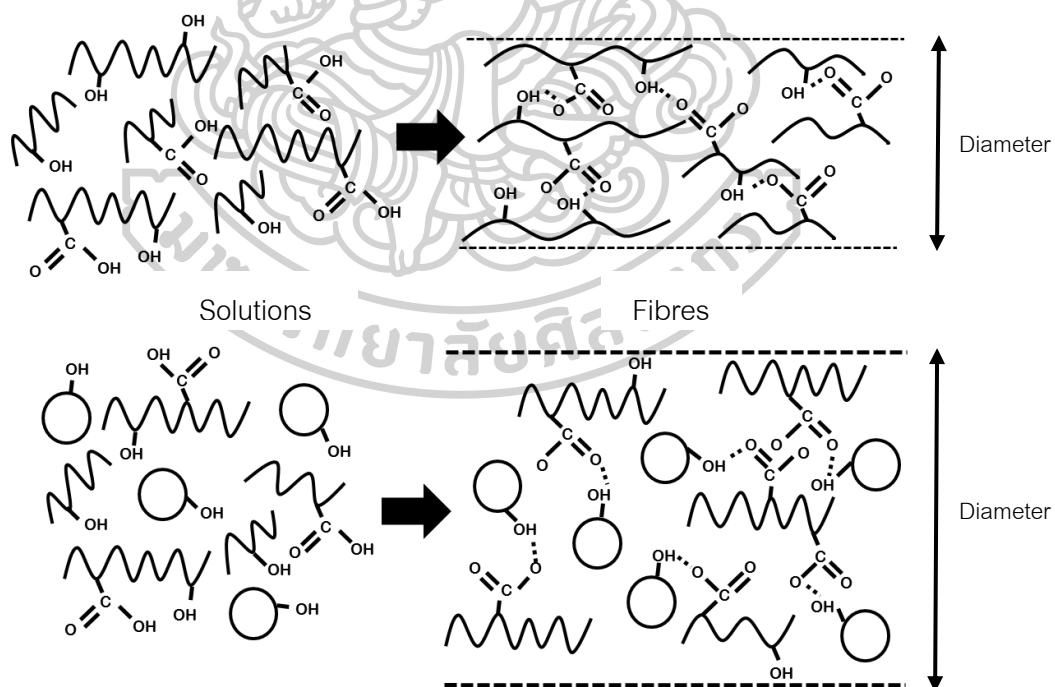


Figure 28 Schematic diagram representing the influence of ML on fibre diameter.

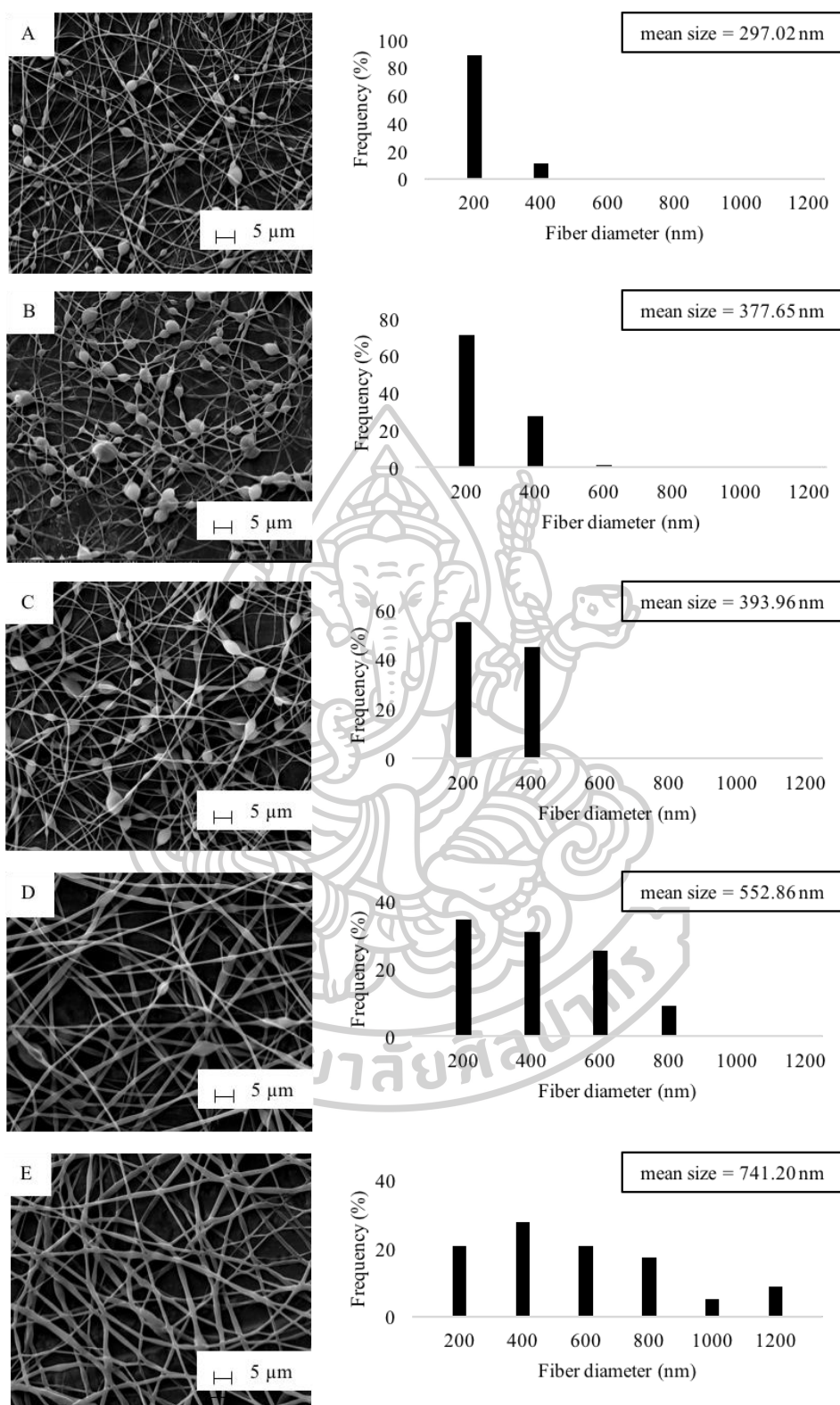


Figure 29 SEM images and diameter distribution of SHL-ML nanofibers at the weight ratio of (A) 35: 1, (B) 35: 3, (C) 37.5: 2, (D) 40: 1 and (E) 40: 3.

According to the analytical results shown in Table 20, the prediction of the models would be reliable referring to the P values of the models which were less than 0.05. Moreover, the lack of fit was not significant with P values of 0.1157(Y_1) and 0.0827(Y_2) indicating that these models were suitable. The coefficients represented the magnitude and direction of the factor effects. As presented in Table 18, SHL content (X_1) was the most influential parameter on the nanofiber diameter and bead amount with positive and negative relationships respectively, corresponding to the results from Pareto diagrams (Figure 27) and two-dimensional contour plots (Figure 30) which were also displayed in order to estimate the effect of each factor on the responses. Based on Figure 30A, the small fibres could be generated from the low amounts of SHL and ML. Meanwhile, the beadless fibres might be obtained from the high concentration of SHL regardless of the amount of SHL as depicted in Figure 30B.

Table 20 Analytical results for diameter and bead amount of SHL-ML fibres.

Responses	Coefficients	* P value	Std. Dev.	%CV	Mean value	R^2	F-value
Y_1 (nanofiber diameter)			106.87	19.68	542.89	0.7480	
X_1	173.81	< 0.0001					
X_2	60.69	0.0373					
Intercept	542.89						
Model		< 0.0001					23.74
Lack of fit		0.1157					8.06
Y_2 (bead amount)			0.22	45.08	0.48	0.7527	
X_1	-0.39	< 0.0001					
Intercept	0.48						
Model		< 0.0001					51.73
Lack of fit		0.0827					11.52

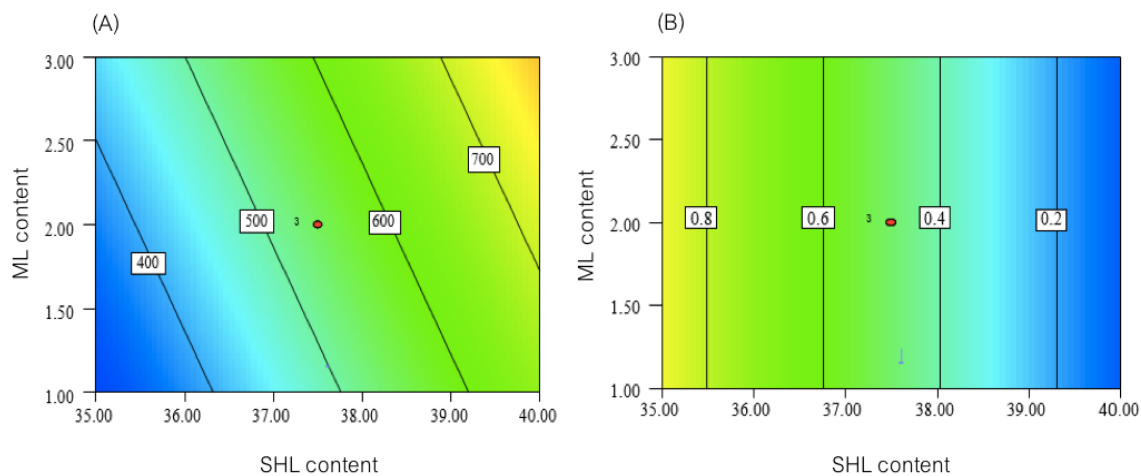


Figure 30 Two-dimensional contour plots presenting the effects of SHL and ML contents on (A) fibre diameter and (B) bead amount.

5.2.3.2 Optimization of SHL-ML nanofibers

The graphical model was presented with the aim of exploring the optimal region leading to the fabrication of the desired nanofibers. There are two types of the represented graph which are generally displayed as the three-dimensional response surface and the contour plot illustrated by the plane surface (69). In this study, an overlay contour plot was depicted as shown in Figure 31. The chosen desirable ranges of fibre diameter and bead-to-fibre ratio were 300-500 nm and 0-0.5, respectively. Based on the overlay plot, the yellow region illustrates the optimized area for the preparation of small (≤ 500 nm) and beadless (≤ 0.5) nanofibers. The example of the optimum conditions for the fabrication of SHL-ML nanofibers with thinner diameter (~ 488 nm) and beadless (~ 0.48) was attained at the SHL and ML contents of 37.5% and 1.1% w/w respectively, with the applied voltage of 18 kV and the flow rate of 0.8 mL/h.

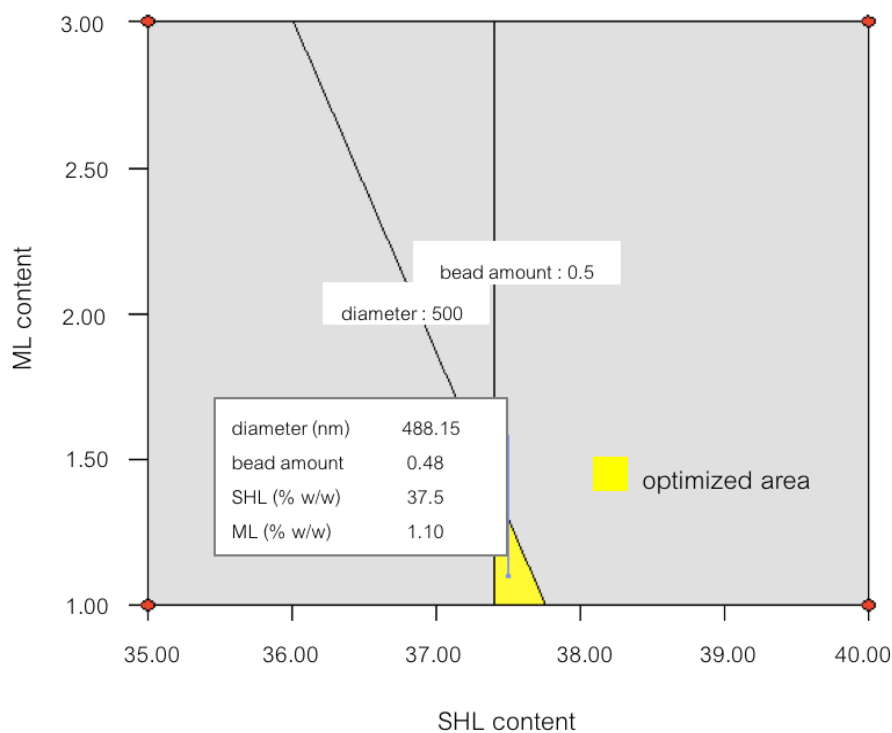


Figure 31 Overlay plot for optimization of SHL nanofibers loaded with ML.

5.2.3.3 The validation of the models

The obtained mathematic equations were validated for their efficiency to accurately predict fibre diameter and bead amount by using the replicated data set. As illustrated in Table 21, the measured data values and the values predicted by the estimated equations demonstrated a relative correlation as indicated by the RMSE values of 10.06 and 0.001 for diameter and bead amount, respectively. Thus, these resultant models were effective in predicting the fibre diameter and bead amount.

Table 21 Comparison between the actual and predicted values of diameter and bead amount of test data set.

	Diameter (nm)			Bead amount		
	Actual value	Predicted value	RMSE	Actual value	Predicted value	RMSE
SHL-ML (40:2) #1 (18 kV / 0.8 mL/h)	704.88	716.71	10.06	0.094	0.092	0.01
SHL-ML (40:2) #2 (18 kV / 0.8 mL/h)	723.06			0.082		
SHL-ML (40:2) #3 (18 kV / 0.8 mL/h)	727.81			0.100		

5.2.4 Time-kill kinetic study

In this work, time-kill kinetic study was carried out in order to determine the pharmacodynamics of ML, providing a profile of antimicrobial effect against *S. aureus*, *E. coli* and *C. albicans* which represented Gram-positive and Gram-negative bacteria and fungi, respectively, at different time periods. The percentage of living cells of *S. aureus*, *E. coli* and *C. albicans* over a period of time was presented in Figure 32. With regard to Figure. 32A, the number of *S. aureus* exposed to SHL-ML nanofibers gradually decreased as compared to those treated with ML solution which provided immediate killing potential, estimating that the release of ML from SHL nanofibers was dependent on the solubility of SHL in TSB media (pH ~ 7.3). Thus, the antibacterial action of SHL-ML nanofibers tended to be relatively sustained. The mode of action was previously reported. ML, a lipophilic compound, might be accumulated into the membrane bilayer, and consequently disintegrates the microbial membrane by fluidizing the lipids and phospholipids in the envelope of the organism, changing of the hydrogen bonding and the dipole-dipole interaction between acyl chains exerting bactericidal effects (42).

Nevertheless, many studies reported that *E. coli* was found to be less affected by ML (45). The difference in the killing effects of lipids against Gram-negative bacteria might depend on the differences in the outer membrane. Based on the structure of *E. coli*, the external membrane consists of proteins and lipopolysaccharides (LPS) which are composed of the O-polysaccharide chains

demonstrating a hydrophilic surface property. Therefore, lipids, which are hydrophobic molecules, could have difficulty in entering the bilayer, and be hardly diffused in the cytoplasm (46,47). This was consistent with the result as shown in Figure 32B. Both of SHL nanofibers loaded with ML and ML solution did not display activity against *E. coli*. The number of living cells was significantly increased over time.

As mentioned before, ML also has an antifungal effect by inhibiting spore germination and preventing the radial growth (43). Figure 32C demonstrated that some of *C. albicans* were killed by the ML released from fibres. However, after a period of 3 h, the amount of *C. albicans* then slightly increased, while the number of *C. albicans* exposed to ML in a solution form obviously declined without re-increasing. This might be explained by the effect of pH media on the solubility of SHL. According to the study of Limmatvapirat et al. (34), SHL with a pKa of 6.9–7.5 could be dissolved at pH above 7. Therefore, the solubility limitation of SHL in SDB media, which has an approximate pH value of 5.6, might occur. The release of ML from SHL carrier seemed to be incomplete which was due to the low pH of the liquid medium. During the initial period of exposure, only some of ML, especially at the surface of nanofibers was rapidly released and partially eradicated the *C. albicans* while most of ML was expected to be trapped in the SHL matrix and slowly released which was considered as the prolonged exposure time. As a result, the concentration of ML was not enough to inhibit the regrowth of living microorganisms after a 3-h exposure to SHL-ML nanofibers. Thus, the application of SHL-ML nanofibers in chronic wound management might be effective due to the predominant alkaline pH of chronic wounds (7.1–8.9), while treatment of acute wounds, which have low pH values of 5–6, seems to be restricted (70).

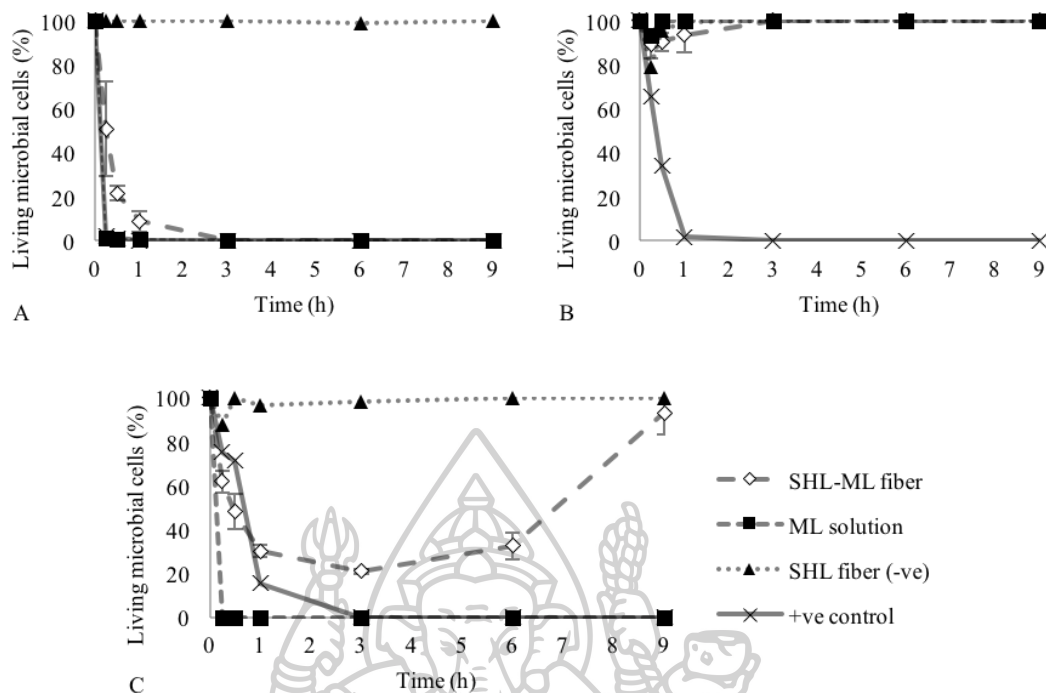


Figure 32 Kill kinetics of nanofibers for (A) *S. aureus*, (B) *E. coli* and (C) *C. albicans* over a period of 9 h.

5.3 Conclusions

SHL nanofibers loaded with ML could be developed for wound dressing application in order to prevent the delayed wound healing resulting from microbial infection. The main and interaction effects of factors on the morphology of nanofibers were investigated by using a full factorial design with three replicated centre points. According to the results, the SHL content was the major parameter affecting the fibre diameter, while the loaded ML content might be the minor parameter. The study of parameters on bead amount was evaluated revealing that the SHL content was the most significant negative impact on bead amount. The optimum conditions for the fabrication of small and beadless nanofibers were studied. The desired fibres could be obtained at the SHL and ML concentrations of 37.5% and 1.1% w/w respectively, with the applied voltage of 18 kV and the flow rate of 0.8 mL/h. Moreover, time–kill assays were performed in order to study the pharmacodynamics of antimicrobial agents, showing a profile of antimicrobial activity over time. The results showed that SHL nanofibers loaded with ML provided an excellent antibacterial activity against *S.*

aureus whereas *E. coli* was less affected. ML also exhibited antifungal effect against *C. albicans*. However, the release of ML might depend on the solubility of SHL carrier. Therefore the effect of pH in wound environment was considerable. The application of SHL-ML nanofibers in chronic wound management might be effective due to the predominant alkaline pH of chronic wounds, while treatment of acute wounds, which have low pH values, seems to be restricted.



CHAPTER 6
**Design and characterisation of electrospun
shellac/polyvinylpyrrolidone blended nanofibers loaded with
monolaurin for application in wound healing**

- 6.1 Introduction
- 6.2 Results and discussion
 - 6.2.1 Evaluation of physical characteristics and compatibility of SHL-PVP nanofibers loaded with ML
 - 6.2.1.1 Powder X-ray diffractometry (PXRD)
 - 6.2.1.2 Differential scanning calorimetry (DSC)
 - 6.2.1.3 Fourier transform infrared spectroscopy (FTIR)
 - 6.2.2 Evaluation of SHL-PVP-ML solution properties
 - 6.2.3 Experimental design
 - 6.2.3.1 Effects of the independent parameters on the morphology of SHL-PVP nanofibers loaded with ML
 - 6.2.3.2 Effects of the independent parameters on the mechanical properties of SHL-PVP nanofibers loaded with ML
 - 6.2.3.3 Effects of the independent parameters on the absorbency of SHL-PVP nanofibers loaded with ML
 - 6.2.4 The antimicrobial activity of SHL-PVP nanofibers loaded with ML
 - 6.2.5 Cell attachment assay
- 6.3 Cytotoxicity screening by the MTT bioassay
- 6.4 Conclusions

6.1 Introduction

Regarding the earlier part, SHL nanofibers loaded with ML were prepared successfully and exhibited significant antimicrobial activity. However, nanofibers comprising only SHL carry some disadvantages, including hydrophobicity, a lack of cell affinity and poor mechanical properties. To address these problems, the fabrication of electrospun nanofibers from the blended solutions of SHL with another polymer that possesses higher hydrophilicity, higher mechanical strength and better cell adhesion should be investigated. Polyvinylpyrrolidone (PVP), a water-soluble synthetic polymer, has been frequently used for biomedical applications, such as in hydrogels for skin substitutes and wound healing, due to its biocompatibility, biodegradability, low toxicity and good mechanical properties (12,13). However, the highly hygroscopic characteristic of PVP might pose problems for storage and rapid dissolution. Therefore, the blending of SHL with PVP might produce an excellent nanofiber mat for wound dressing with improved physiological properties.

This work aimed to fabricate an antimicrobial patch from electrospun SHL-PVP blended nanofibers through Design of Experiment. In this part, the effect of flow rate on the studied responses was ignored based on the results obtained from previous part. Therefore, the main effect of SHL ratio in an SHL-PVP blended solution, ML content and applied voltage, and their interactions on multiple observed responses, including morphology, mechanical properties, hydrophilicity and absorbability were examined. The physicochemical characteristics of the polymer-drug blend were analysed using differential scanning calorimetry, powder X-ray diffraction and FTIR spectroscopy. Cell attachment and antimicrobial activity assays were also performed to measure the wound-healing capacity of the resultant nanofibers.

6.2 Results and discussion

6.2.1 Evaluation of physical characteristics and compatibility of SHL-PVP nanofibers loaded with ML

The thermal behaviour, crystalline properties, molecular structure and interactions of ML-loaded SHL-ML blended nanofibers were investigated using PXRD, DSC and FTIR.

6.2.1.1 Powder X-ray diffractometry (PXRD)

According to the diffraction spectrum of ML powder demonstrated in Figure 33, obvious sharp peaks were observed at 2θ values of 9.6° , 19.6° , 20.5° and 23.0° , identifying its crystalline characteristics. Meanwhile, the PXRD patterns of SHL and PVP powders indicated the amorphous nature of the powder, as characterised by a broad halo pattern. Based on our previous study, the maximum concentration of ML loaded onto SHL nanofibers was approximately 7% w/w (71). The loaded content of ML seemed to be enhanced significantly when PVP was added. As illustrated in Figure 33, ML in the concentration range of 5%-20% w/w might be completely encapsulated in the SHL and PVP blended matrix, as described by the absence of crystalline peaks of ML in the obtained nanofibers, indicating that ML was completely dissolved and embedded in the polymeric matrix. However, the crystallinity appeared to be increased in the presence of a high level of loaded ML. Small crystalline peaks were presented in the PXRD profiles of electrospun SHL/PVP nanofibers comprising 35% w/w of ML, suggesting the incomplete entrapment of ML in the SHL and PVP blended matrix. In addition, the crystalline peak intensity of 35% w/w of ML loaded onto SHL/PVP blended nanofibers in a ratio of 25 to 75 seemed to be lower than those of the same amount of ML loaded onto SHL/PVP nanofibers in the ratio of 75 to 25, implying that ML was likely to be incorporated into the PVP portion.

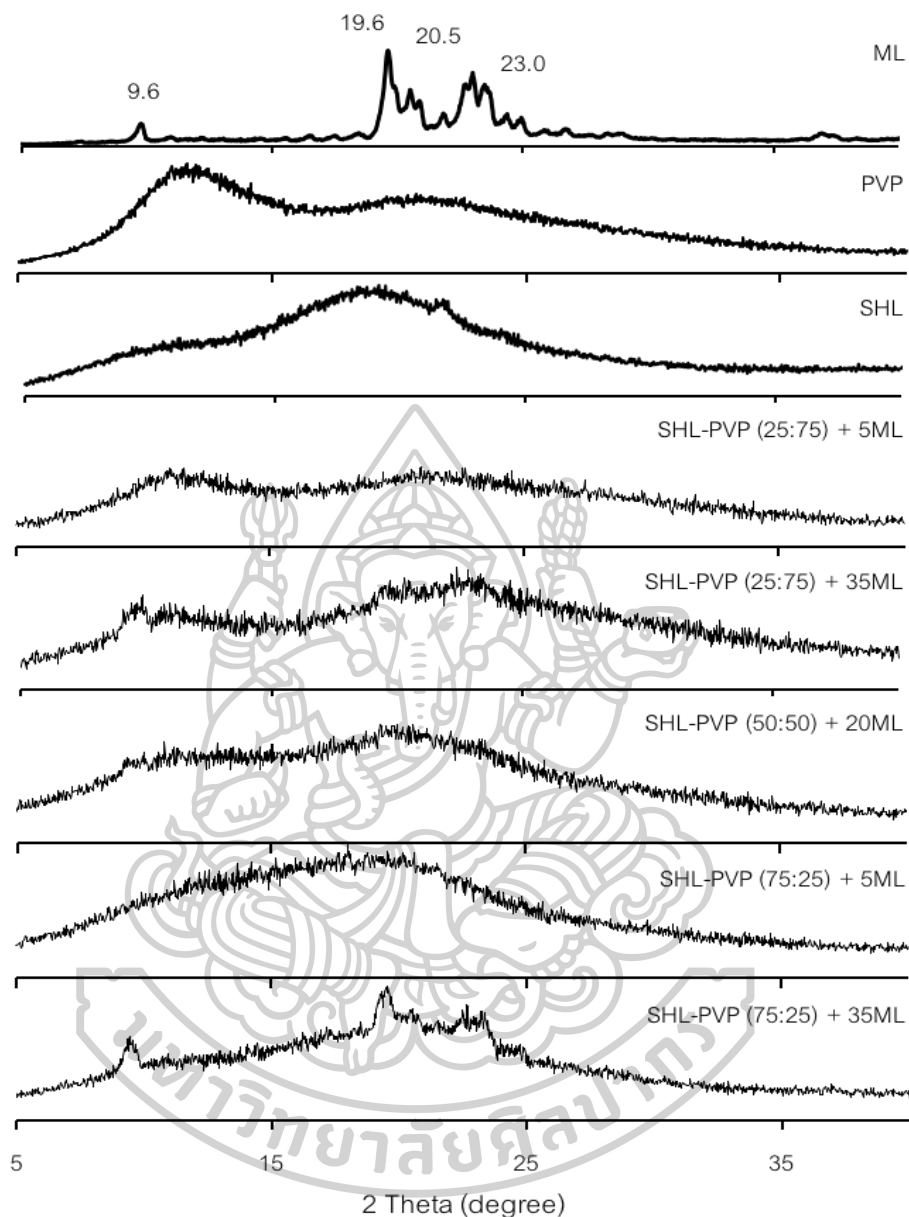


Figure 33 Powder X-ray diffraction patterns of ML, PVP, SHL and nanofibers at various ratios of SHL and PVP, and different amounts of loaded ML.

6.2.1.2 Differential scanning calorimetry (DSC)

Differential scanning calorimetry has been used to determine interactions between different compounds. Regarding the DSC thermogram of ML powder displayed in Figure 34, a large endothermic peak at about 66 °C, which was the melting point of ML, was clearly observed. Whereas, the melting peaks of SHL

and PVP powders were respectively obtained at about 69 °C and 141 °C. Similar to the results of PXRD described earlier, ML ranging from 5% to 20% w/w should be completely incorporated in the SHL/PVP polymer blended matrix during the process of electrospinning, as explained by the disappearance of endothermic peak of ML in the obtained electrospun nanofibers, suggesting that the crystalline state of ML was changed to the molecular state and interacted with the polymer matrix. Nevertheless, the DSC profiles of the nanofibers loaded with 35% w/w of ML also provided the endothermic peak, indicating that incomplete loading of ML might have occurred. Besides the melting peak, the enthalpy of melting was calculated from the obtained peak area. Referring to the results, the fusion heat of nanofibers was significantly increased from 0 to 59.38 J/g as an increase in the concentration of ML ranging from 5% to 35% w/w, which could be explained by the crystalline behaviour of high-ML-loaded nanofibers. Moreover, when comparing the enthalpy values of two different ratios of SHL and PVP in blended nanofibers comprising the same high percentage of ML (35% w/w), it was found that ML was more interactive and incorporated into the PVP part as described by the lower enthalpy value of 46.42 J/g for the SHL/PVP blend nanofibers in a ratio of 25 to 75. The enthalpy value for the SHL/PVP blend nanofibers in a ratio of 75 to 25 was 59.38 J/g.



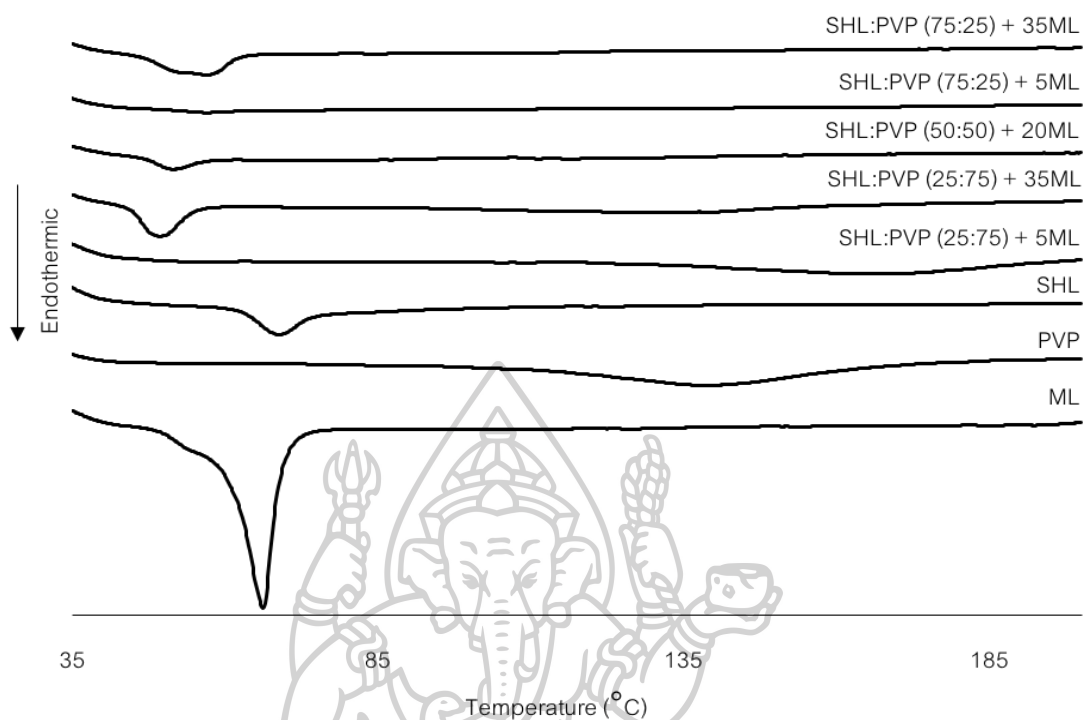


Figure 34 DSC thermograms of ML, PVP, SHL and nanofibers at various ratios of SHL and PVP, and different amounts of loaded ML.

6.2.1.3 Fourier transform infrared spectroscopy (FTIR)

The intermolecular interaction between the loaded ML and the polymeric matrix was further investigated by FTIR. Regarding the resultant FTIR spectra (Figure 35), ML exhibited the peaks at 1182 and 1731 cm^{-1} assigned to the C-O stretching of lauryl ester and the carbonyl (C=O) stretching, respectively. A broad peak with maxima around 3314 cm^{-1} was attributed to the O-H stretching of the hydroxyl groups on the glycerol backbone (65). The spectra of SHL consisted of a different broad O-H stretching band at 3420 cm^{-1} , a carbonyl (C=O) stretching peak at 1716 cm^{-1} , an alkenyl (C=C) peak at 1636 cm^{-1} and a C-O stretching peak at 1255 cm^{-1} (66). The appearance peaks of carbonyl (C=O) stretching vibration at 1655 cm^{-1} , and C-N vibration at 1292 and 1017 cm^{-1} were observed for the spectra of PVP (72). The spectra after loading ML onto the SHL and PVP blended matrix illustrated a slight shift of broad O-H and carbonyl peaks, indicating that coordination bonds

might have occurred. Moreover, the peak intensity of ML (1182 cm^{-1}) was obviously decreased, especially in the concentration range of 5%-20% w/w after incorporation into SHL-PVP fibres. The results confirmed the interaction of ML within the SHL-PVP blended matrix.



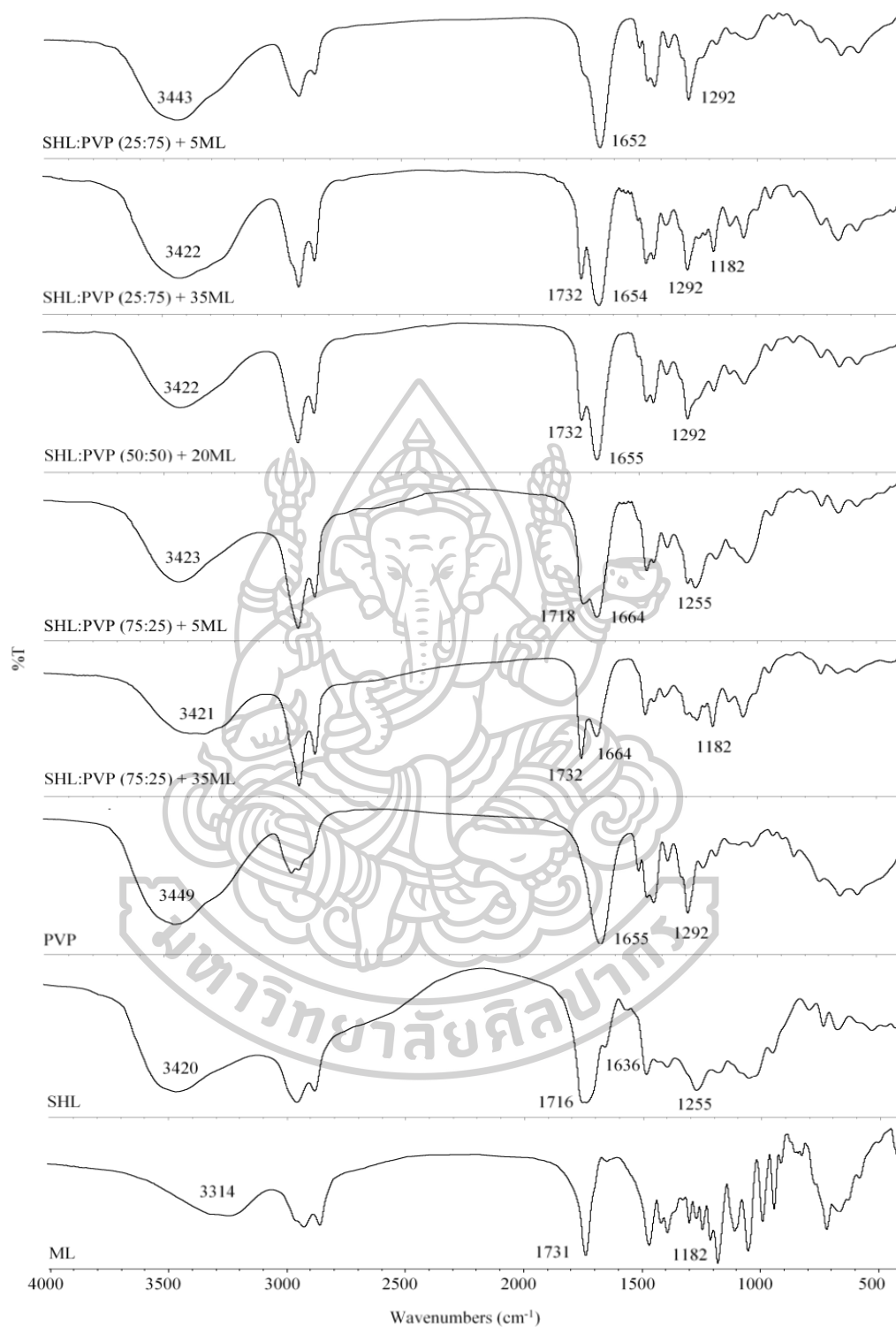


Figure 35 FTIR spectra of ML, PVP, SHL and nanofibers at various ratios of SHL and PVP, and different amounts of loaded ML.

6.2.2 Evaluation of SHL-PVP-ML solution properties

The morphology of the fabricated nanofibers can be controlled by properties of the electrospun solution, including conductivity, viscosity and surface tension, which might affect the stretching capacity as the solution is ejected from the needle during the process of electrospinning (19). According to Table 22, the increased ratio of SHL in the SHL/PVP blended solution contributed to the largely increased viscosity and conductivity, whereas the surface tension was not significantly different. The enhanced viscosity might be related to a dominant increase in chain entanglement as the amount SHL in the blended solutions was increased. A great decrease in electrical conductivity might have resulted mainly from an increase in non-ionised PVP content correlated with the relatively low conductivity of PVP compared with SHL. Based on the results of surface tension measurement, no significant difference was observed. This may imply that the dispersed polymer molecules in the solution were not projected to the surface.

Table 22 Effect of SHL ratio in blended solution and ML content on the solution properties.

SHL ratio in blended solution	ML content [% w/w]	Solution properties		
		Viscosity [mPa.s]	Conductivity [μ S]	Surface tension [mN/m]
25	5	186.4	13.40	23.1
25	35	182.1	11.95	22.6
50	20	205.2	23.90	22.8
75	5	348.5	30.57	22.7
75	35	336.8	28.80	22.4

Additionally, the presence of ML had an important impact on the solution properties. As illustrated in Table 22, an increase in the ML concentration could lead to a slight drop in viscosity and conductivity. The decreased viscosity might have occurred because the entrapment of ML between the polymeric chains was increased, resulting in a reduction in the entanglement of polymeric chains, in concordance with a previous report (71). The reduced electrical conductivity was typically due to an increase in the content of non-ionic molecules of ML (68). Nevertheless, the addition of ML did not lead to a significant change in the surface tension value. This effect could be explained in the same manner as discussed earlier.

6.2.3 Experimental design

6.2.3.1 Effects of the independent parameters on the morphology of SHL-PVP nanofibers loaded with ML

A 2^3 full factorial design with three replicated centre points was carried out. According to the Pareto charts (Figure 36) and the diameter distributions of nanofibers (Figure 37), the ratio of SHL in the SHL/PVP blended solution (X_1) was the most significant parameter affecting the fibre diameter. The minor factors were the content of ML (X_2) and the interaction between the SHL ratio and ML content (X_1X_2), respectively. Conversely, a negative relationship between the applied voltage (X_3) and the fibre diameter was observed.

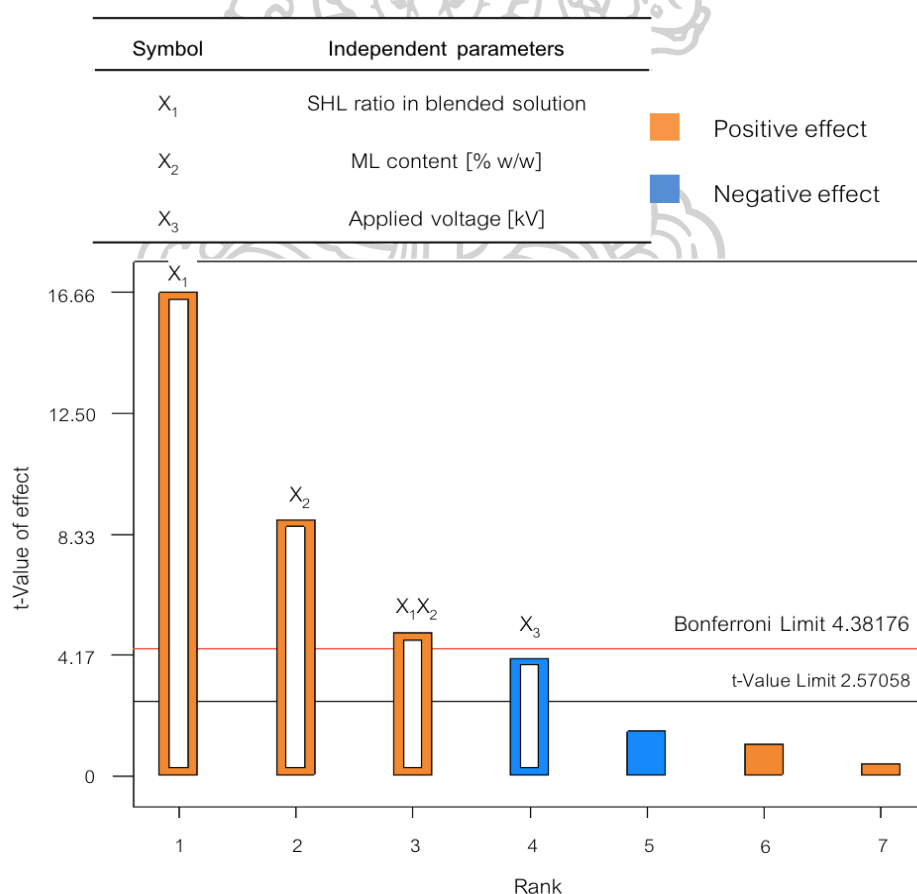


Figure 36 Pareto charts of nanofiber diameter.

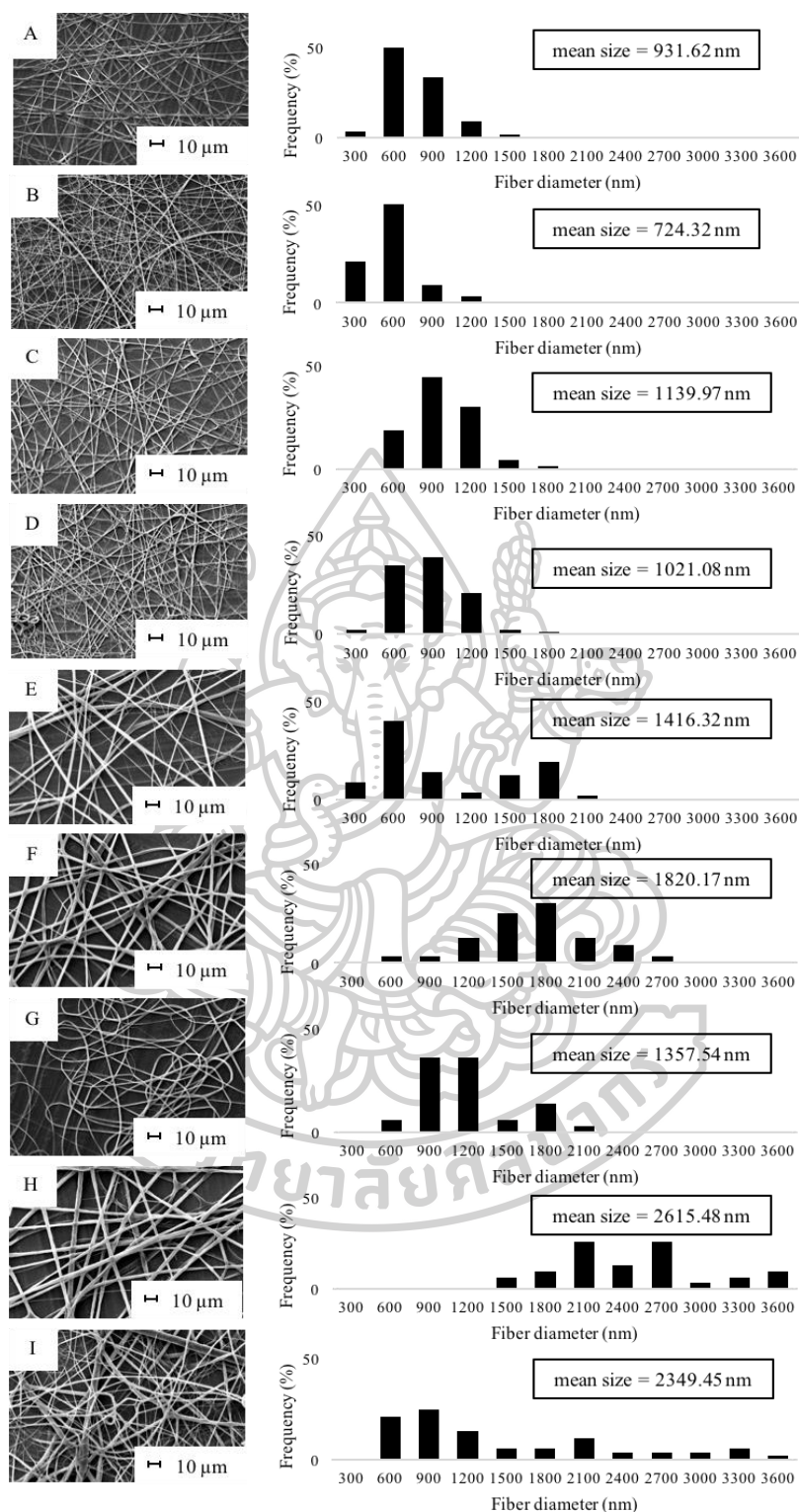


Figure 37 SEM images and diameter distributions of (A) SHL:PVP (25:75) + 5ML at 9 kV, (B) SHL:PVP (25:75) + 5ML at 27 kV, (C) SHL:PVP (25:75) + 35ML at 9 kV, (D) SHL:PVP (25:75) + 35ML at 27 kV, (E) SHL:PVP (50:50) + 20ML at 18 kV, (F) SHL:PVP (75:25) + 5ML at 9 kV, (G) SHL:PVP (75:25) + 5ML at 27 kV, (H) SHL:PVP (75:25) + 35ML at 9 kV and (I) SHL:PVP (75:25) + 35ML at 27 kV.

As discussed earlier, the presence of large nanofibers was apparently attributed to a decline in the stretching ability of the electrospun solution associated with an increasing SHL ratio in the blended solution (19). The concentration of ML was also significant. The obtained nanofibers tended to be thicker when the amount of ML was increased. This effect could be described as impairment of the elastic force within the jet because of the increased encapsulation of ML between the polymeric chains, along with the reduced charge density (71). Another important factor might be the interaction between the SHL ratio in the blended solution and the ML content. As shown in the interaction graph given in Figure 38, an increase in the fibre diameter seemed to be correlated with an increase in the loading ML concentration, especially at a high proportion of SHL. This may indicate a synergistic effect of these two factors. However, the fibre diameter may have been inversely related to the voltage applied. An elevation in applied voltage could lead to the fabrication of small fibres due to the contribution of increased charge repulsion and the strong electrical field to increased jet stretching (19).

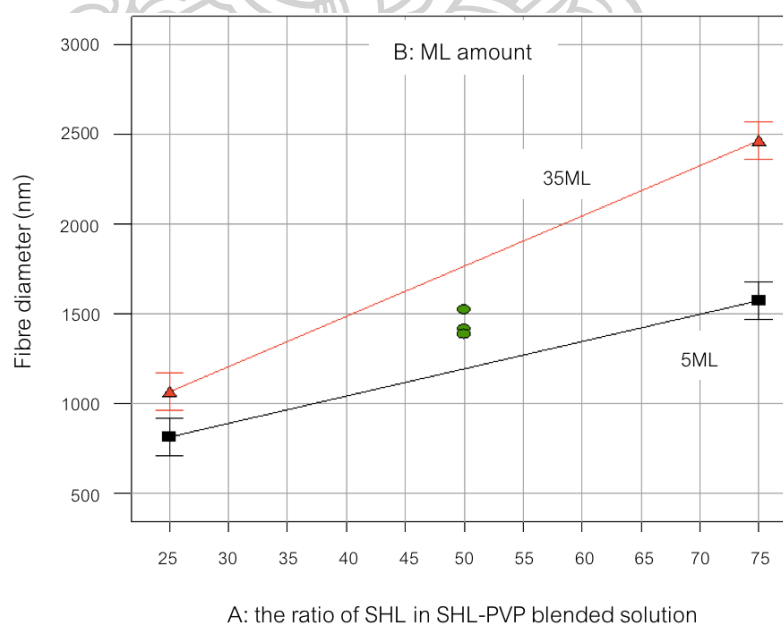


Figure 38 Interaction graph between the ratio of SHL in blended solution and ML amount.

The mathematical model in terms of coded factors presented in the following equation (Eq. 5) was created with the aim of predicting the effect of various

parameters on the morphology of the obtained fibres. The analytical results illustrated in Table 23 revealed that the predictive model was reliable, with a P value of less than 0.05. In addition, the P value for the lack-of-fit was 0.3863 (more than 0.05), indicating the suitability of the model. The good fit of the model was indicated by the R^2 value of 0.9858.

$$\text{Diameter} = 1480.55 + 540.63(X_1) - 286.38(X_2) - 131.87(X_3) + 0.427(X_1X_2) \quad (5)$$

Table 23 Analytical results for different responses, including morphology and mechanical properties.

Responses	Coefficients	* P value	Std. Dev.	%CV	Mean value	R^2	F-value
Y_1 (fibre diameter)			89.57	6.05	1480.55	0.9858	
X_1	540.63	< 0.0001					
X_2	286.38	0.0001					
X_3	-131.87	0.0059					
X_1X_2	160.13	0.0023					
Intercept	1480.55						
Model		< 0.0001					104.04
Lack of fit		0.3863					1.81
Y_2 (tensile strength)			5.223×10^{-3}	1.90	0.27	0.9997	
X_1	-0.086	< 0.0001					
X_2	0.10	< 0.0001					
X_3	0.059	< 0.0001					
X_1X_2	-0.012	0.0066					
X_1X_3	-0.052	< 0.0001					
X_2X_3	-4.986×10^{-3}	0.0738					
$X_1X_2X_3$	0.080	< 0.0001					
Intercept	0.27						
Model		< 0.0001					1301.19
Lack of fit		0.2858					2.08
Y_3 (elongation)			0.65	28.75	2.25	0.9834	
X_1	-1.78	0.0044					
X_2	-0.28	0.3036					
X_3	0.59	0.0829					
X_1X_2	0.20	0.4375					
X_1X_3	-0.97	0.0243					
X_2X_3	-1.40	0.0088					
$X_1X_2X_3$	1.67	0.0053					
Intercept	2.25						
Model		0.0113					25.43
Lack of fit		0.4225					1.00

According to our previous works, the morphology of nanofibers prepared from an SHL solution appeared to be relatively beaded and disordered (71,73). However, in this study, the formation of bead defects was not observed. The primary explanation for this phenomenon could be that the addition of PVP in the SHL solution seemed to improve the stretching of the liquid jet, owing to its excellent mechanical behaviour, leading to the fabrication of uniform nanofibers with no bead formation instead of discontinuous nanofibers with beads (13,19).

6.2.3.2 Effects of the independent parameters on the mechanical properties of SHL-PVP nanofibers loaded with ML

Due to the poor mechanical properties of SHL, the stress resistance of the fabricated SHL nanofibers tended to be limited. In order to provide mechanical protection and improve flexibility, SHL should be blended with another polymer with favourable mechanical properties. In this work, PVP, a synthetic material with good mechanical characteristics, was selected. The tensile strength and elongation at the breaking point were evaluated. According to the Pareto charts (Figure 39A), the tensile strength of the resultant mat was primarily dependent on the concentration of loaded ML (X_2). Meanwhile, the SHL ratio in a blended solution (X_1) was the second factor negatively correlated with tensile strength. Consequently, the applied voltage (X_3) and the interactions between these factors were significant.

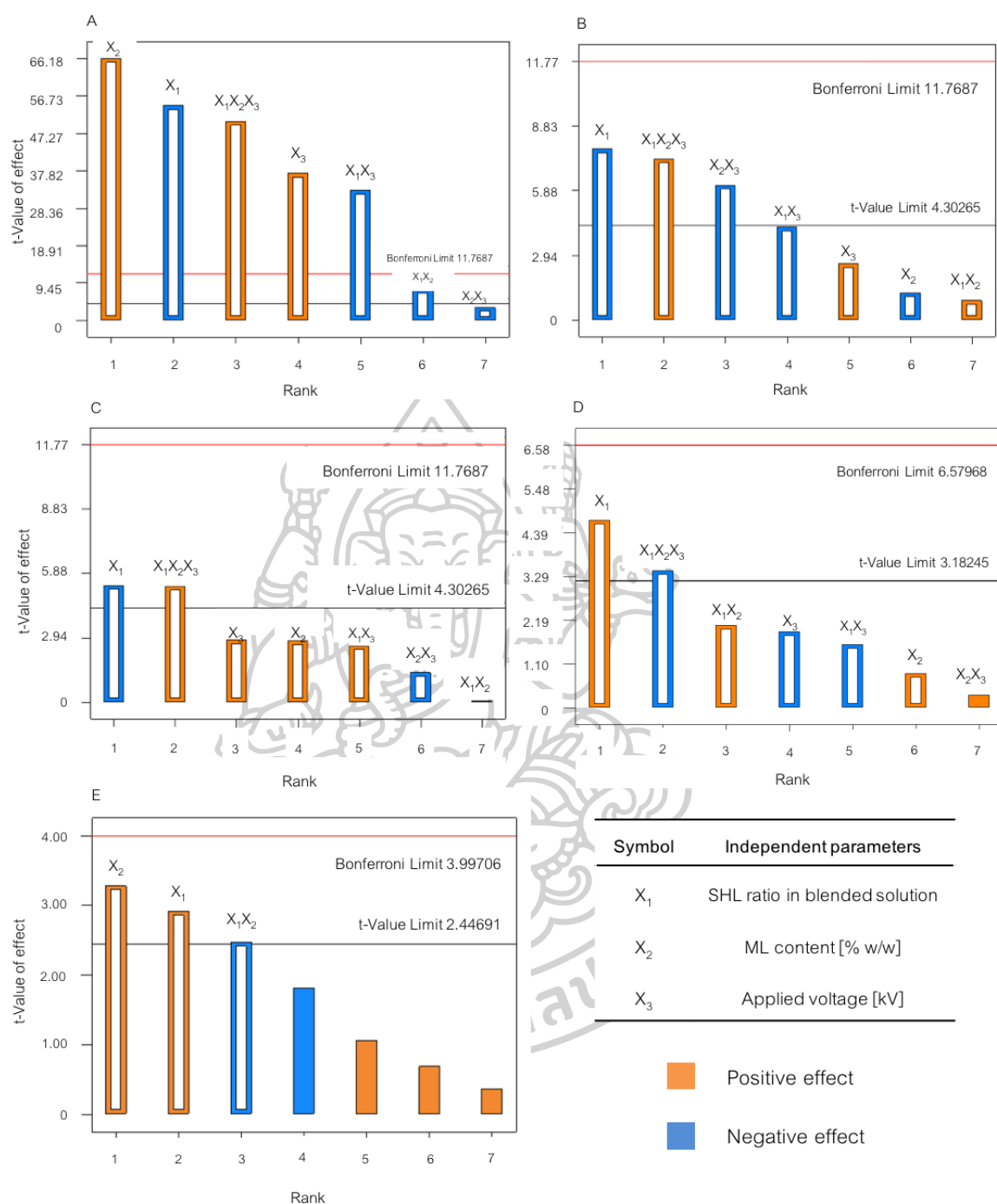


Figure 39 Pareto charts of (A) tensile strength, (B) elongation, (C) contact angle, (D) polarity and (E) absorbency.

An increase in tensile strength owing to the addition of ML suggested a strong interaction between loaded ML and the polymeric carrier after encapsulation. Bonding interactions seemed to play a significant role in promoting the stress durability of the obtained nanofibers. Moreover, based on the characteristic of ML as

a plasticiser, the incorporation of ML into electrospun SHL-PVP fibres might result in a reduction of fracture behaviour, along with an improvement of tensile strength (74). Another important factor was the SHL ratio in a blended solution. The tensile strength was greatly enhanced as the SHL to PVP ratio decreased. The introduction of PVP was found to improve stress resistance due to its good mechanical properties, whereas SHL, which is a kind of natural resinous oligomer consisting of a few units of monomer ($MW \approx 1000$ D), could be brittle (75). An effect of voltage on tensile strength was also observed. A high voltage might lead to increased tensile behaviour. During the electrospinning process, the polymer stretch was remarkably extended as the applied voltage was increased. As a result, finer nanofibers with small diameters were obtained; these nanofibers were densely packed and uniformly oriented, contributing to the enhancement of force resistance (76). The ideal wound dressing should be flexible and resilient in order to conform to shapes of wounds located on different body parts, resulting in excellent coverage and protection of the wound from infection. The elongation value could be used to determine the elasticity of the fibres. As shown in Figure 39B, the SHL ratio in a blended solution might have an inverse effect on the elongation of nanofiber mats. The improved elongation was particularly due to the increased content of PVP, a synthetic material with good mechanical properties.

The predictive models were performed and displayed in Eq. (6) and Eq. (7) in order to determine the influence of factors on the mechanical properties of nanofibers including tensile strength and elongation, respectively.

$$\text{Sqrt}(\text{tensile strength}) = 0.27 - 0.086(X_1) + 0.10(X_2) + 0.059(X_3) - 0.012(X_1X_2) - 0.052(X_1X_3) - 4.986 \times 10^{-3}(X_2X_3) + 0.080(X_1X_2X_3) \quad (6)$$

$$\text{Elongation} = 2.25 - 1.78(X_1) - 0.28(X_2) + 0.59(X_3) + 0.20(X_1X_2) - 0.97(X_1X_3) - 1.40(X_2X_3) + 1.67(X_1X_2X_3) \quad (7)$$

According to the ANOVA results (Table 23), the P values of the models were less than 0.05, indicating their reliability. The P values for the lack-of-fit test were 0.2858(Y_2) and 0.4225(Y_3), indicating that these models might be suitable for prediction. The R^2 values were 0.9997(Y_2) and 0.9834(Y_3), illustrating the

goodness-of-fit of these models.

6.2.3.3 Effects of the independent parameters on the wettability of SHL-PVP nanofibers loaded with ML

An effective wound dressing should be easily placed onto the wound bed and remain firmly adhered to the wound surface during the healing process. In addition, an ideal wound dressing is designed to provide a moist wound environment, stimulating the process of wound healing. Therefore, a nanofibrous wound dressing with good surface wettability might be a suitable option. The contact angle is the primary indicator of fibre wettability. According to our results, the contact angles of the SHL-PVP nanofiber membranes were all less than 90° , indicating favourable wettability, while the contact angle of SHL fibres was greater than 90° , corresponding to low wettability. Water would reduce its contact with the surface (59). In general, as the PVP content in a blended solution increases, the contact angle of water droplets on the surface of the obtained nanofibers should decrease due to the hydrophilic character of PVP. Conversely, the Pareto charts illustrated in Figure 39C present the possible indirect influence of the SHL ratio in a blended solution on the contact angle. An increase in the concentration of PVP might lead to a reduction in the water contact angle. This unlikely situation could be described by the fusion of the obtained thick layer nanofibers as shown in SEM images (Figure 40), which was attributed to the hygroscopic nature of PVP, resulting in a decrease in the porosity of nanofibers; thus, water could not easily pass through the membrane. Similarly, an increase in the PVP ratio might give a reduction in the calculated polarity (Figure 39D) due to a significant increase in the water contact angle as discussed before.

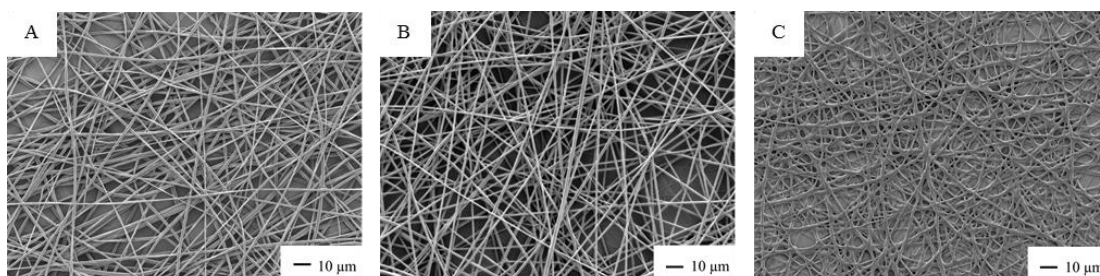


Figure 40 SEM images of SHL-PVP-ML nanofibers at the weight rate of (A) 75:25:5, (B) 50:50:5 and (C) 25:75:5.

The mathematic equations (Eq. 8 and Eq. 9) were employed to examine the individual factor effects on the contact angle and polarity of the fibre mats, respectively.

$$\begin{aligned} \text{Contact angle} = & 29.60 - 10.83(X_1) + 5.69(X_2) + 5.78(X_3) - 0.12(X_1X_2) + 5.24(X_1X_3) \\ & - 2.78(X_2X_3) + 10.73(X_1X_2 X_3) \end{aligned} \quad (8)$$

$$\begin{aligned} \text{Polarity (\%)} = & 32.14 + 6.64(X_1) + 1.21(X_2) - 2.69(X_3) + 2.92(X_1X_2) - 2.24(X_1X_3) - \\ & 4.85(X_1X_2 X_3) \end{aligned} \quad (9)$$

The analytical results, as illustrated in Table 24, reported that the obtained predictive models were reliable, with P values of less than 0.05 for both models. The lack-of-fit P values of both models were greater than 0.05, indicating the suitability of these predictive models. The R^2 value of contact angle and polarity were 0.9585 and 0.9323, indicating the goodness-of-fit of the models.

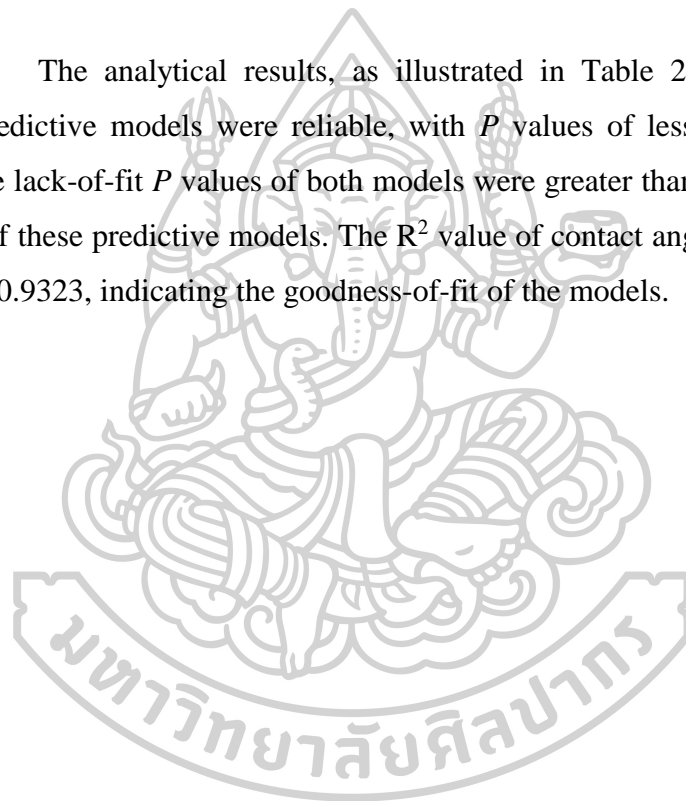


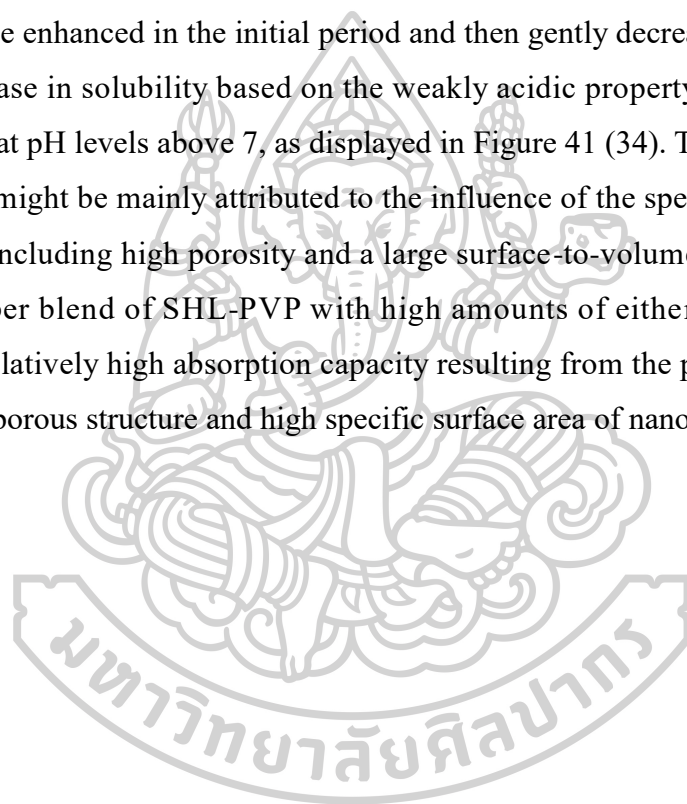
Table 24 Analytical results for different responses, including surface wettability and absorbency.

Responses	Coefficients	*P value	Std. Dev.	%CV	Mean value	R ²	F-value
Y ₄ (contact angle)			6.20	20.96	29.60	0.9585	
X ₁	-10.83	0.0159					
X ₂	5.69	0.0808					
X ₃	5.78	0.0781					
X ₁ X ₂	-0.12	0.9590					
X ₁ X ₃	5.24	0.0968					
X ₂ X ₃	-2.78	0.2943					
X ₁ X ₂ X ₃	10.73	0.0164					
Intercept	29.60						
Model		0.0431					9.90
Lack of fit		0.3456					1.50
Y ₅ (polarity)			3.62	11.25	32.14	0.9323	
X ₁	6.64	0.0065					
X ₂	1.21	0.3965					
X ₃	-2.69	0.1029					
X ₁ X ₂	2.92	0.0844					
X ₁ X ₃	-2.24	0.1545					
X ₁ X ₂ X ₃	-4.85	0.0191					
Intercept	32.14						
Model		0.0251					9.17
Lack of fit		0.8871					0.13
Y ₆ (absorbency)			8.70	199.07	-4.37	0.7591	
X ₁	8.36	0.0299					
X ₂	9.41	0.0184					
X ₁ X ₂	-7.10	0.0545					
Intercept	-4.37						
Model		0.0144					7.35
Lack of fit		0.2817					2.83

6.2.3.4 Effects of the independent parameters on the absorbency of SHL-PVP nanofibers loaded with ML

During the inflammatory stage of wound healing, the levels of mediators such as histamine and bradykinin might be enhanced, leading to vasodilation and thereby producing wound exudate. Excessive exudate could result in skin maceration and excoriation, thus delaying wound healing (77). The absorptive nature of a wound dressing could assist in the management of highly exuding wounds by allowing the dressing to retain some of the exudate. The Pareto charts in

Figure 39E illustrate that the proportion of SHL in a blended solution and the ML content might have crucial impacts on the absorption capacity of the obtained nanofibers. The capacity for absorption tended to increase in parallel with the SHL content and the incorporated ML concentration in blended solutions. This occurrence might be due to the capacity of SHL and ML, which are naturally hydrophobic, to protect PVP from erosion. Generally, the PVP nanofiber mat was found to be completely dissolved in PBS solution (pH 7.4) within a 10-min period due to the highly hydrophilic nature of PVP. In contrast, the absorption capacity of SHL fibres seemed to be enhanced in the initial period and then gently decreased, together with a slight increase in solubility based on the weakly acidic property of SHL, favouring dissolution at pH levels above 7, as displayed in Figure 41 (34). The initial increase in absorption might be mainly attributed to the influence of the specific structure of the nanofiber, including high porosity and a large surface-to-volume ratio. Accordingly, the nanofiber blend of SHL-PVP with high amounts of either SHL or ML might possess a relatively high absorption capacity resulting from the protection of PVP as well as the porous structure and high specific surface area of nanofibers themselves.



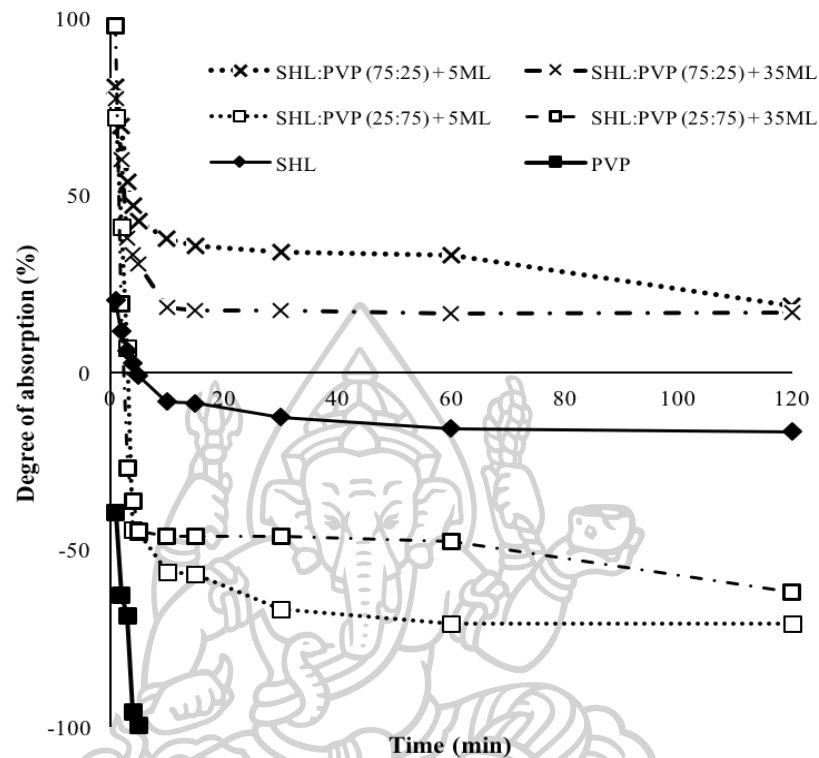


Figure 41 The degree of absorption of nanofibers (at 27 kV) over a period of 15 min.

The following mathematical model (Eq. 10) was employed to evaluate the relationship between the independent factors and the absorbency of the resultant fibres as the response variable.

$$\text{Absorbency} = 0.71302(\text{SHL ratio}) + 1.57375(\text{ML content}) - 0.018923(\text{SHL ratio} \times \text{ML content}) - 52.57523 \quad (10)$$

The analytical results shown in Table 24 indicated that a good predictive model with no significant lack of fit ($P > 0.05$) and an R^2 value of 0.7591 was developed.

6.2.4 The antimicrobial activity of SHL-PVP nanofibers loaded with ML

Time-kill kinetics of SHL-PVP fibres loaded with ML against typical skin flora, including *S. aureus* and *C. albicans*, were studied over time. According to Figure 42, all blended nanofibers exhibited excellent antimicrobial activity against *S. aureus*, as illustrated by the rapid decline in the number of colonies at the initial time points. In addition, consistent reduction of *S. aureus* was maintained over a period of 6 h. According to previous reports, the bactericidal mode of action of ML is incorporation into the microbial membrane bilayer and consequent disintegration of lipids and phospholipids, the composition of the cell envelope, due to the lipophilic nature of ML (42). Thus, the solubility of SHL in SDB media (approximate pH value of 5.6) might be relatively restricted. During the initial exposure period, the rapid release of ML from the polymeric carrier occurred, based on the high solubility of PVP and the presence of ML on the fibre surface. After a prolonged exposure time, the number of *C. albicans* tended to decrease slightly as a result of the slow release of entrapped ML from the SHL matrix.

As stated earlier, ML could inhibit the germination of spores and also prevent radial growth of fungi (43). Regarding the antifungal results (Figure 43), the abundance of *C. albicans* appeared to gradually decrease over time as compared with the antibacterial effect on *S. aureus*. It might be estimated that the release of ML would depend on the dissolution of PVP as well as SHL in a liquid medium. Shellac could be effectively dissolved at a pH above 7, owing to its pK_a of 6.9–7.5 (34). Another factor affecting the release of ML from the nanofibers was the amount of incorporated ML. The blended nanofibers comprising 5% w/w of ML demonstrated incomplete fungicidal activity against *C. albicans*. This could be explained by the viscosity effect. The release of ML from the viscous polymeric carrier, especially with the high proportion of PVP, seemed to be retarded, as indicated by the high total amount of fibres added to media broth to give the same final concentration of 2 mg/mL. The influence of applied voltage on the release of ML was also significant. As discussed earlier, finer fibres could be fabricated with the use of a high-voltage power supply. An increase in charge repulsion and the electrical field might lead to an increase in jet stretching. An electrospun nanofiber with a small diameter would have

high specific surface area and porosity, contributing to the increased release of ML as shown in Figure 43B.

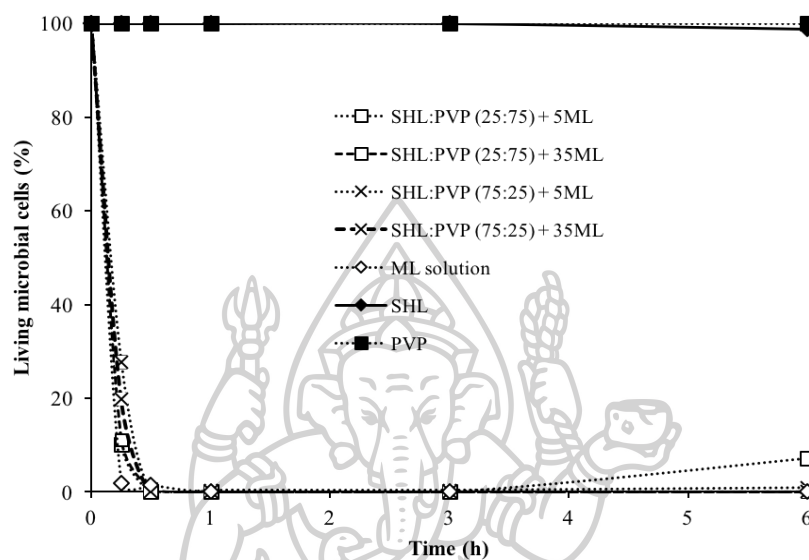


Figure 42 Kill kinetics of nanofibers (at 27 kV) for *S. aureus* over a period of 6 h.



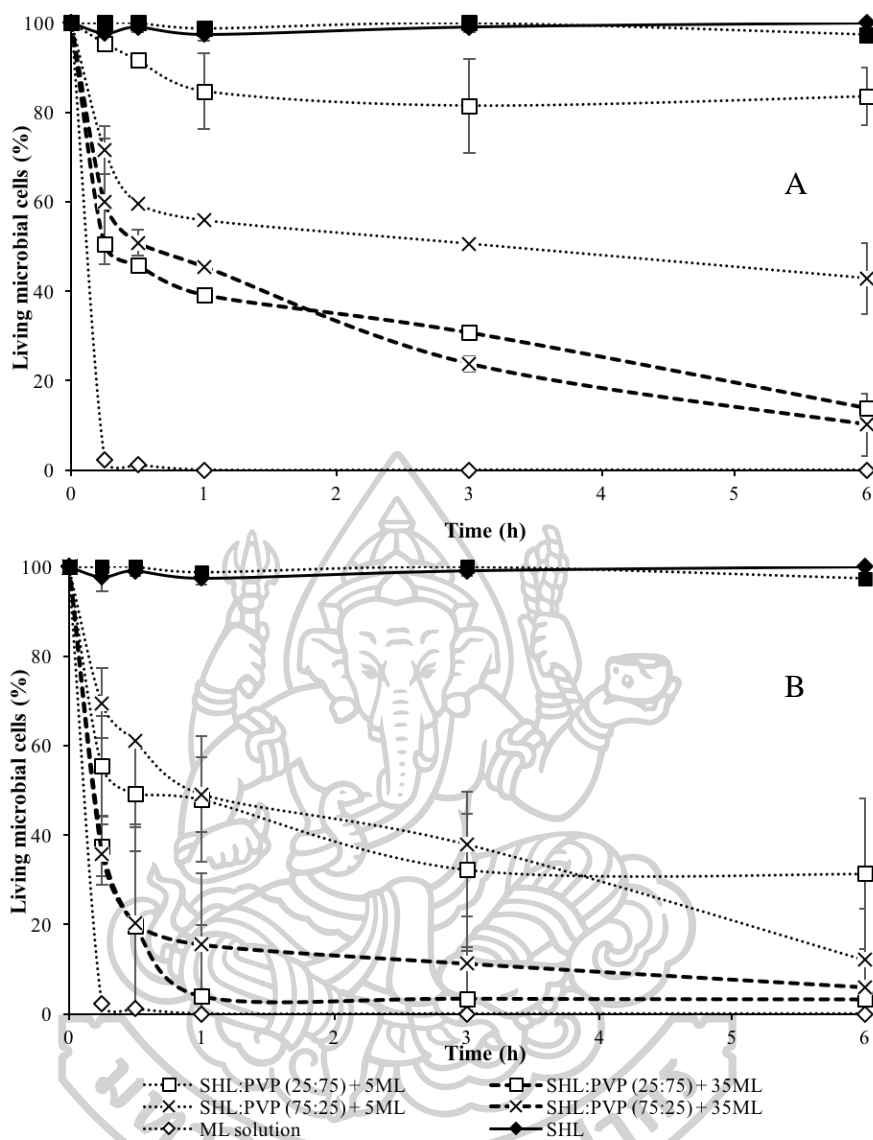


Figure 43 Kill kinetics of nanofibers at (A) 9 kV and (B) 27 kV for *C. albicans* over a period of 6 h.

6.2.5 Cell attachment assay

The healing of a full-thickness skin wound might generally require the synthesis and remodelling of dermal and epidermal elements, especially fibroblasts, which might play a significant role in supporting the wound-healing process by migrating to the wound site, undergoing proliferation and changing the wound-healing environment, leading to wound contraction (78). Figure 44 illustrates the morphology of cells seeded on nanofibers at different time points. The results showed that a nanofiber blend of SHL-PVP with high ratio of PVP could remarkably promote

cell attachment in the initial period, whereas the affinity of cell adhesion after 40 min of seeding seemed to be dramatically decreased with increasing dissolution of PVP. This implies that enhanced cell attachment might be attributed to the high water solubility of PVP. Conversely, when the proportion of SHL was increased, the number of remaining adherent cells tended to increase gradually due to the erosion protection and sustained dissolution of PVP over a period of time, which was in accordance with the earlier absorbency results. However, the effect of the loaded ML content on cell attachment was likely to be less significant.

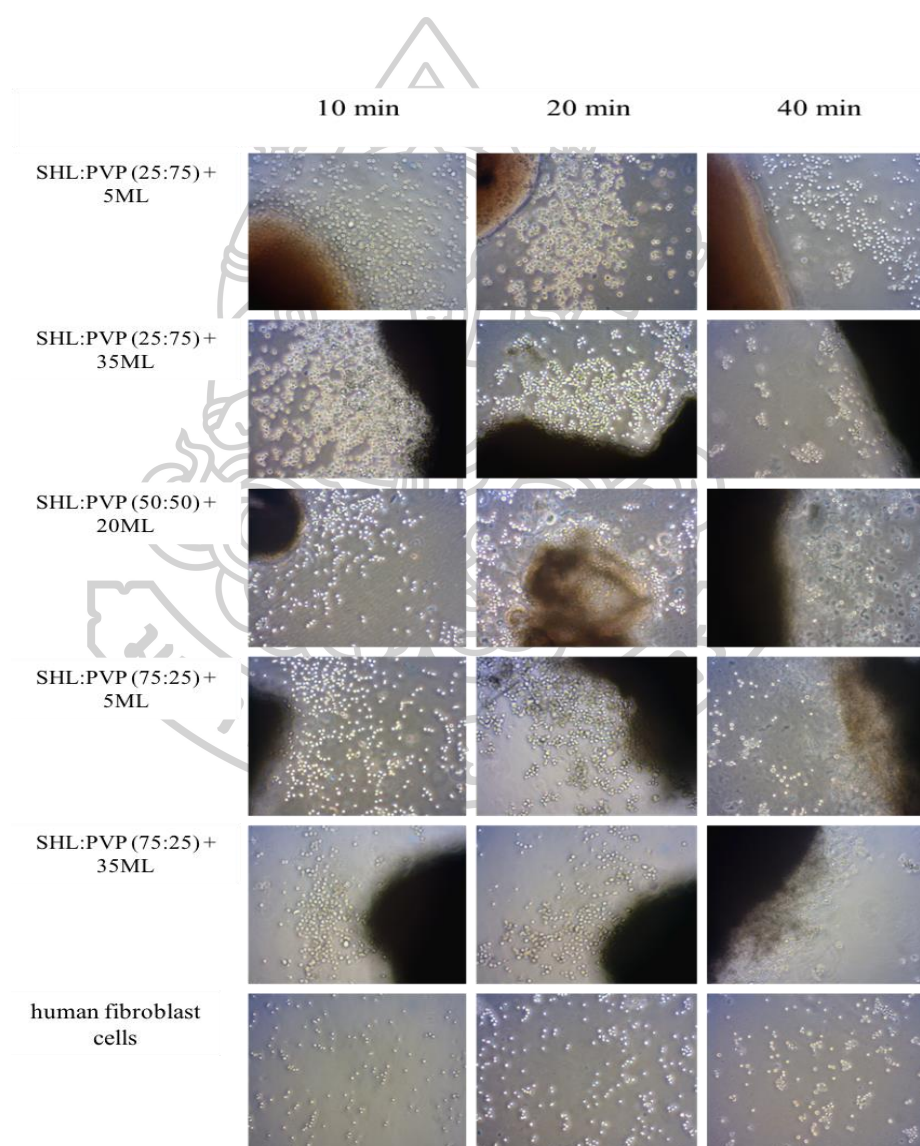


Figure 44 The morphology of cell after seeding on nanofibers at different time points.

6.3 Cytotoxicity screening by the MTT bioassay

As described previously, wound dressings are supposed to be directly placed over the wound surface; therefore, they should be non-toxic and compatible with cells. The MTT colorimetric assay is one of the most largely used for determining the cytotoxic potential of materials due to its precision and rapidity. The evaluation of cell viability is performed by converting a water soluble yellow tetrazolium dye MTT 3-(4,5-dimethylthiazol-2-yl)-2,5-diphenyltetrazolium bromide into insoluble purple formazan by mitochondrial enzymes in living cells. The proportion of survival cells is related with the concentration of generated formazan crystals (79).

As illustrated in Figure 45A, the percentages of cell survival in the cultures treated with SHL and PVP were significantly higher than those treated with ML, chitosan and SHL/PVP blended nanofibers loaded with ML, indicating the higher safety of both SHL and PVP. For example (Figure 45B), the percentage of cell viability for 0.001 mg/mL of SHL and PVP was 100 which presented the non-toxic property of these materials. Whereas, the percentage of cell viability of ML, chitosan and blended nanofibers loaded with ML were 48.43, 30.11 and 43.64, respectively. According to the previous study, chitosan, a cationic polysaccharide, has been widely employed as a biomedical material due to its low toxicity and biological properties such as antimicrobial and antitumor activities (80). In this study, when compared with chitosan, ML exhibited the higher percentage of cell survival at the same concentration. This occurrence could be explained by the electrical interaction between chitosan and cell surface, resulting in cell disintegration (81). However, ML seemed to be relatively involved in cell disintegration by disrupting the cell membrane, owing to its emulsifying property. The hydrophobic chain of ML could possibly penetrate into the cell membrane, leading to cell rupture (81). In addition, SHL/PVP fibres incorporated with 20% w/w ML also exhibited the moderate percentage of cell viability in the same manner as described previously.

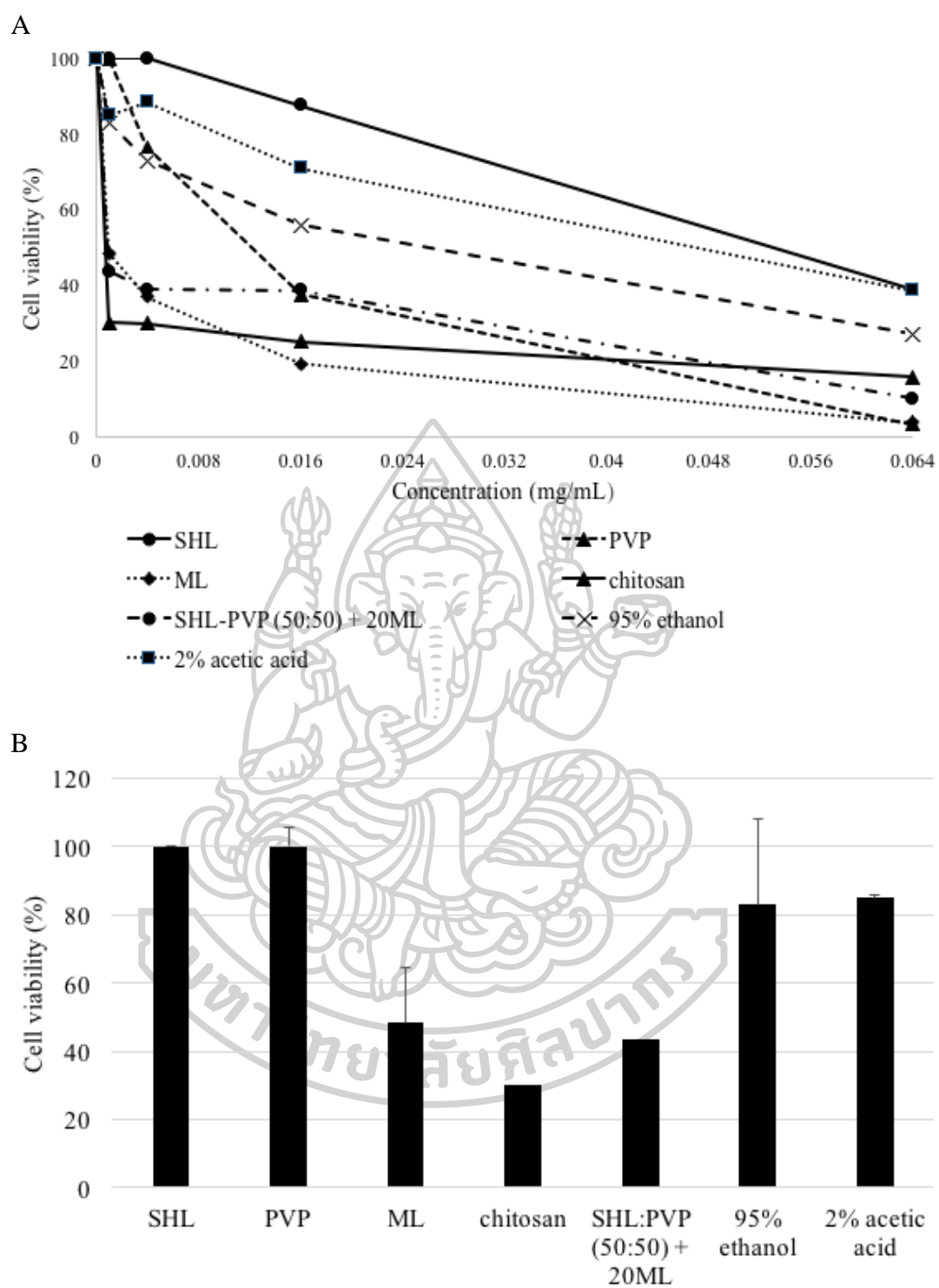


Figure 45 Percentage of cell viability at (A) different concentrations and (B) 0.001 mg/mL.

6.4 Conclusions

Shellac provides an excellent protective barrier and good electrospinnability. However, it is hydrophobic and has unfavourable mechanical properties and low cell affinity. In contrast, SHL blended with PVP, a hydrophilic, water-soluble synthetic polymer possessing high mechanical strength, could produce the nanofibers required for use in wound healing. The main and interaction effects of parameters on various responses were studied using a 2^3 full factorial design with three replicated centre points. As a result, the SHL ratio in a blended solution was the crucial factor affecting nanofiber diameter. An increase in SHL content would result in a reduction in stretching ability. The presence of PVP could lead to a relative improvement in mechanical properties, cell adhesion and drug release from nanofibers, owing to its hydrophilicity and good mechanical strength. However, the hygroscopic nature and rapid erosion of PVP might retard the wettability and absorbency of the fibres. The applied voltage was also significant. According to our results, small fibres, which tended to be uniformly oriented and densely packed, were obtained by applying high electrical voltage, leading to an increase in tensile strength and antimicrobial activities, especially against *C. albicans*, resulting from the improved dissolution of fibres. Additionally, the encapsulation of ML in an SHL-PVP carrier might cause a strong interaction, resulting in enhanced mechanical strength; however, the elastic force was impaired, contributing to an increased diameter.

CHAPTER 7

Summary and general conclusions

Electrospun SHL nanofibers might be potentially used for wound dressing application due to its natural origin and excellent protective properties. In the first part, a full factorial design with three replicated centre points was performed in order to investigate the main and interaction effects of SHL content (35%-40% w/w), applied voltage (9-27 kV) and flow rate (0.4-1.2 mL/h) on the morphology of SHL nanofibers. A total of 11 experiments were conducted. The response variables were the diameter of nanofibers, the distribution of diameter and the amount of beads. The results showed that the concentration of SHL was the most significant impact on SHL nanofiber diameter, while applied voltage, interaction between SHL content and voltage, and feed rate were minor factors, respectively. SHL content and applied voltage had negative relationships with bead amount. When reducing the concentration of SHL and voltage, the amount of beads was increased. However, the influence of these parameters on diameter distribution seemed to be not significant. Based on response surface plot, nanofibers with thinner diameter (~ 493 nm) and less number of beads (~ 0.47) could be obtained at the optimum conditions; the SHL content of 38.5% w/w, the voltage of 21 kV and the feed rate of 0.4 mL/h.

SHL nanofibers loaded with ML, a natural antimicrobial lipid, could be developed for wound dressing application in order to prevent the delayed wound healing resulting from microbial infection and also minimize the increasing antibiotic resistance. The aim of this part was to elucidate the optimized fabrication factors influencing the formation and properties of SHL nanofibers loaded with ML. The main and interaction effects of formulation and process parameters including SHL content (35%-40% w/w), ML content (1%-3% w/w), applied voltage (9-27 kV) and flow rate (0.4-1.2 mL/h) on the characteristic of nanofibers were investigated through a total of 19 experiments based on a full factorial design with three replicated centre points. As a result, the SHL content was the major parameter affecting fibre diameter. Another response result revealed that the SHL content would be also the most significant negative impact on amount of beads. An increase in the concentration of

SHL led to a reduction in the amount of beads. From the results of characterization study, it was proved that ML might be entrapped between the chains of SHL during the electrospinning process exhibiting an excellent encapsulation. According to the response surface area, small (~ 488 nm) and beadless (~ 0.48) fibres were obtained with the SHL and ML contents of 37.5% and 1.1% w/w respectively, at the applied voltage of 18 kV and the flow rate of 0.8 mL/h. In addition, the results of the kinetic studies showed that SHL nanofibers loaded with ML exhibited an excellent antibacterial activity against *S. aureus*, while *E. coli* was less affected due to the hydrophilic structure of its outer membrane. ML also exerted an antifungal activity by reducing the number of *C. albicans* colonies. Based on their structural and antimicrobial properties, SHL nanofibers containing ML could be potentially used as a medicated dressing for wound treatment.

Nevertheless, the fabricated nanofibers using only SHL as a polymeric carrier exhibited some drawbacks due to the absence of hydrophilicity, cell affinity and good mechanical properties. In this part, PVP was introduced to be blended with SHL in order to improve the physiological properties. This part aimed to examine the factors influencing the fabrication and properties of electrospun SHL/PVP blended nanofibers loaded with ML. A total of 11 runs based on a 2^3 full factorial design with three centre-point replications was performed in order to elucidate the main and interaction impacts of the SHL ratio in an SHL-PVP blended solution (25–75), ML content (5%–35% w/w) and applied voltage (9–27 kV) on the characteristics of the obtained nanofibers. The results demonstrated that an increase in the ML content and SHL ratio in an SHL-PVP blended solution could mainly lead to an increase in nanofiber diameter due to the impairment of elastic force and stretching ability, whereas an increase in the voltage applied would result in the formation of small fibres due to the enhancement of charge repulsion contributing to an increase in jet stretching. The effect of various factors on the mechanical properties of nanofibers was also studied. The enhanced ML concentration and applied voltage might induce an increase in the tensile strength of the fibres owing to the strong interaction between encapsulated ML and the polymeric carrier and the resultant densely packed and uniformly oriented nanofibers, respectively. When the SHL ratio was high, the tensile

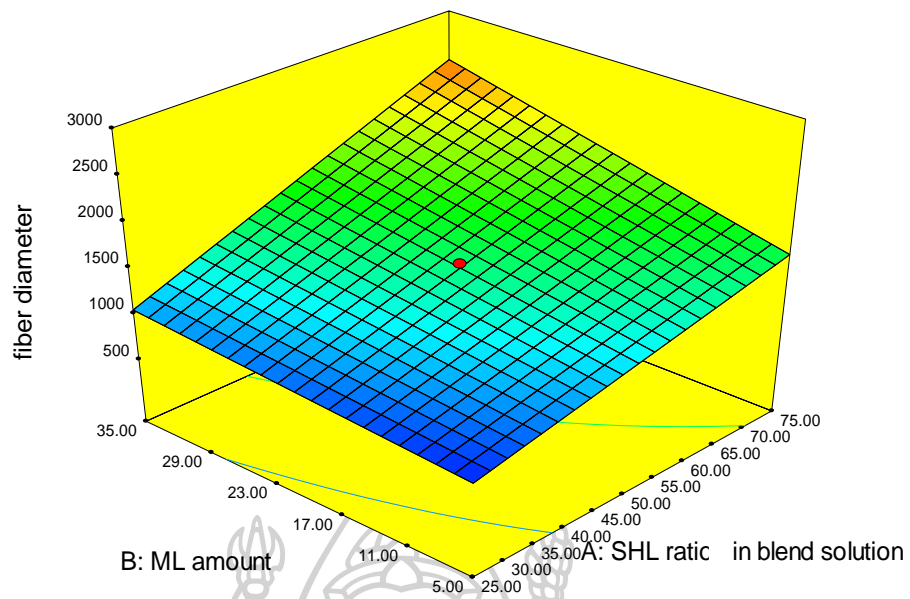
strength and elongation tended to be low, owing to the brittle nature of SHL. Other response results, including absorbency and wettability, revealed that the absorbency increased as the SHL ratio and ML content increased. This may have been due to the protective effect of SHL and ML, both of which are hydrophobic, against erosion of PVP. Nevertheless, a rise in the PVP ratio could apparently lead to an increase in water contact angle and polarity, as a result of a reduction in fibre porosity due to the hygroscopic property of PVP. Furthermore, according to the results of the kill-kinetic and cell attachment assays, the obtained blended nanofibers loaded with ML displayed excellent activity against *S. aureus* and *C. albicans* and exhibited enhanced cell adhesion ability. Thus, SHL/PVP blended nanofibers loaded with ML might be used effectively for wound-healing management.

Regarding the experimental results obtained from all parts of the study, it might be concluded that the contents of SHL and ML might significantly contribute to the fabrication of large diameter nanofibers. However, the effect of applied voltage on fibre diameter seemed to be varied. When PVP was added to the electrospun solution, the small fibres were obtained at high applied voltage during the electrospinning process which was different from the earlier parts. Furthermore, the introduction of PVP could lead to an improvement in drug loading capacity and dissolution rate. The appearance of smooth fibres might be occurred resulting from an increase in the mechanical strength associated with an increase in the PVP content. The fabricated nanofibres loaded with ML also demonstrated non-toxic property, cell adhesion ability and antimicrobial activity.

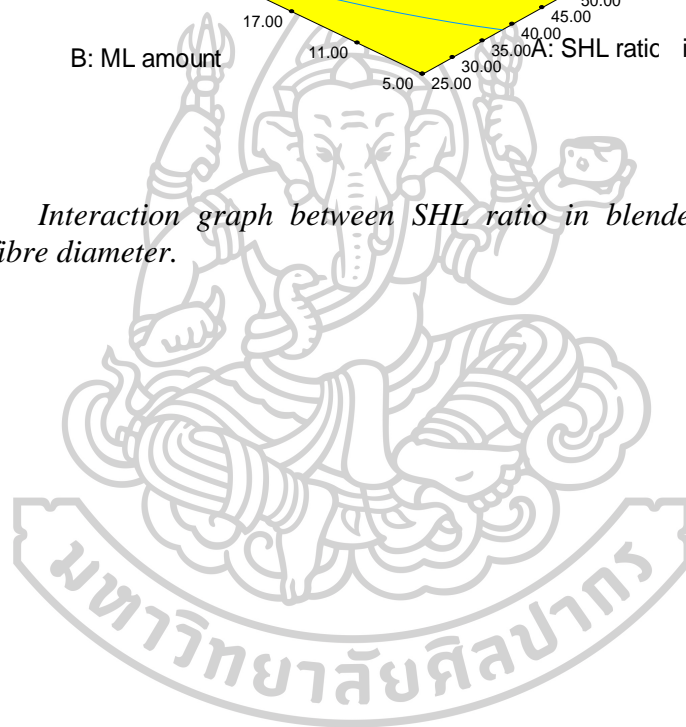
APPENDIX

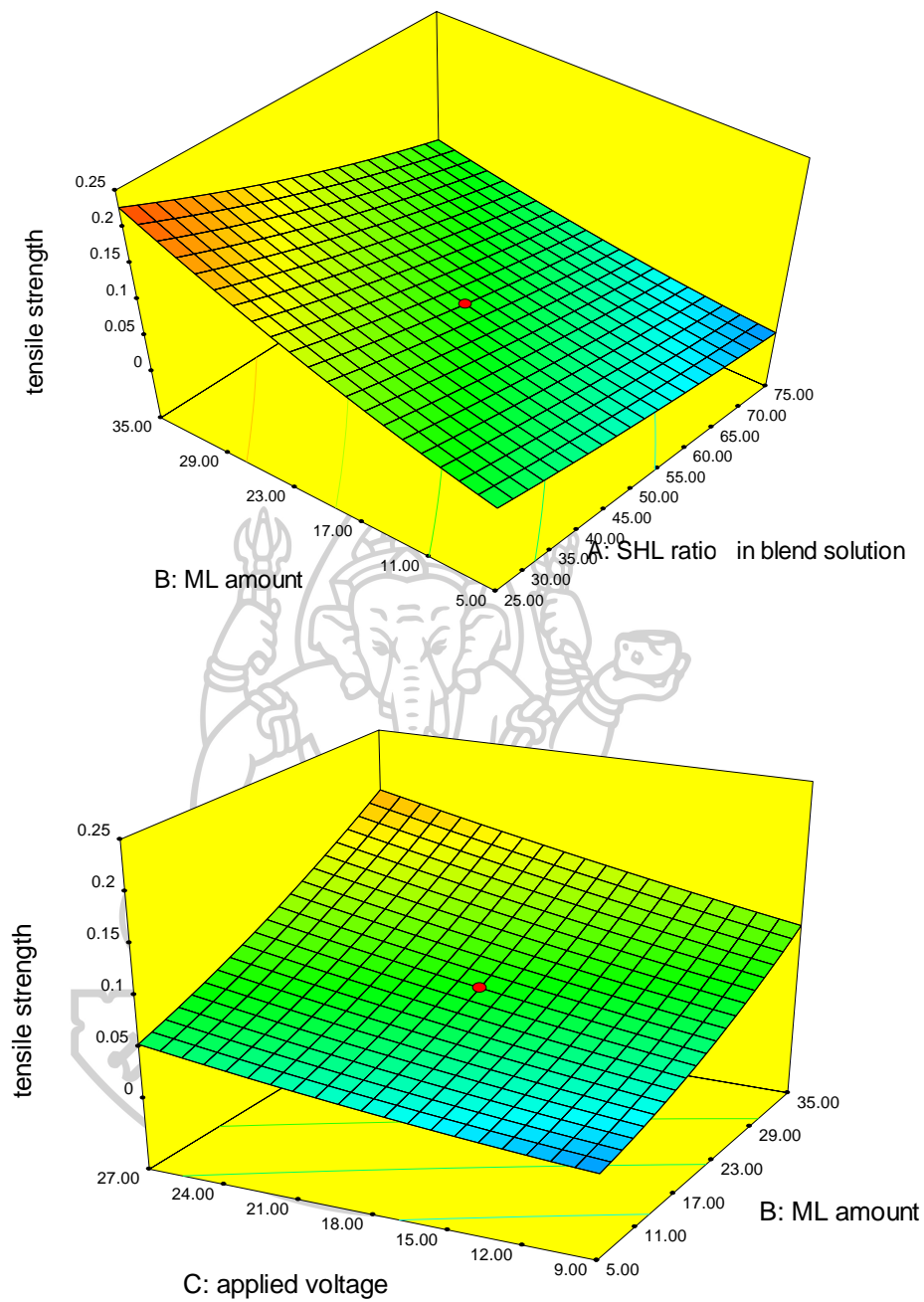
Appendix 1 The experimental values of independent factors, including SHL ratio in blended solution, ML amount, and applied voltage, and the measured response values of tensile strength, elongation, contact angle, polarity and absorbency.

X ₁	X ₂	X ₃	Y ₁	Y ₂	Y ₃	Y ₄	Y ₅	Y ₆
SHL ratio in blended solution	ML amount	applied voltage (kV)	diameter (nm)	tensile strength (MPa)	elongation (mm)	contact angle (°)	polarity (%)	absorbency (%)
25	5	9	932	0.0024	0.014	19.28	33.35	-34.4
25	5	27	724	0.1938	9.266	47.36	21.84	-19.8
25	35	9	1140	0.205	5.184	57.91	19.33	0.74
25	35	27	1021	0.2555	2.144	31.97	29.03	11.1
50	20	18	1524	0.0755	1.186	32.68	35.92	-3.61
50	20	18	1387	0.0748	2.322	27.51	31.16	-12.19
50	20	18	1416	0.071	2.292	38.98	26.29	-14.49
75	5	9	1820	0.0274	1.323	8.83	35.56	12.98
75	5	27	1358	0.0009	0.018	14.97	34.51	-5.34
75	35	9	2615	0.0403	0.618	4.07	52.64	7.6
75	35	27	2349	0.1324	0.407	41.99	33.96	9.31

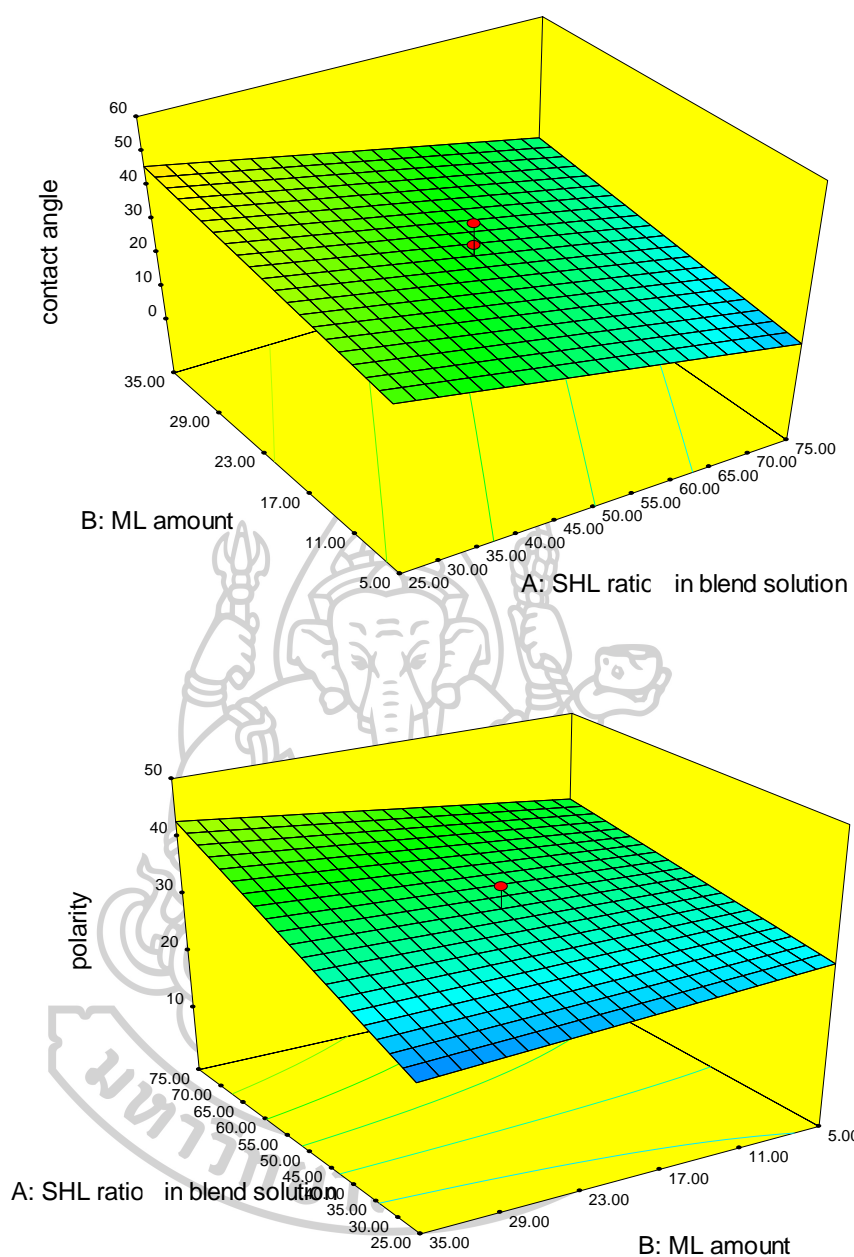


Appendix 2 Interaction graph between SHL ratio in blended solution and ML content on fibre diameter.





Appendix 3 Interaction graphs between SHL ratio in blended solution, ML content and applied voltage on tensile strength.



Appendix 4 Interaction graphs between SHL ratio in blended solution and ML content on contact angle and polarity.

REFERENCES



1. Abdelrahman T, Newton H. Wound dressings: principles and practice. Surg [Internet]. 2011;29(10):491–5. Available from: <http://www.sciencedirect.com/science/article/pii/S0263931911001281>
2. D. Winter G. Formation of the Scab and the Rate of Epithelization of Superficial Wounds in the Skin of the Young Domestic Pig. Vol. 193, Nature. 1962. 293-294 p.
3. Stashak TS, Farstvedt E, Othic A. Update on wound dressings: Indications and best use. Clin Tech Equine Pract [Internet]. 2004 Jun 1 [cited 2018 Jan 15];3(2):148–63. Available from: <https://www.sciencedirect.com/science/article/pii/S1534751604000460>
4. Engel E, Michiardi A, Navarro M, Lacroix D, Planell JA. Nanotechnology in regenerative medicine: the materials side. Trends Biotechnol [Internet]. 2008;26(1):39–47. Available from: <http://www.sciencedirect.com/science/article/pii/S0167779907002892>
5. Pelipenko J, Kocbek P, Janković B, Rošić R, Baumgartner S, Kristl J. The Topography of Electrospun Nanofibers and Its Impact on the Growth and Mobility of Keratinocytes. Vol. 84, European journal of pharmaceutics and biopharmaceutics : official journal of Arbeitsgemeinschaft fur Pharmazeutische Verfahrenstechnik e.V. 2012.
6. Unnithan AR, Gnanasekaran G, Sathishkumar Y, Lee YS, Kim CS. Electrospun antibacterial polyurethane–cellulose acetate–zein composite mats for wound dressing. Carbohydr Polym [Internet]. 2014;102:884–92. Available from: <http://www.sciencedirect.com/science/article/pii/S0144861713010990>
7. Hu X, Liu S, Zhou G, Huang Y, Xie Z, Jing X. Electrospinning of polymeric nanofibers for drug delivery applications. J Control Release [Internet]. 2014;185:12–21. Available from: <http://www.sciencedirect.com/science/article/pii/S0168365914002363>
8. Okamoto, M. Y.; Ibanez PS. Final Report on the Safety Assessment of Shellac. J Am Coll Toxicol [Internet]. 1986;5(5):309–27. Available from: <http://www.informaworld.com/openurl?genre=article&doi=10.1080/10915810802550835&magic=crossref%7C%7CD404A21C5BB053405B1A640AFFD44AE3>
9. Alzahrani H, Bedir Y, Al-Hayani A. Efficacy of shellac, a natural product, for the prevention of wet gangrene. Vol. 41, The Journal of international medical research. 2013.
10. Porter SC. Coating of pharmaceutical dosage forms. In: Lieberman HA, editor. Pharmaceutical Dosage Forms: Tablet. New York: Marcel Dekker Inc.; 1990. p. 77–160.
11. Limmatvapirat S, Thammachat T, Sriamornsak P, Luangtana-Anan M, Nunthanid J, Limmatvapirat C. Preparation and Characterization of Shellac Fiber as a Novel Material for Controlled Drug Release. 2011. 1232-1235 p.
12. Razzak MT, Zainuddin, Erizal, Dewi SP, Lely H, Taty E, et al. The characterization of dressing component materials and radiation formation of PVA–PVP hydrogel. Radiat Phys Chem [Internet]. 1999;55(2):153–65. Available from: <http://www.sciencedirect.com/science/article/pii/S0969806X9800320X>
13. Baccaro S, Pajewski LA, Scoccia G, Volpe R, Rosiak JM. Mechanical

- properties of polyvinylpyrrolidone (PVP) hydrogels undergoing radiation. *Nucl Instruments Methods Phys Res Sect B Beam Interact with Mater Atoms* [Internet]. 1995;105(1):100–2. Available from: <http://www.sciencedirect.com/science/article/pii/0168583X95005196>
14. Thormar H, Hilmarsson H. The role of microbicidal lipids in host defense against pathogens and their potential as therapeutic agents. *Chem Phys Lipids* [Internet]. 2007 Nov [cited 2018 Jan 15];150(1):1–11. Available from: <http://www.ncbi.nlm.nih.gov/pubmed/17686469>
 15. Carpo BG, Verallo-Rowell VM, Kabara J. Novel antibacterial activity of monolaurin compared with conventional antibiotics against organisms from skin infections: an in vitro study. *J Drugs Dermatol* [Internet]. 2007 Oct [cited 2018 Jan 15];6(10):991–8. Available from: <http://www.ncbi.nlm.nih.gov/pubmed/17966176>
 16. Lieberman S, Enig MG, Preuss HG. A Review of Monolaurin and Lauric Acid: *Natural Virucidal and Bactericidal Agents*. *Altern Complement Ther* [Internet]. 2006 Dec 11 [cited 2018 Jan 15];12(6):310–4. Available from: <http://www.liebertonline.com/doi/abs/10.1089/act.2006.12.310>
 17. Filip V. Inhibition of *Aspergillus niger* DMF 0801 by Monoacylglycerols Prepared from Coconut Oil. 2002.
 18. Nobmann P, Smith A, Dunne J, Henahan G, Bourke P. The antimicrobial efficacy and structure activity relationship of novel carbohydrate fatty acid derivatives against *Listeria* spp. and food spoilage microorganisms. *Int J Food Microbiol* [Internet]. 2009 Jan 15 [cited 2018 Jan 15];128(3):440–5. Available from: <http://www.ncbi.nlm.nih.gov/pubmed/19012983>
 19. Ramakrishna S. An introduction to electrospinning and nanofibers [Internet]. World Scientific; 2005 [cited 2018 Jan 15]. 382 p. Available from: https://books.google.co.th/books/about/An_Introduction_to_Electrospinning_and_N.html?id=QHkyRdb2TicC&redir_esc=y
 20. Montgomery DC. Design and analysis of experiments. 8th ed. New Jersey: John Wiley & Sons, Inc.; 2013.
 21. Turner TD. The Development of Wound Management Products. In: Krasner DL, Rodeheaver GT, Sibbald RG, editors. *Chronic Wound Care: A Clinical Source Book for Healthcare Professionals*. 3rd ed. Wayne, PA: HMP Communications; 2001. p. 293–310.
 22. Zahedi P, Rezaeian I, Ranaei-Siadat S-O, Jafari S-H, Supaphol P. A review on wound dressings with an emphasis on electrospun nanofibrous polymeric bandages. *Polym Adv Technol* [Internet]. 2009 Feb 1 [cited 2018 Jan 15];21(2):n/a-n/a. Available from: <http://doi.wiley.com/10.1002/pat.1625>
 23. Weller C, Sussman G. Wound Dressings Update. *J Pharm Pract Res* [Internet]. 2006 Dec 1 [cited 2018 Jan 15];36(4):318–24. Available from: <http://doi.wiley.com/10.1002/j.2055-2335.2006.tb00640.x>
 24. Sussman G. Wound care module. In: Affairs DoV, editor. Victoria: Monash University; 2008. p. 1–29.
 25. Barot M, Gokulgandhi M, Ray A, Mitra A. Nanofiber. In: Mitra A, Lee C, Cheng K, editors. *Advanced Drug Delivery*. 1st ed. New York: John Wiley & Sons, Inc.; 2014. p. 219–30.
 26. Huang Z-M, Zhang Y-Z, Kotaki M, Ramakrishna S. A review on polymer

- nanofibers by electrospinning and their applications in nanocomposites. *Compos Sci Technol* [Internet]. 2003;63(15):2223–53. Available from: <http://www.sciencedirect.com/science/article/pii/S0266353803001787>
27. Leung V, Hartwell R, Yang H, Ghahary A, Ko F. Bioactive Nanofibres for Wound Healing Applications. Vol. 4, *Journal of Fiber Bioengineering and Informatics*. 2011. 1-14 p.
 28. Liao N, Unnithan AR, Joshi MK, Tiwari AP, Hong ST, Park C-H, et al. Electrospun bioactive poly (ϵ -caprolactone)–cellulose acetate–dextran antibacterial composite mats for wound dressing applications. *Colloids Surfaces A Physicochem Eng Asp* [Internet]. 2015 Mar 20 [cited 2018 Apr 25];469:194–201. Available from: <https://www.sciencedirect.com/science/article/pii/S0927775715000412>
 29. Unnithan AR, Barakat NAM, Tirupathi Pichiah PB, Gnanasekaran G, Nirmala R, Cha Y-S, et al. Wound-dressing materials with antibacterial activity from electrospun polyurethane–dextran nanofiber mats containing ciprofloxacin HCl. *Carbohydr Polym* [Internet]. 2012 Nov 6 [cited 2018 Apr 25];90(4):1786–93. Available from: <https://www.sciencedirect.com/science/article/pii/S0144861712007448>
 30. Hadipour-Goudarzi E, Montazer M, Latifi M, Aghaji AAG. Electrospinning of chitosan/sericin/PVA nanofibers incorporated with in situ synthesis of nano silver. *Carbohydr Polym* [Internet]. 2014 Nov 26 [cited 2018 Apr 25];113:231–9. Available from: <https://www.sciencedirect.com/science/article/pii/S0144861714006602>
 31. Vasita R, Katti DS. Nanofibers and their applications in tissue engineering. *Int J Nanomedicine* [Internet]. 2006 Mar;1(1):15–30. Available from: <http://www.ncbi.nlm.nih.gov/pmc/articles/PMC2426767/>
 32. Utracki LA. *Polymer Blends Handbook*. Dordrecht: Kluwer Academic Publishers; 2002.
 33. Pawar MD, Rathna GVN, Agrawal S, Kuchekar BS. Bioactive thermoresponsive polyblend nanofiber formulations for wound healing. *Mater Sci Eng C* [Internet]. 2015;48:126–37. Available from: <http://www.sciencedirect.com/science/article/pii/S0928493114007383>
 34. Limmatvapirat S, Limmatvapirat C, Luangtana-anan M, Nunthanid J, Oguchi T, Tozuka Y, et al. Modification of physicochemical and mechanical properties of shellac by partial hydrolysis. *Int J Pharm* [Internet]. 2004 Jun 18 [cited 2018 Apr 25];278(1):41–9. Available from: <https://www.sciencedirect.com/science/article/pii/S0378517304001747>
 35. Limmatvapirat S, Limmatvapirat C, Puttipatkhachorn S, Nuntanid J, Luangtana-Anan M. Enhanced enteric properties and stability of shellac films through composite salts formation. *Eur J Pharm Biopharm*. 2007 Nov;67(3):690–8.
 36. Kanokpanont S, Damrongsakkul S, Ratanavaraporn J, Aramwit P. Physicochemical properties and efficacy of silk fibroin fabric coated with different waxes as wound dressing. *Int J Biol Macromol*. 2013 Apr;55:88–97.
 37. Himly N, Darwis D, Hardiningsih L. Poly(n-vinylpyrrolidone) hydrogels: 2. Hydrogel composites as wound dressing for tropical environment. *Radiat Phys Chem* [Internet]. 1993 Oct 1 [cited 2018 Apr 25];42(4–6):911–4.

Available from:

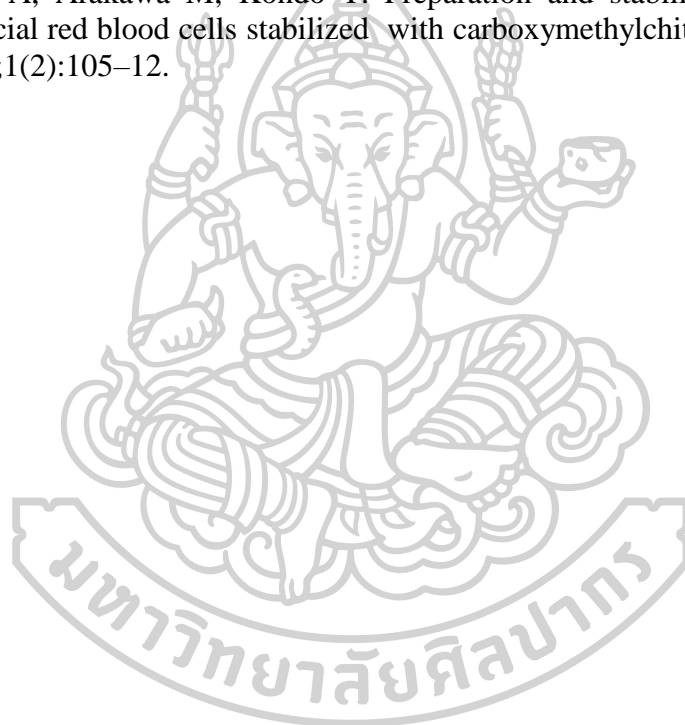
<https://www.sciencedirect.com/science/article/pii/S0969806X93904000>

38. Isaacs CE, Litov RE, Thormar H. Antimicrobial activity of lipids added to human milk, infant formula, and bovine milk. *J Nutr Biochem*. 1995 Jul;6(7):362–6.
39. Wille JJ, Kydonieus A. Palmitoleic acid isomer (C16:1 Δ 6) in human skin sebum is effective against gram-positive bacteria. *Skin Pharmacol Appl Skin Physiol*. 2003;16(3):176–87.
40. DebMandal M, Mandal S. Coconut (*Cocos nucifera* L.: Areaceae): in health promotion and disease prevention. *Asian Pac J Trop Med*. 2011 Mar;4(3):241–7.
41. Temelli F, King JW, List GR. Conversion of oils to monoglycerides by glycerolysis in supercritical carbon dioxide media. *J Am Oil Chem Soc* [Internet]. 1996;73(6):699–706. Available from: <https://doi.org/10.1007/BF02517943>
42. Tangwatcharin P, Khopaibool P. Activity of virgin coconut oil, lauric acid or monolaurin in combination with lactic acid against *Staphylococcus aureus*. *Southeast Asian J Trop Med Public Health*. 2012 Jul;43(4):969–85.
43. Řiháková Z, Filip V, Plocková M, Šmidrkal J, Červenková R. Inhibition of *Aspergillus niger* DMF 0801 by monoacylglycerols prepared from coconut oil. Vol. 20, *Czech Journal of Food Sciences*. 2018. 48-52 p.
44. Lin Y-C, Schlievert PM, Anderson MJ, Fair CL, Schaeffers MM, Muthyala R, et al. Glycerol monolaurate and dodecylglycerol effects on *Staphylococcus aureus* and toxic shock syndrome toxin-1 in vitro and in vivo. *PLoS One*. 2009 Oct;4(10):e7499.
45. Skřivanová E, Marounek M, BENDA V, BREZINA P. Susceptibility of *Escherichia coli*, *Salmonella* sp. and *Clostridium perfringens* to organic acids and monolaurin. Vol. 51, *Veterinarni Medicina*. 2006.
46. Bergsson G, Steingrímsson O, Thormar H. Bactericidal effects of fatty acids and monoglycerides on *Helicobacter pylori*. *Int J Antimicrob Agents*. 2002 Oct;20(4):258–62.
47. Ouattara B, Simard RE, Holley RA, Piette GJ, Begin A. Antibacterial activity of selected fatty acids and essential oils against six meat spoilage organisms. *Int J Food Microbiol*. 1997 Jul;37(2–3):155–62.
48. Razavi Rohani SM, Griffiths M. The Effect of Mono and Polyglycerol Laurate on Spoilage and Pathogenic Bacteria Associated With Foods. Vol. 14, *Journal of Food Safety*. 2007. 131-151 p.
49. Altieri C, Bevilacqua A, Cardillo D, Sinigaglia M. Effectiveness of fatty acids and their monoglycerides against Gram-negative pathogens. Vol. 44, *International Journal of Food Science & Technology*. 2008. 359-366 p.
50. Thormar H, Isaacs CE, Brown HR, Barshatzky MR, Pessolano T. Inactivation of enveloped viruses and killing of cells by fatty acids and monoglycerides. *Antimicrob Agents Chemother*. 1987 Jan;31(1):27–31.
51. Strandberg KL, Peterson ML, Lin Y-C, Pack MC, Chase DJ, Schlievert PM. Glycerol monolaurate inhibits *Candida* and *Gardnerella vaginalis* in vitro and in vivo but not *Lactobacillus*. *Antimicrob Agents Chemother*. 2010 Feb;54(2):597–601.

52. Perera SEF and R. A response surface methodology based damage identification technique. *Smart Mater Struct* [Internet]. 2009;18(6):65009. Available from: <http://stacks.iop.org/0964-1726/18/i=6/a=065009>
53. Yanilmaz M, Kalaoglu F, Karakas H. Investigation on the Effect of Process Variables on Polyurethane Nanofibre Diameter Using a Factorial Design. Vol. 98, *Fibres and Textiles in Eastern Europe*. 2013. 19-21 p.
54. Sarlak N, Nejad MAF, Shakhshi S, Shabani K. Effects of electrospinning parameters on titanium dioxide nanofibers diameter and morphology: An investigation by Box–Wilson central composite design (CCD). *Chem Eng J* [Internet]. 2012;210:410–6. Available from: <http://www.sciencedirect.com/science/article/pii/S1385894712011527>
55. Gonen SO, Erol Taygun M, Akturk A, Kucukbayrak S. Fabrication of nanocomposite mat through incorporating bioactive glass particles into gelatin/poly(epsilon-caprolactone) nanofibers by using Box-Behnken design. *Mater Sci Eng C Mater Biol Appl*. 2016 Oct;67:684–93.
56. Dhekale N, Kunti HB, Y. Kirankumar K, Gore DA, Anbhule P, Kolekar G. Development and optimization of a multivariate RP-UPLC method for determination of telmisartan and its related substances by applying a two-level factorial design approach: Application to quality control study. Vol. 6, *Analytical Methods*. 2014. 5168 p.
57. Willmott CJ. Some Comments on the Evaluation of Model Performance. *Bull Am Meteorol Soc* [Internet]. 1982 Nov 1;63(11):1309–13. Available from: [https://doi.org/10.1175/1520-0477\(1982\)063%3C1309:SCOTEO%3E2.0.CO](https://doi.org/10.1175/1520-0477(1982)063%3C1309:SCOTEO%3E2.0.CO)
58. Hild M, Al Rez MF, Aibibu D, Toskas G, Cheng T, Laourine E, et al. Pcl/Chitosan Blended Nanofibrous Tubes Made by Dual Syringe Electrospinning. Vol. 15, *Autex Research Journal*. 2015.
59. Yuan Y, Lee TR. Contact Angle and Wetting Properties BT - Surface Science Techniques. In: Bracco G, Holst B, editors. Berlin, Heidelberg: Springer Berlin Heidelberg; 2013. p. 3–34. Available from: https://doi.org/10.1007/978-3-642-34243-1_1
60. Archana D, Dutta J, Dutta PK. Evaluation of chitosan nano dressing for wound healing: characterization, in vitro and in vivo studies. *Int J Biol Macromol*. 2013 Jun;57:193–203.
61. Demir MM, Yilgor I, Yilgor E, Erman B. Electrospinning of polyurethane fibers. *Polymer (Guildf)* [Internet]. 2002;43(11):3303–9. Available from: <http://www.sciencedirect.com/science/article/pii/S0032386102001362>
62. Schlievert PM, Peterson ML. Glycerol Monolaurate Antibacterial Activity in Broth and Biofilm Cultures. Kaufmann GF, editor. *PLoS One* [Internet]. 2012 Jul 11;7(7):e40350. Available from: <http://www.ncbi.nlm.nih.gov/pmc/articles/PMC3394780/>
63. Seleem D, Chen E, Benso B, Pardi V, Murata RM. In vitro evaluation of antifungal activity of monolaurin against *Candida albicans* biofilms. *PeerJ*. 2016;4:e2148.
64. Van Dooren AA. Design for Drug-Excipient Interaction Studies. *Drug Dev Ind Pharm* [Internet]. 1983 Jan 1;9(1–2):43–55. Available from: <https://doi.org/10.3109/03639048309048544>
65. Chen X, Wu D, He Y, Liu S. Detecting the quality of glycerol monolaurate: a

- method for using Fourier transform infrared spectroscopy with wavelet transform and modified uninformative variable elimination. *Anal Chim Acta*. 2009 Apr;638(1):16–22.
66. Limmatvapirat S, Panchapornpon D, Limmatvapirat C, Nunthanid J, Luangtana-Anan M, Puttipipatkachorn S. Formation of shellac succinate having improved enteric film properties through dry media reaction. *Eur J Pharm Biopharm*. 2008 Sep;70(1):335–44.
 67. Kumar MM. Solution properties of shellac, 4. Solubility parameter of shellac. *Die Angew Makromol Chemie* [Internet]. 2018 Jul 4;147(1):107–12. Available from: <https://doi.org/10.1002/apmc.1987.051470110>
 68. Blaszyk M, Holley RA. Interaction of monolaurin, eugenol and sodium citrate on growth of common meat spoilage and pathogenic organisms. *Int J Food Microbiol*. 1998 Feb;39(3):175–83.
 69. Vera Candiotti L, De Zan MM, Cámara MS, Goicoechea HC. Experimental design and multiple response optimization. Using the desirability function in analytical methods development. *Talanta* [Internet]. 2014;124:123–38. Available from: <http://www.sciencedirect.com/science/article/pii/S0039914014000459>
 70. Schneider LA, Korber A, Grabbe S, Dissemond J. Influence of pH on wound-healing: a new perspective for wound-therapy? *Arch Dermatol Res* [Internet]. 2007;298(9):413–20. Available from: <https://doi.org/10.1007/s00403-006-0713-x>
 71. Chinatankul N, Limmatvapirat C, Nunthanid J, Luangtana-Anan M, Sriamornsak P, Limmatvapirat S. Design and characterization of monolaurin loaded electrospun shellac nanofibers with antimicrobial activity. *Asian J Pharm Sci* [Internet]. 2017 Dec 27 [cited 2018 Apr 25]; Available from: <https://www.sciencedirect.com/science/article/pii/S1818087617308206>
 72. Koczur KM, Mourdikoudis S, Polavarapu L, Skrabalak SE. Polyvinylpyrrolidone (PVP) in nanoparticle synthesis. *Dalton Trans*. 2015 Nov;44(41):17883–905.
 73. Chinatankul N, Pengon S, Limmatvapirat C, Limmatvapirat S. Design of Experiment Approach for Fabrication Process of Electrospun Shellac Nanofibers Using Factorial Designs. *Key Eng Mater* [Internet]. 2017;757:120–4. Available from: <https://www.scientific.net/KEM.757.120>
 74. Moradi M, Tajik H, Razavi Rohani SM, Mahmoudian A. Antioxidant and antimicrobial effects of zein edible film impregnated with *Zataria multiflora* Boiss. essential oil and monolaurin. *LWT - Food Sci Technol* [Internet]. 2016;72:37–43. Available from: <http://www.sciencedirect.com/science/article/pii/S0023643816302109>
 75. Cockeram HS, Levine SA. The physical and chemical properties of shellac. *J Soc Cosmet Chem*. 1961;12:316–23.
 76. Lim CT, P. S. Tan E, Y. Ng S. Effects of crystalline morphology on the tensile properties of electrospun polymer nanofibers. *Appl Phys Lett*. 2008 May 1;92:141908.
 77. Vickery C. Exudate: what is it and what is its function? In: Cherry GW, Harding K, editors. *Management of wound exudate: Abstracts from the first combined meeting of the European Tissue Repair Society and the European*

- Wound Management Association at Green College, University of Oxford. London: Churchill Communications; 1997.
78. Halloran CM, Slavin JP. Pathophysiology of Wound Healing. Surg [Internet]. 2002;20(5):i–v. Available from: <http://www.sciencedirect.com/science/article/pii/S0263931906702150>
 79. Ciapetti G, Cenni E, Pratelli L, Pizzoferrato A. In vitro evaluation of cell/biomaterial interaction by MTT assay. Biomaterials [Internet]. 1993;14(5):359–64. Available from: <http://www.sciencedirect.com/science/article/pii/0142961293900557>
 80. Qi L, Xu Z, Jiang X, Li Y, Wang M. Cytotoxic activities of chitosan nanoparticles and copper-loaded nanoparticles. Bioorg Med Chem Lett [Internet]. 2005;15(5):1397–9. Available from: <http://www.sciencedirect.com/science/article/pii/S0960894X05000478>
 81. Kato A, Arakawa M, Kondo T. Preparation and stability of liposome-type artificial red blood cells stabilized with carboxymethylchitin. J Microencapsul. 1984;1(2):105–12.



VITA

NAME Nawinda Chinatangkul

DATE OF BIRTH 31 Jan 1983

INSTITUTIONS ATTENDED - Bachelor of Pharmacy, Faculty of Pharmacy, Silpakorn University, Thailand
- Master of Pharmaceutical Science, University of Tasmania, Australia

HOME ADDRESS 201/10 M.5 Petkasem Rd. Tammasala Muang Nakhon Pathom

PUBLICATION - Chinatangkul N, Phosrithong N, Nuchtavorn N, Rattanapit T, Mongkol C, Chutipanyaboot P. Formulation and Physicochemical Evaluation of Topical Preparations Containing Extract of Clerodendrum disparifolium. Adv Mater Res [Internet]. 2015;1060:95–8. Available from: <https://www.scientific.net/AMR.1060.95>

- Chinatangkul N, Pengon S, Limmatvapirat C, Limmatvapirat S. Design of Experiment Approach for Fabrication Process of Electrospun Shellac Nanofibers Using Factorial Designs. Key Eng Mater [Internet]. 2017;757:120–4. Available from: <https://www.scientific.net/KEM.757.120>

- Chinatangkul N, Limmatvapirat C, Nunthanid J, Luangtana-Anan M, Sriamornsak P, Limmatvapirat S. Design and characterization of monolaurin loaded electrospun shellac nanofibers with antimicrobial activity. Asian J Pharm Sci [Internet]. 2017 Dec 27 [cited 2018 Apr 25]; Available from: <https://www.sciencedirect.com/science/article/pii/S1818087617308206>

- Pengon S, Chinatangkul N, Limmatvapirat C, Limmatvapirat S. The effect of surfactant on the physical properties of coconut oil nanoemulsions. Asian J Pharm Sci [Internet]. 2018 Mar 17 [cited 2018 Apr 25]; Available from: <https://www.sciencedirect.com/science/article/pii/S1818087617308267>